A STUDY OF THE POTENTIAL BENEFITS OF USING LOWER-DENSITY ABLATORS FOR PROTECTING MANNED LIFTING-BODY ENTRY VEHICLES

A Thesis

Presented to

the Faculty of the School of Engineering and Applied Science

University of Virginia

In Partial Fulfillment

of the Requirements for the Degree

Master of Aerospace Engineering

---

by

James N. Moss

June 1968

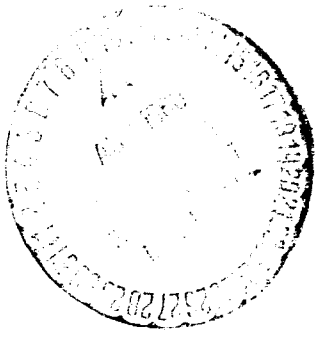

APPROVAL SHEET

This thesis is submitted in partial fulfillment of

the requirements for the degree of

Master of Aerospace Engineering

James N. Moss

Author

Approved:

Ricardo Zapata

Faculty Advisor

Dean, School of Engineering and
Applied Science

June 1968

ACKNOWLEDGMENT

The author is indebted to the National Aeronautics and Space Administration for permitting material obtained from research conducted at the Langley Research Center to be used in this thesis. The author is grateful to William A. Brooks, Jr., Head of Entry Structures Branch, for his comments on the thesis and for serving as an off-campus advisor.

The author also appreciates the assistance of Dr. Ricardo N. Zapata of the University of Virginia in preparing this thesis.

TABLE OF CONTENTS

LIST OF TABLES

LIST OF FIGURES

FIGURE PAGE

FIGURE PAGE

FIGURE PAGE

LIST OF SYMBOLS

A	constant in mass loss rate equation corresponding to specific reaction rate, lb/ft^2-sec-atm
B	constant in exponential of mass loss rate equation corresponding to activation temperature, ^oR
C_e	oxygen concentration by weight at edge of boundary layer, per cent
C_{hs}	heat capacity of heat sink $(\rho C_p X)_{heat\ sink}$, Btu/ft^2-^oF
C_L	lift coefficient
C_w	oxygen concentration by weight at wall, per cent
c_p	specific heat, Btu/lb-^oF
$\bar{c}_p$	specific heat of gaseous products of pyrolysis, Btu/lb-^oF
E	ablative effectiveness, defined as qt_{300}/w where t_{300} is the time for a back-surface temperature rise of 300^oF, Btu/lb
g	initial temperature distribution, ^oF
H	altitude, ft
h_e	total enthalpy at edge of boundary layer, Btu/lb
h_w	total enthalpy of fluid at wall, Btu/lb
Δh_c	heat of combustion, Btu/lb
Δh_p	heat of pyrolysis, Btu/lb
k	thermal conductivity, Btu/ft-sec-^oF

l	length of vehicle, ft
L/D	lift-drag ratio
M	constant defined in Equation (17)
$\dot{m}_c$	rate of char loss, lb/ft^2-sec
$\dot{m}_p$	rate of loss of uncharred material, lb/ft^2-sec
$\dot{m}_{(O_2)}$	rate at which oxygen diffuses to surface, lb/ft^2-sec
N	constant defined in Equation (18)
N_{Le}	Lewis number
$P_{O_2,w}$	partial pressure of oxygen at the wall
$p_{t,2}$	stagnation pressure behind normal shock, atm
p_w	total pressure at the wall, atm
Q	heat load, Btu/ft^2
$\bar{Q}$	total heat absorbed, Btu
q	convective heating rate to a cold-wall with no mass transfer, Btu/ft^2-sec
q_{net}	hot-wall convective heating rate corrected for transpiration, Btu/ft^2-sec
R	sphere radius, ft
Re	free-stream Reynolds number based on length of vehicle
T	temperature, ^oF or ^oR
t	time, sec
u_e	velocity at edge of boundary layer, ft/sec
V	velocity, ft/sec
w	weight per unit area of uncharred ablation material, lb/ft^2
$\bar{w}$	total weight of ablation material, lb

X	thickness or chordwise distance, ft
$\bar{X}$	distance from initial outer surface to outer surface of char layer, ft
y	distance from initial outer surface of char layer, ft
α	angle of attack, deg
α_c	weighting factor for transpiration effectiveness of char mass loss
α_p	weighting factor for transpiration effectiveness of pyrolysis products
γ	flight-path angle from horizontal, deg
ϵ	emissivity
λ	weight of char removed per unit weight of oxygen
ρ	density, lb/ft^3
σ	Stefan-Boltzmann constant, $Btu/sec\text{-}ft^2\text{-}{}^oF^4$
τ	aerodynamic shear stress, lb/ft^2
φ	roll angle, measure from the most windward streamline, deg
ψ	ratio of molecular weight of mixture to molecular weight of oxygen at the wall

Subscripts:

i	initial value
max	maximum
s	stagnation
∞	free stream
1, 2	different environments

Abbreviations:

Mic	phenolic Microballoons
Ny	powdered nylon
Ph	powdered phenolic resin

Primed symbols refer to uncharred material

ABSTRACT

Results are presented of an experimental investigation of low-density (10- to 20-lb/ft^3) phenolic-nylon ablative materials and of an analysis of the ablative heat shield weight requirements of a 13° blunted half-cone entry vehicle for various entry attitudes (lift). The ablative effectiveness of some of the low-density materials was found to be about 1.5 times that of a 36-lb/ft^3 phenolic-nylon ablator. Furthermore, it was found that a 14-lb/ft^3 ablator provided high ablative effectiveness while maintaining good structural char integrity when exposed to a range of test conditions that was inclusive of most of the environmental conditions experienced by a manned lifting-body entry vehicle. Analysis shows that the ablative heat-shield weight requirements are strongly dependent on the entry attitude, decreasing with increasing lift; and that a 34 per cent reduction in the total weight of the ablative heat shield may be obtained by using a 14-lb/ft^3 rather than a 36-lb/ft^3 phenolic-nylon ablator.

CHAPTER I

INTRODUCTION

In recent years, much study has been directed toward the lifting vehicle concept for manned near-earth missions such as logistic ferry applications. One important aspect of these studies has been the heat-shield requirement for this type of vehicle, the manned lifting-body entry vehicle. Some of the studies have indicated that the heat-shield weights for lifting vehicles may range from 20 to 30 per cent of vehicle gross weight. Hence, the importance of the heat shield becomes readily apparent not only from the view point of its primary mission, that of protecting the vehicle's main structure and occupants from the hyper-thermal environment, but also from a weight view point.

Of the basic heat shield concepts available (ablative, radiation cooled, and transpiration cooled), the ablative heat shields are generally recommended (Ref. 1 to 4) because of their high efficiency for the environment experienced by manned lifting-body entry vehicles. Of the ablation materials available, studies (Ref. 5) have shown that the lower-density, char-forming ablators provide the most effective protection. The reason for the effectiveness of the char-forming ablators is attributed to the presence of three characteristics that are desirable of ablation materials; namely, a reradiating outer surface provided by the carbonaceous char, a passive transpiration cooling capability provided by the pyrolysis gases that are generated when the uncharred

material is thermally degraded, and an insulative capability provided by the charred and uncharred materials.

For the detailed heat shield design studies that use charring ablators, such as those reported in References 2, 3, and 4, considerations are given not only to the ablation material per se, but also to the means by which the ablation material may be used most effectively either alone or in combination with structural and insulative materials in providing the most desirable heat shield with respect to such factors as reliability, weight, refurbishability, and cost. Of the heat-shield designs that incorporate an ablative material, they may be classified as single-wall or double-wall heat shields.

The single-wall heat shield is one in which the ablation material is affixed to the load-carrying structure that it is intended to protect. The most attractive aspect of the single-wall heat shield is its reliability. However, with respect to weight and refurbishability, the single-wall heat shield is not as advantageous as the double-wall heat shield. Nevertheless, the single-wall concept becomes more competitive with the double-wall concept with respect to refurbishability when the ablation material is bonded to a thin sheet of material such that the shield can be fabricated independently of the space vehicle and affixed to the vehicle at the most convenient time by mechanical fasteners.

For the double-wall heat shield, the ablation material is affixed to a honeycomb structure which is attached to the main structure by means of stand-offs. The space between the honeycomb and main structure is filled with a low density insulator. The double-wall heat shield is

less desirable with respect to reliability than the single-wall heat shield. Nevertheless, the results of the studies reported in References 3 and 4 show that a double-wall heat shield is desirable for the HL-10 lifting entry vehicle because of weight advantages and ease of refurbishment. However, the results were obtained for ablation materials having densities of 36 to 40 lb/ft^3.

The primary environmental factors influencing the selection of a heat shield for lifting entry vehicles are the relatively low heating rates and long entry time resulting in a high total heat load. This heating is predominantly convective since radiative heating is negligible for entry from near-earth orbits. As is shown in Reference 6, the heating rates and heat loads experienced by an entry vehicle can be altered significantly by altering the vehicle attitude (lift) on entry. Furthermore, it was observed (Ref. 6) that, in general, no one point or line on a vehicle can possibly show a variation of entry heating rate with angle of attack that is typical of the entire vehicle. Consequently, the heat shield requirements must be determined by examining the heating experienced by the entire area for which an ablative heat shield is required.

Since large areas of lifting-body entry vehicles encounter relatively low heating rates over rather long time intervals, the use of charring ablators having densities less than 36 to 40 lb/ft^3, that is, densities less than that for which all of the heat-shield design studies have been made, may be desirable if the lower-density ablators can perform reliably. A possible implication of developing

lower-density ablators with improved insulation characteristics would be an alteration in the present heat-shield design philosophy, that is, the use of a single-wall heat shield as opposed to the double-wall heat shield. For these reasons, emphasis has been directed recently toward the development of low density ablation materials (Refs. 7 and 8).

The present investigation was undertaken to evaluate the performance of low-density (10-to-20 lb/ft^3) phenolic-nylon ablative materials when subjected to test environments representative of that experienced by lifting-body entry vehicles and to determine by analysis the potential weight savings that may be realized by using a 14-lb/ft^3 ablator as opposed to a 36-lb/ft^3 ablator for a lifting entry vehicle at various entry attitudes (lift). The analysis includes the determination of the trajectory parameters and the aerodynamic and heating characteristics of the vehicle (one-half of a 13° half-angle cone with a spherically blunt tip) at the various entry attitudes.

CHAPTER II

CHARRING ABLATOR PROGRAM

The charring ablator program (Ref. 9) used in the parametric study and the application analysis study is a one-dimensional numerical computer program that solves the equations governing the transient response of ablators subjected to a heating environment. The description of the ablator program includes only those aspects of the program that relate to the ablation analysis made in this paper.

Qualitative Description of Ablation

Figure 1 shows a schematic diagram of a charring ablator and the analytical model used. When the outer surface of a charring ablator is exposed to a high-temperature environment, a char layer is formed as the material is thermally degraded. The char layer provides both insulation and a high-temperature outer surface for reradiation. The heat passing through the char is partially absorbed by pyrolysis at the interface between the char layer and the uncharred material. The remaining heat is conducted into the uncharred material. The gases generated during pyrolysis are heated as they transpire through the char and are injected into the boundary layer. The heat that the gases of pyrolysis absorb as they transpire through the char reduces the quantity of heat that is conducted to the pyrolysis interface. When the gases are injected into the boundary layer, the convective heating rate to the surface is reduced. This process of reducing the convective heating is commonly

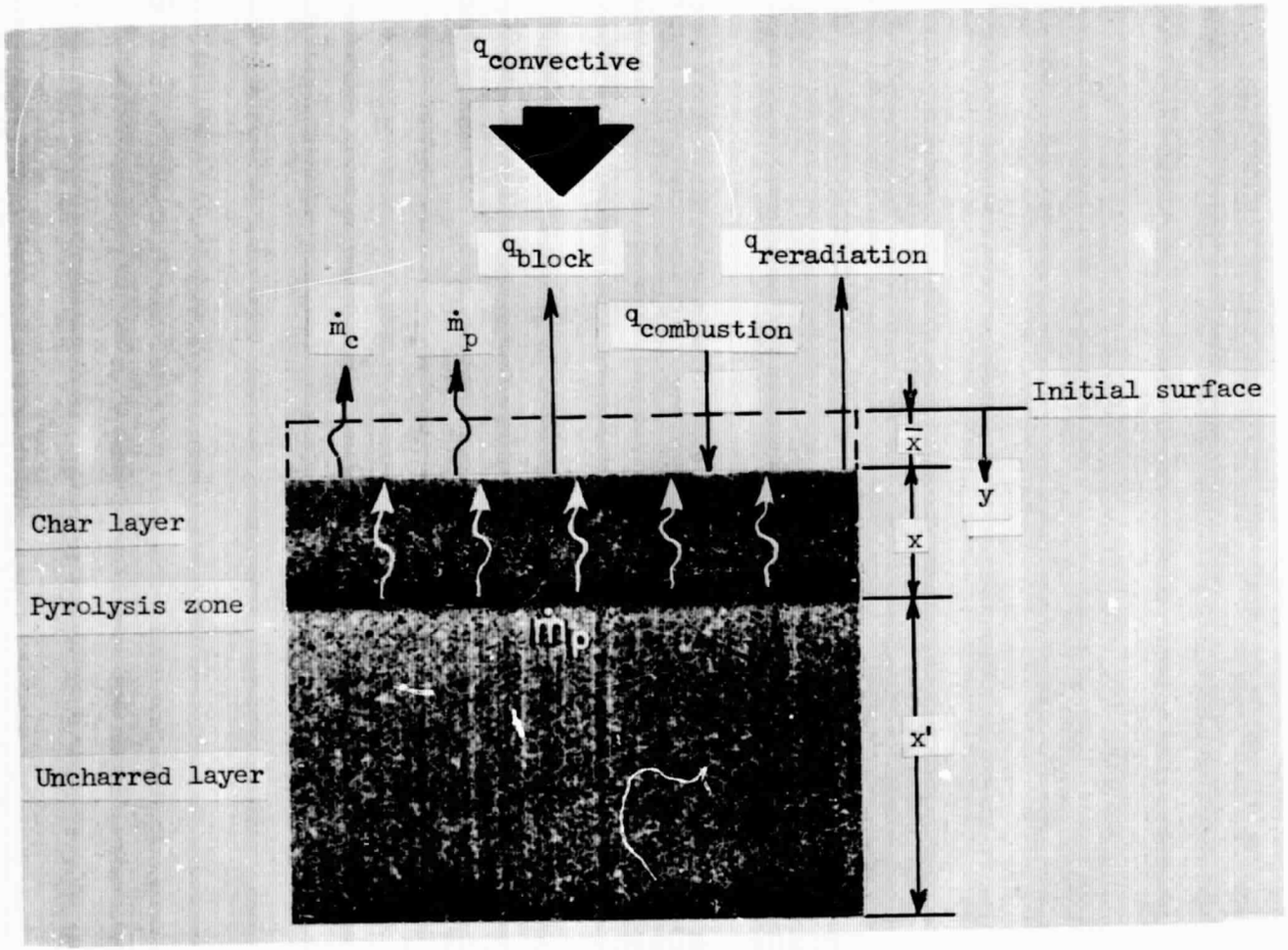

Figure 1.- Schematic diagram of charring ablator and analytical model.

referred to as aerodynamic blocking and has the same effect as that obtained with subliming ablators such as teflon. As the processes of pyrolysis, transpiration, and injection are taking place, char removal may also be taking place as a result of thermal, chemical, or mechanical processes. Thus, the char thickness may increase or decrease depending upon the relative rates of formation and removal of the char. The various processes discussed are related quantitatively in the following sections.

Basic Heat Conduction Equations

It is assumed that the thermal properties of a given layer of material are functions of only temperature, that all heat flow is normal to the surface, and that gases transpiring through the char are at the same temperature as the char. Then the differential equation governing the heat transfer within the char layer ($\bar{X} \leq y \leq \bar{X} + X$) is:

$$\frac{\partial}{\partial y}\left(k \frac{\partial T}{\partial y}\right) + \dot{m}_p \bar{c}_p \frac{\partial T}{\partial y} = \rho c_p \frac{\partial T}{\partial t} \tag{1}$$

This equation accounts for the heat conducted within the char, the heat absorbed by the gases transpiring through the char, and the heat stored within the char.

For the uncharred material ($\bar{X} + X \leq y \leq X_i + X_i'$), the heat transfer is governed by the following differential equation:

$$\frac{\partial}{\partial y}\left(k' \frac{\partial T'}{\partial y}\right) = \rho' c_p' \frac{\partial T'}{\partial t} \tag{2}$$

Initial and Surface Boundary Conditions

The initial temperature distribution is assumed to be given as a function of position:

$$T(y,o) = g(y) \tag{3}$$

In addition, the initial mass-transfer rates must be specified.

Two boundary conditions must be specified at the heated surface of the char. One must determine either the rate of removal of material at the surface or the surface temperature. The second surface boundary condition is provided by an energy balance.

In general, the relative importance of the various mechanisms involved in char removal are not well established. However, it has been established (Ref. 10) that oxidation of the char surface is an important mechanism responsible for char removal. The calculations made in this study used oxidation as the only surface removal mechanism.

The rate of oxidation of carbon for a first order reaction can be determined from the following equation (Ref. 11):

$$\dot{m}_c = Ae^{-B/T} p_{O_2,w} \tag{4}$$

where the constant A corresponds to the specific reaction rate and the constant B corresponds to the activation temperature. The rate at which char is removed by oxygen must be proportional to the net rate at which oxygen diffuses to the surface. From Reference 12, this rate is

$$\dot{m}_{(O_2)} = \frac{N_{Le}^{0.6}\, q_{net}}{h_e - h_w}\left(C_e - C_w\right) = \frac{\dot{m}_c}{\lambda} \tag{5}$$

By combining Equations (4) and (5), the resulting equation for char removal rate using first-order oxidation is obtained:

$$\dot{m}_c = \frac{A e^{-B/T} p_w C_e \psi}{1 + \dfrac{A e^{-B/T} p_w \left(h_e - h_w\right) \psi}{q_{net} \lambda N_{Le}^{0.6}}} \tag{6}$$

where q_{net} is the hot-wall convective heating rate corrected for transpiration (see Eq. (7)). The surface energy balance, when transpiration theory is used and radiative heating is neglected, is given as follows:

$$\underbrace{q \underbrace{\left(1 - \frac{h_w}{h_e}\right)}_{\text{Hot-wall correction}} \underbrace{\left[1 - \left\{0.724 \frac{h_e}{q}\left(\alpha_c \dot{m}_c + \alpha_p \dot{m}_p\right) - 0.13\left(\frac{h_e}{q}\right)^2 \left(\alpha_c \dot{m}_c + \alpha_p \dot{m}_p\right)^2\right\}\right]}_{\text{Aerodynamic blocking}}}_{\substack{\text{Cold-wall convective heating rate} \\ \text{Net convective heating rate}}} \tag{7}$$

$$\underbrace{+ \dot{m}_c \Delta h_c}_{\substack{\text{Combustive} \\ \text{heating rate}}} = \underbrace{\sigma \epsilon T^4}_{\substack{\text{Reradiation}}} - \underbrace{\left(k \frac{\partial T}{\partial y}\right)_{surface}}_{\substack{\text{Conduction to} \\ \text{interior}}}$$

The net convective heating rate term in the surface energy balance equation is written such that the approximate net heating to a vehicle

can be obtained without simultaneously solving the boundary layer equations accounting for the coupling that occurs between ablation and the flow field properties. The approximate expression for the net convective heating is formulated such that the effect of heat and mass transfer can be uncoupled. That is, the required convective heating rate input for the charring ablator program is the cold-wall convective heating to a non-ablating body. The approximate net convective heating rate with mass transfer is then obtained by using the hot-wall and aerodynamic blocking terms. Consequently, the net convective heating does not account for any coupling between the flow parameters and aerodynamic blocking that may result from homogeneous reactions within the boundary layer due to the injection of the ablation products. However, as discussed in Reference 13, homogeneous reactions that occur within the boundary layer have only a secondary effect on heat transfer despite the importance of the reactions in determining the thermodynamic state of the gas throughout the flow field. This condition exists as long as the Lewis number N_{Le} is approximately one and the surface is catalytic to recombinations. Consequently, neglecting the effect of homogeneous reactions due to mass transfer on the net heat transfer to a charring ablator appears to be a reasonable approximation.

The aerodynamic blocking term in Equation (7) is a second-degree approximation of the exact solution obtained from boundary-layer solutions for air-to-air injection (Ref. 9). The evaluation of the coefficients in the blocking term is discussed in Reference 9. The

char-removal rate $\dot{m}_c$, due to combustion at the surface, is given by Equation (6) and the pyrolysis rate $\dot{m}_p$ is given by Equation (10).

The pyrolysis-interface boundary condition ($y = \bar{X} + X$) is given as follows:

$$- k \frac{\partial T}{\partial y} = \dot{m}_p \Delta h_p - k' \frac{\partial T'}{\partial y} \tag{8}$$

where the heat conducted to the pyrolysis interface must be either absorbed by pyrolysis reactions or conducted into the uncharred material. In addition, the temperature in the char and in the uncharred material must be equal at the interface: that is, at $y = \bar{X} + X$

$$T = T' \tag{9}$$

The approach used for calculating the rate of pyrolysis was to assume that the rate of pyrolysis is a known function of temperature of the following form:

$$\dot{m}_p = A' e^{-B'/T(\bar{X} + X)} \tag{10}$$

The specific reaction rate constant A' and activation energy constant B' can be determined by employing thermoanalytical techniques (Ref. 14) such as thermogravimetric analysis (TGA).

The boundary condition at the back surface of the ablation material is given as follows:

$$- k' \frac{\partial T'}{\partial y} = C_{hs} \frac{\partial T'}{\partial t} \tag{11}$$

This boundary condition accounts for the fact that the uncharred ablation material is attached to a thermally thin plate which functions as a concentrated heat sink. The heat capacity C_{hs} of the heat sink used in the parametric and application studies had a value of 0.235 $Btu/ft^2-{}^oF$, which corresponds to an aluminum sheet having a thickness of approximately 0.08-inches.

Numerical Solution

The previously discussed differential equations along with their respective boundary conditions were transformed to a coordinate system in which the coordinates themselves move to accommodate the changes in the locations of the surfaces of the charred and uncharred layers. The transformed equations and boundary conditions were then placed into a form suitable for numerical calculation by deriving the equations in finite-difference form and then solving them by an iteration procedure on a high-speed digital computer. Details regarding the coordinate transformations and the finite-difference representation of the equations are included in Reference 9.

The numerical solution yields temperature distributions, dimensional changes, rates of char loss $\dot{m}_c$, rates of pyrolysis $\dot{m}_p$, net convective heating q_{net}, combustive heating, and reradiative heating as functions of time. To obtain these results, it is necessary to specify certain environmental and material properties. The ablative heat shield weight requirements obtained in this study were obtained by iterating on the thickness of ablation material required to limit the back-surface temperature rise to 300^oF.

CHAPTER III

PARAMETRIC STUDY

To obtain an idea of the potential ablative heat-shield weight savings that may be realized by using lower-density ablation materials, a parametric ablative study was conducted whereby the local ablative weight requirements were calculated for a typical manned lifting-body entry vehicle by using a numerical charring ablation program. For this study, all of the ablative material parameters were considered as fixed parameters with the exception of the density of the char and the density and thermal conductivity of the uncharred material. The thermal conductivity of the uncharred material was included as a variable parameter since reducing the density of ablation materials is usually accompanied by a reduction in the uncharred thermal conductivity as indicated in Reference 7.

Material Properties

The material properties used in the parametric study as inputs in the charring ablator program, with the exception of the densities and the thermal conductivity of the uncharred material, are listed in Table I as the properties for the 36-lb/ft^3 material. The properties listed in Table I for the 36-lb/ft^3 phenolic-nylon ablator are those that have been used previously (Ref. 15) to obtain good agreement between calculated and experimental results. It was assumed that the density of the char was always one-half that of the uncharred material and that the thermal conductivity and specific heat of the char and the

specific heat of the uncharred material were not a function of the density of the uncharred material.

Environment

The environmental conditions used in the parametric study are those experienced by a typical lifting-body entry vehicle (Ref. 16) characterized by a maximum lift-drag ratio of 1.5 at an angle of attack of 27°. Entry begins at an altitude of 400,000 ft with an entry angle of -1.5° and a velocity of 26,000 ft/sec. When the entry angle reaches 0°, the vehicle is roll modulated to prevent skip-out and to maintain a constant altitude trajectory. The vehicle is flown at constant altitude until the roll angle returns to 0°. Following the constant altitude maneuver, the vehicle flies an equilibrium-glide trajectory at the maximum lift-drag ratio to touchdown. The stagnation enthalpy and cold-wall heating rate histories encountered by this vehicle are shown in Figure 2. The enthalpy and heating rate histories along with the free stream composition are the required environmental inputs to the charring ablator program. Additional details regarding the vehicle, trajectory, and environmental parameters encountered during entry may be obtained in Reference 16.

The heating rate used in the parametric study was 40 per cent that of the stagnation value. Consequently, the maximum heating rate used in the parametric study had a value of 38 Btu/ft^2-sec. The lower value of heating rate was used since the stagnation heating is much too high

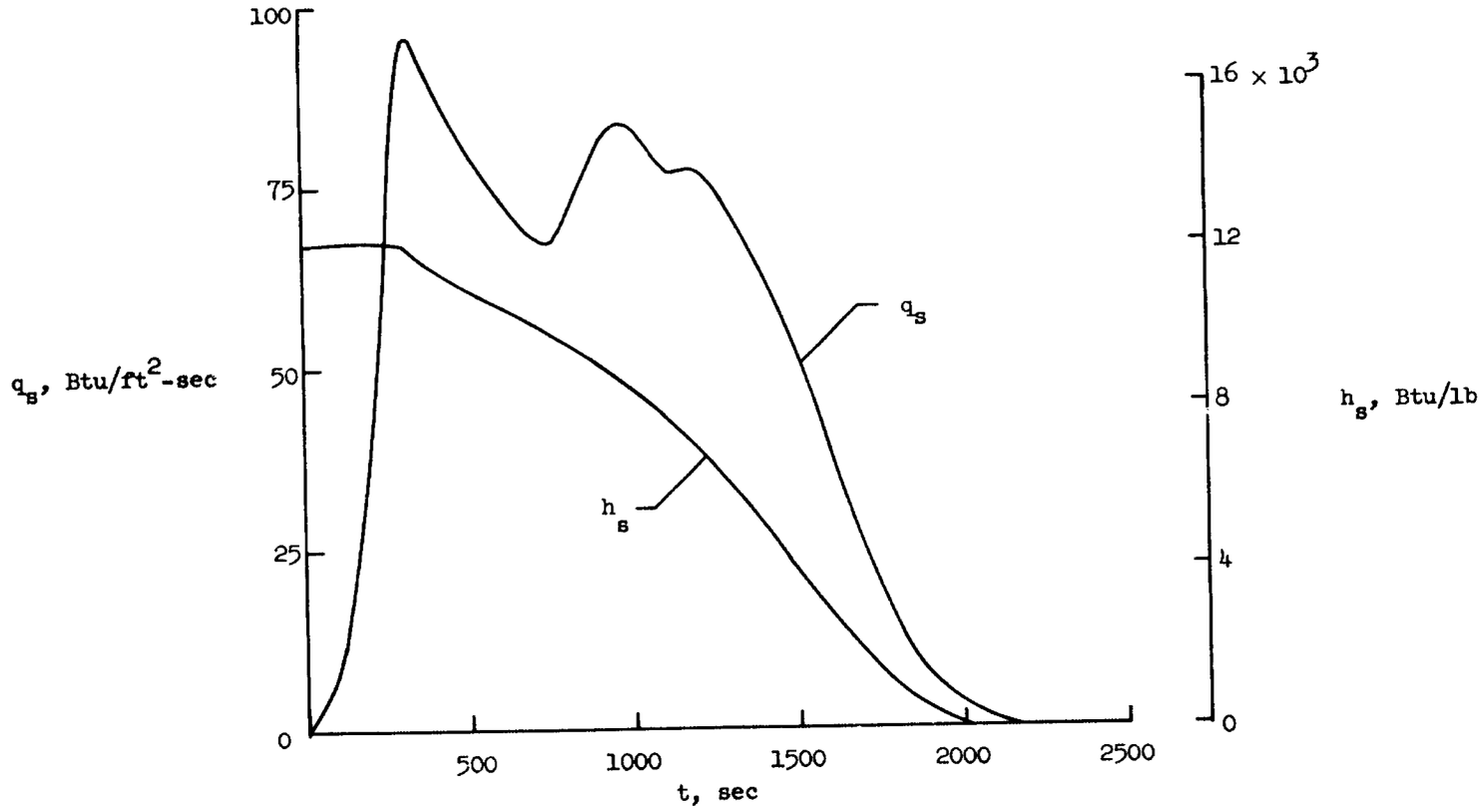

Figure 2.- Enthalpy and stagnation cold-wall heating rate histories experienced by typical manned lifting-body entry vehicle.

for that experienced by most of the area of an entry vehicle. The total heat load accommodated, corresponding to 40 per cent stagnation condition, was 44,000 Btu/ft^2.

Local Weight Requirements

The local unit weight of ablation material required to limit the back-surface temperature rise to 300° F for an ablator having various densities and thermal conductivities is shown as a carpet plot in Figure 3. This is the amount of material that must accommodate a total heat load of 44,000 Btu/ft^2 over an entry time of 2200-seconds. The data indicate that the unit weight of ablation material can be reduced by decreasing the density or the thermal conductivity of the uncharred material.

Since many of the ablation material characterization and heat-shield design studies presently being conducted are concerned with materials having densities of 35 to 40 lb/ft^3 and thermal conductivities of 1.8×10^{-5} to 2.2×10^{-5} Btu/ft-sec-°F, a significant improvement in the ablative material weight requirements could be realized if the density of the ablation materials could be reduced to 10 to 15 lb/ft^3. If a reduction in thermal conductivity can be realized with decreasing density as has been indicated in Reference 7, then the potential of the lower-density ablators would be increased even more.

With the parametric study indicating the potential that lower-density ablators have for protecting entry vehicles on a weight basis, an experimental investigation was initiated to determine whether phenolic-nylon ablators could be fabricated that would perform

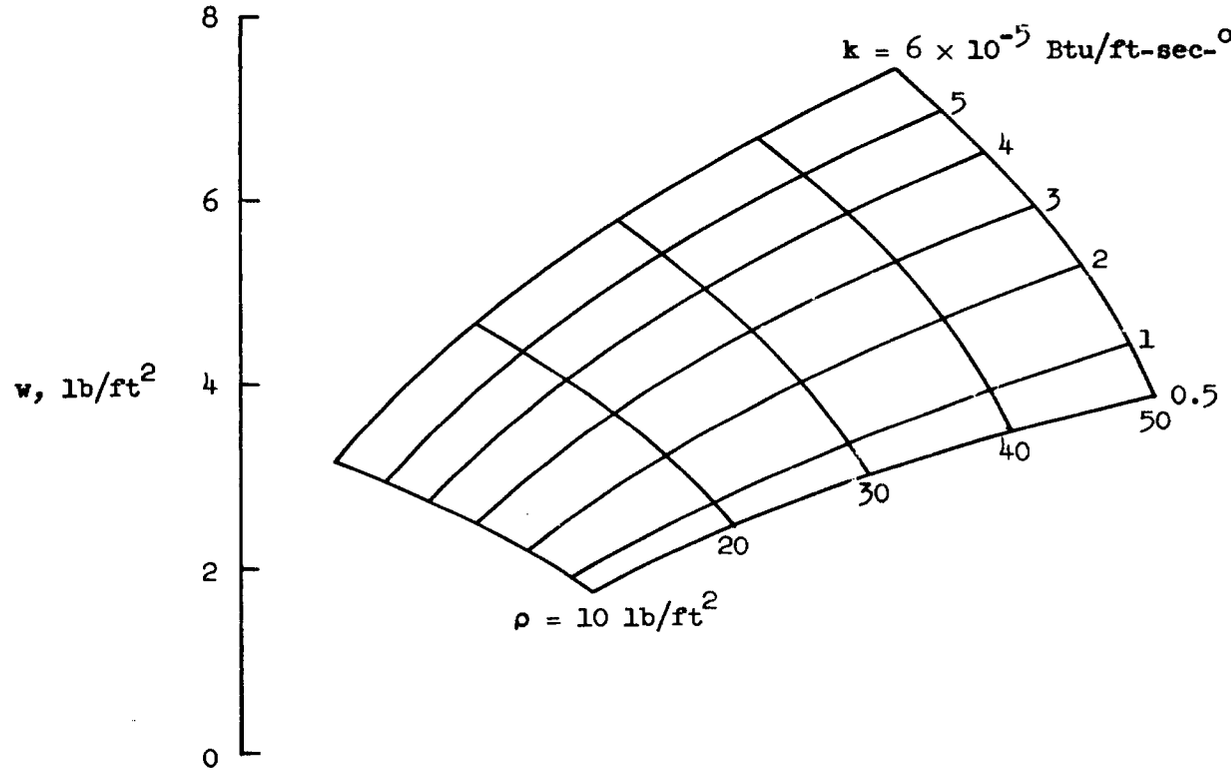

Figure 3.- Effect of density and thermal conductivity of uncharred ablator on the local unit weight of ablation material required for a lifting-body entry vehicle.

satisfactorily when subjected to environments similar to those experienced by manned lifting-body entry vehicles. The experimental test program is discussed in the following chapter.

CHAPTER IV

EXPERIMENTAL

With the parametric study previously discussed providing an indication of the potential that lower-density ablators have for reducing the ablative weight requirement for manned lifting-body entry vehicles, an experimental test program to evaluate such materials was initiated. The objective of the experimental program was to determine whether low-density (10-20 lb/ft^3) phenolic-nylon ablation materials that could be fabricated would perform satisfactorily when exposed to simulated entry environments obtainable in supersonic arc test facilities.

The experimental study was directed initially toward determining the ablative performance of a number of low-density phenolic-nylon ablators having different densities and compositions and subjected to a test condition having the nominal parameters: cold-wall heating rate of 20 Btu/ft^2-sec, total-stream enthalpy of 1700 Btu/lb, and a stagnation pressure of 0.04 atm. Once this phase of the experimental study was completed, one ablator was selected for a more extensive evaluation by exposing it to a number of test environments. A description of the test models, test facilities, and results and discussion of the experimental study follows.

Albation Test Models

The phenolic-nylon ablation models considered in this study consisted of various percentages of powdered phenolic bonding material, nylon powders, and phenolic Microballoons as listed in Table III. Details regarding the material processing and fabrication of these materials are available in Reference 8.

The test models were obtained by machining the fabricated phenolic-nylon composites into 3-inch disks with a thickness of 0.38 inches. The instrumentation and model configuration are shown in Figure 4. A 3/8-inch diameter 1/32-inch thick copper calorimeter was affixed to the back surface of the ablation material with a thermocouple silver soldered to the back surface of the calorimeter. A mounting block was bonded to the back surface of the ablation models with a room-temperature vulcanizing elastomeric rubber. The mounting block afforded a means of attachment to the test facility and isolated the calorimeter from the test environment.

Arc Tunnel Tests

All of the ablation models were tested in supersonic arc tunnels at the Langley Research Center. The models listed in Table III and part of the models in Table IV were tested in a 5-megawatt a.c. arc-powered tunnel while the remaining models in Table IV were tested in a 1-megawatt d.c. arc-powered tunnel. It was necessary to use the 1-megawatt facility in order to obtain cold-wall heating rates to the 3-inch diameter flat-face models in excess of 50 Btu/ft^2-sec with $p_{t,2}$ values of 0.05 atm.

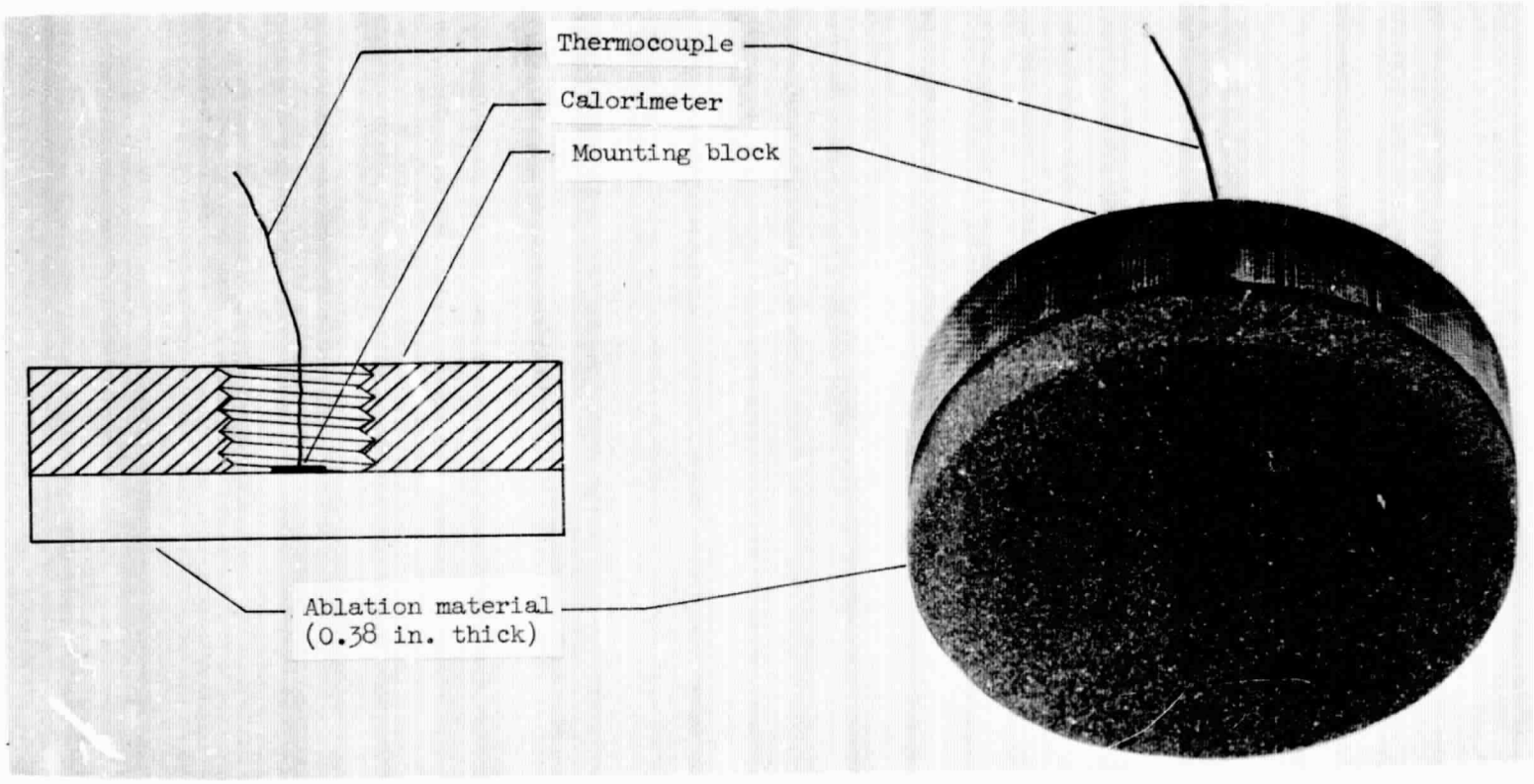

Figure 4.- Instrumentation and model configuration.

The 5-megawatt facility. A schematic of the 5-megawatt facility is shown in Figure 5. The range of operational parameters for this facility equipped with a 9.65° conical nozzle with a 1.5-inch-diameter throat and a 6-inch-diameter exit, as used in this study, are included in Table II. The arc facility utilizes three electrode pairs in the arc chamber (settling chamber) to heat the test gas that is injected near the base of each of the electrode pairs. Each electrode pair consists of a centrally located water-cooled copper annulus surrounded by a water-cooled copper helix. Each electrode pair was energized by one phase of a three-phase alternating-current power source, and the arc formed between the helix and annulus was rotated in the plane of the electrodes by a magnetic field produced by field coils that surround the arc chamber. The test gas is forced through the arcing region, heated, discharged through the water-cooled supersonic nozzle onto the test model, and collected in a vacuum sphere. The only limitation with respect to operating time for this facility is the vacuum capability, that is, the ability to maintain the desired pressure in the test section.

As shown in Figure 5, the test section had four pneumatically operated inserter arms, each of which had a sting for supporting a model. Three of the inserter arms were used in this study: one for supporting the ablation model, one for supporting the pressure probe, and one for supporting the heat transfer calorimeter.

The 1-megawatt facility. The 1-megawatt facility has essentially the same test section as the 5-megawatt facility but has a vortex-stabilized constricted arc unit and the diffuser is connected to a

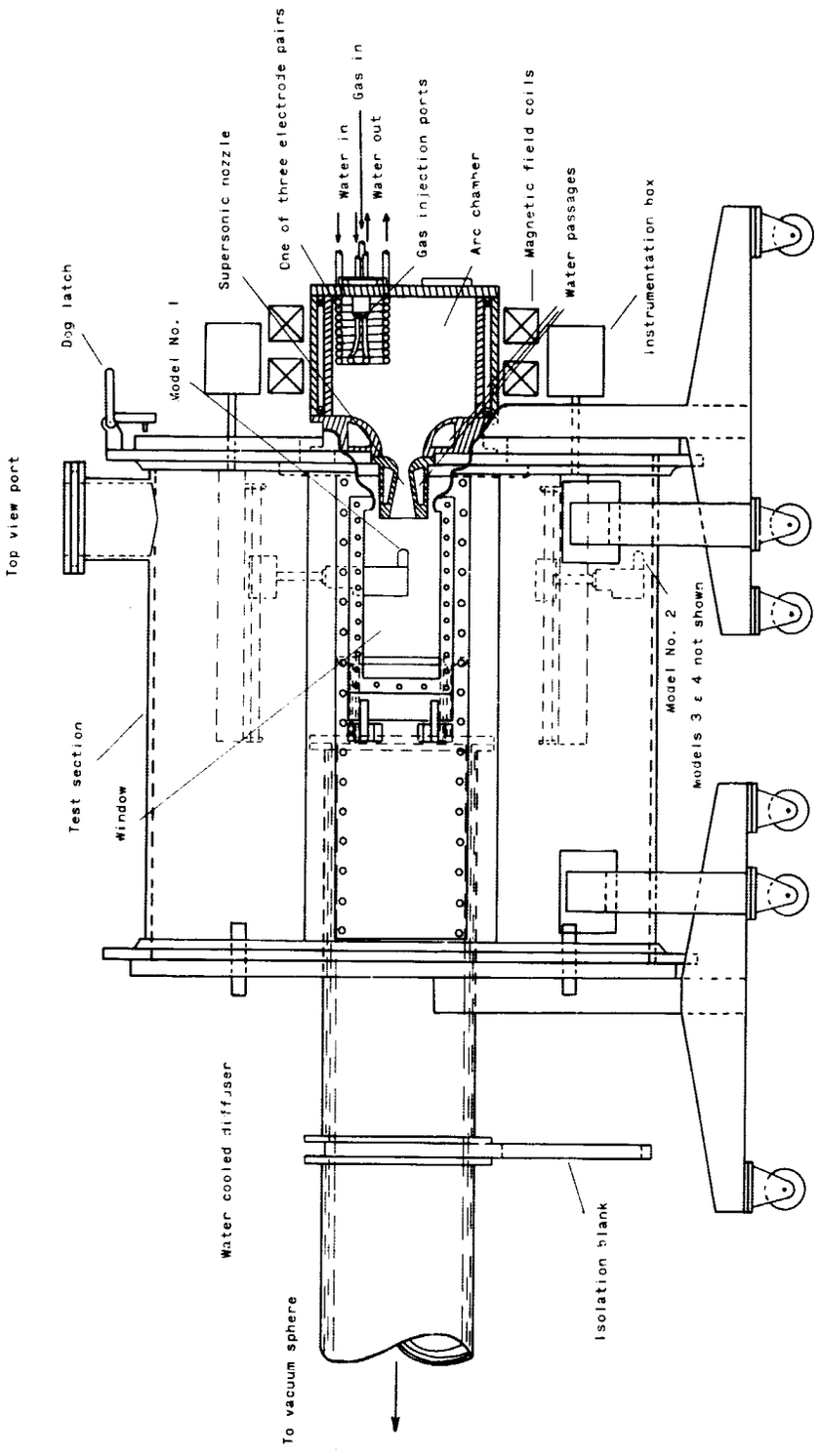

Figure 5.- Schematic of 5-megawatt supersonic arc test facility.

steam ejector rather than to a vacuum sphere. The operational parameters for this facility when using a 8.18° conical nozzle with a 1-inch diameter throat and a 4-inch diameter exit, as used in this study, are included in Table II.

Test conditions. The nominal test conditions obtained in the 5-megawatt facility for the ablation models listed in Table III were: cold-wall heating rate of 20 Btu/ft^2-sec, total-stream enthalpy of 1700 Btu/lb, Mach number of 3.9, stagnation pressure of 0.04 atm, and a mass flow rate of 0.10 lb/sec. The test gas used was a 3-per cent oxygen and 97-per cent nitrogen mixture. The remaining ablation models along with their respective test conditions are listed in Table IV.

Test procedure. Prior to the test of the ablation models, the desired test condition was determined and calibrated with respect to heating rate and pressure. The procedure for each model tested was to start the facility and allow enough time for the test condition to become stable. A heat-transfer measurement, obtained by the transient calorimetry technique, was taken and the test model was inserted with the model surface normal to the flow. The model exposure time was such that the copper calorimeter on the back surface of the model would experience a temperature rise of 300° F. During the model exposure, the output from the thermocouple attached to the copper calorimeter and the test-facility temperature and pressure data were recorded at 2-second intervals on digital tape. A second heating rate was obtained as soon as the test model was retracted from the test stream to obtain an

average heating rate. The charred models were then cross sectioned, photographed, and measured to determine surface recession.

Experimental Results and Discussion

The results of the arc tunnel tests of phenolic-nylon materials are listed in Tables III and IV. The results of these tests will be subsequently discussed in detail.

Extent of entry environment simulation. In an assessment of the results of an ablation test program in which a material is subjected to a simulated entry environment, the observations or conclusions must always be made by considering the extent by which the tests have simulated the actual entry parameters. If the experimental test environments previously discussed are compared with the environments representative of that experienced by manned lifting-body entry vehicles (Figure 18 and Reference 16), an indication of the extent by which the test conditions have simulated the flight conditions may be obtained. From such a comparison it is evident that the test condition can only simulate the entry environment at some instant in the entry trajectory. This is due to the fact that the entry parameters are time-dependent parameters whereas the test parameters are constant. Therefore, in selecting the test condition or conditions, one must select either a condition that is "typical" of the entry environment, as was done for the materials listed in Table III, or a number of test conditions that represent the entry environment at different times during the entry trajectory, as was done for the material subjected to the various test conditions listed in Table IV.

In comparing the test conditions with the entry conditions, it is also obvious that a number of entry parameters or combination of parameters are not simulated in the test environment. The inability to provide a more complete simulation of the entry conditions is due to the limitations of the present state-of-the-art of ground test facilities.

Since it is not possible, in general, to provide a complete simulation of entry conditions in ground test facilities for ablation studies, the approach has been to determine the more important environmental parameters involved in the ablation process and to concentrate on scaling the test environment such that these parameters are simulated. Reference 17 suggests that environmental parameters affect ablative performance only at the heated surface; therefore, any two environments so related that the inputs at the surface are the same should result in the same performance of the material.

Theoretical equations in Reference 17 indicate the necessary relations between different environments that are required to produce the same material performance. These relations were developed by considering that the aerodynamic inputs to an ablating surface could be classified as thermal, chemical, and mechanical. Because of the formal similarity between the governing boundary-layer equations, the convective inputs are related approximately as

$$\frac{q_{net}}{h_e - h_w} = \frac{\dot{m}(O_2)}{C_e - C_w} = \frac{\tau_w}{u_e} \qquad (12)$$

where all inputs are those which are obtained with a given mass transfer into the boundary layer.

No satisfactory general theory of the effects of mechanical inputs on the performance of charring ablators is available. However, experimental data indicate that at low shear stress levels, such stress has no effect on thermal performance and can be neglected. Then, the relations between two environments which produce the same thermal performance are, for convective heating only, as follows:

$$\left(q_{net}\right)_1 = \left(q_{net}\right)_2 \tag{13}$$

$$\left(\dot{m}_{(O_2)}\right)_1 = \left(\dot{m}_{(O_2)}\right)_2 \tag{14}$$

$$\frac{\left(C_e - C_w\right)_1}{\left(C_e - C_w\right)_2} = \frac{\left(h_e - h_w\right)_1}{\left(h_e - h_w\right)_2} \tag{15}$$

Then from Equation (7), the convective heating rate is

$$\left(\frac{q}{h_e} - M + N\frac{h_e}{q}\right)_1 = \left(\frac{q}{h_e} - M + N\frac{h_e}{q}\right)_2 \frac{\left(h_e - h_w\right)_2}{\left(h_e - h_w\right)_1} \tag{16}$$

where the constants M and N are defined as:

$$M = 0.724\left(\alpha_c \dot{m}_c + \alpha_p \dot{m}_p\right) = M_1 = M_2 \tag{17}$$

$$N = 0.13\left(\alpha_c \dot{m}_c + \alpha_p \dot{m}_p\right)^2 = N_1 = N_2 \tag{18}$$

For the case of diffusion-controlled oxidation reactions, the relation between the composition of the two environments is

$$\frac{\left(C_e\right)_1}{\left(C_e\right)_2} = \frac{\left(h_e - h_w\right)_1}{\left(h_e - h_w\right)_2} \tag{19}$$

The Equations (15) or (19) and (16), therefore, relate convective heating environments which produce the same transient material behavior.

The relations shown in Equations (15) and (19) were the basis for reducing the test stream oxygen concentration for those tests conducted in the relatively low enthalpy environment produced in the 5-megawatt facility. The nominal 3-per cent oxygen and 97-per cent nitrogen test stream, used in making the tests in the 5-megawatt facility, and the nominal 23-per cent oxygen and 77-per cent nitrogen test stream, used in making the tests in the 1-megawatt facility, did not provide the correct ratio of test-stream oxygen concentration to enthalpy for all test conditions. Consequently, the ablative performance of the materials tested in an environment containing an excessive oxygen concentration was conservative, because oxidation has a deleterious

effect on the performance of charring ablators. However, for those tests that were made where the test-stream oxygen concentration was low for the associated test-stream enthalpy, the ablative performance was nonconservative. It is to be noted that it would not have been possible to provide accurately the correct ratio of oxygen concentration to enthalpy for all of the test conditions, because it would not have been possible to maintain the small oxygen flow rates that would have been required.

It is believed that the experimental tests conditions provide a good simulation of the entry conditions experienced by a manned lifting-body entry vehicle at various times during the entry trajectory. This observation is based on the assumption that the net convective heating q_{net}, the stream enthalpy h_e, and the stream oxygen concentration C_e are the important environmental parameters to be considered in determining the ablative performance of phenolic-nylon ablators subjected to environments experienced by manned lifting-body entry vehicles.

Effect of materials. The performance of the phenolic-nylon materials listed in Table III, as well as those in Table IV, were compared on the basis of the ablative effectiveness E and the physical appearance of the charred material. The ablative effectiveness is defined as follows:

$$E = \frac{qt_{300}}{w} \tag{20}$$

where q is the cold-wall heating rate to a nonablative surface, t_{300} is the time for a back surface temperature rise of 300° F, and w is the weight per unit area of ablation material used. The value of this parameter depends on both the mass loss characteristics and the insulating properties of materials. Even though the effectiveness parameter is not suitable for making heat shield designs, it is useful in comparing various materials subjected to similar test environments or in investigating the effect of changes in environment on a particular material.

The combined effect of density and composition on the effectiveness of phenolic-nylon ablation materials is shown in Figure 6. The trend is for the effectiveness to decrease with increasing density; however, the extent of the effect of density varied with the material considered.

The effectiveness values are not believed to provide a complete indication of the usefulness of a material, since the handling characteristics of a material and the physical integrity of the char developed during testing are considered to be important to the selection of a particular material. For example, the material with a density of 10 lb/ft^3 (Fig. 7) was molded without any compaction, so that the model was of a powdery texture and was fragile and difficult to handle. On the other hand, the model having a density of 20 lb/ft^3 was molded so that the mold volume was approximately 50 per cent that of the bulk volume, and the resulting model had a firm texture and was easily machined. The appearance of the charred material, shown in Figure 7,

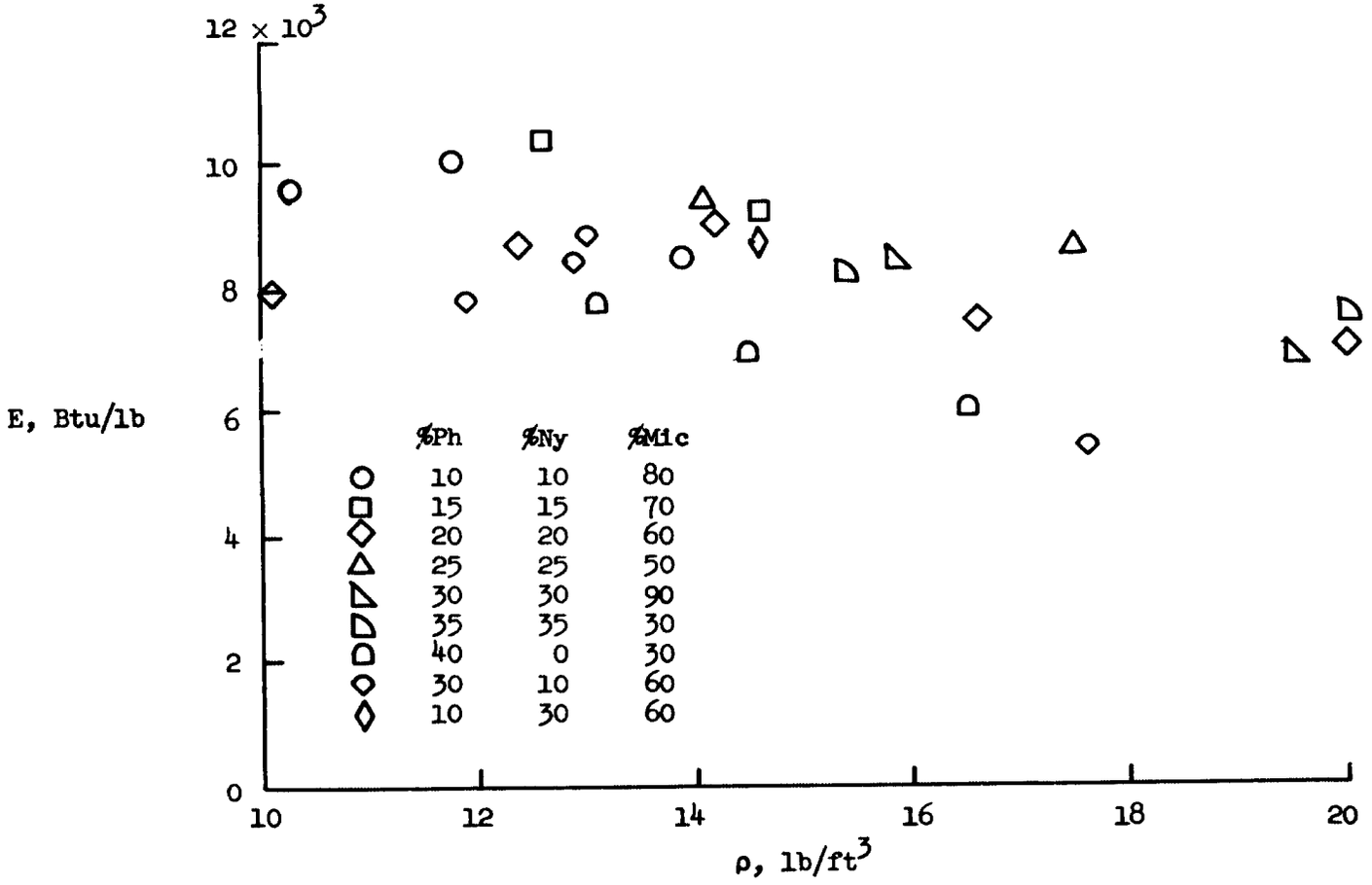

Figure 6.- Combined effect of density and composition on effectiveness of phenolic-nylon composites.

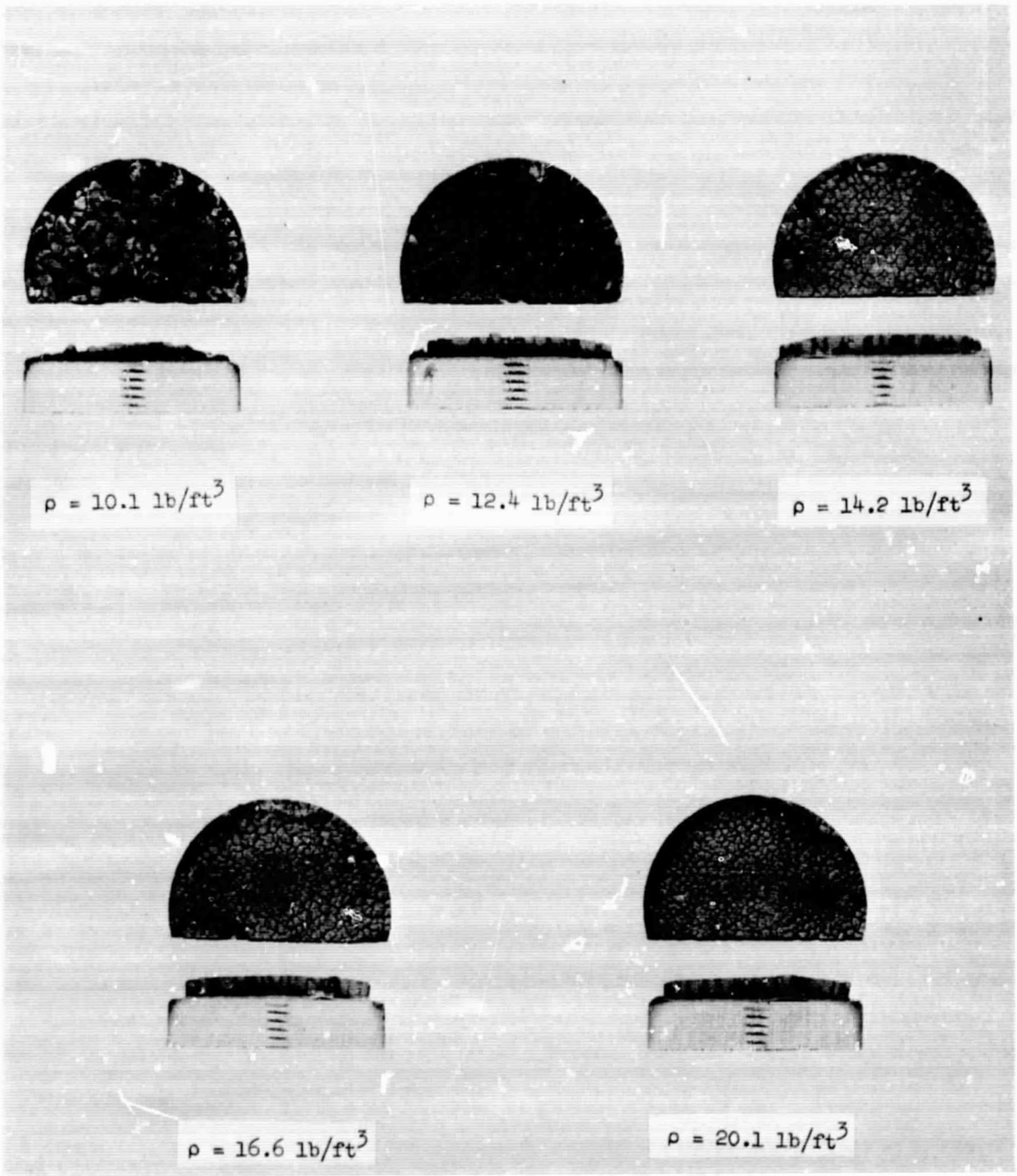

Figure 7.- Surface and cross-section views of various densities of 20 per cent phenolic, 20 per cent nylon, and 60 per cent Microballoons after testing.

indicates that the physical characteristics of the char of the lowest-density model are inferior to those of the higher-density model. For the intermediate densities, the physical characteristics of the chars improved with an increase in density with a substantial improvement occurring as the density increased from 10.1 lb/ft^3 to 14.2 lb/ft^3. The appearance of the chars for various densities of 20 per cent phenolic, 20 per cent nylon, and 60 per cent Microballoons is characteristic of the chars developed for different densities of each of the other phenolic-nylon materials; that is, the characteristics of the char improve with density and the chars have a columnar structure that extends through the depth of the char. The spacing between the columns of material tends to increase as the density decreases and this phenomenon accounts for the weaker char structure.

Since part of the effectiveness variations shown in Figure 6 was due to composition variations, the effect of composition will now be discussed. As the weight percentage of Microballoons was increased with a one-to-one ratio of phenolic powder and nylon (Fig. 8) the effectiveness increased. The data points for each composite are due to different density moldings. The effectiveness curve is a least-squares fit for all data points. A similar plot is shown in Figure 9 where the amount of Microballoons remains constant while the percentages of phenolic powder and nylon were varied. The effectiveness increased as nylon was substituted for the phenolic powders.

Comparison with high-density material. A 36-lb/ft^3 ablator (25 per cent phenolic, 40 per cent nylon, and 35 per cent Microballoons)

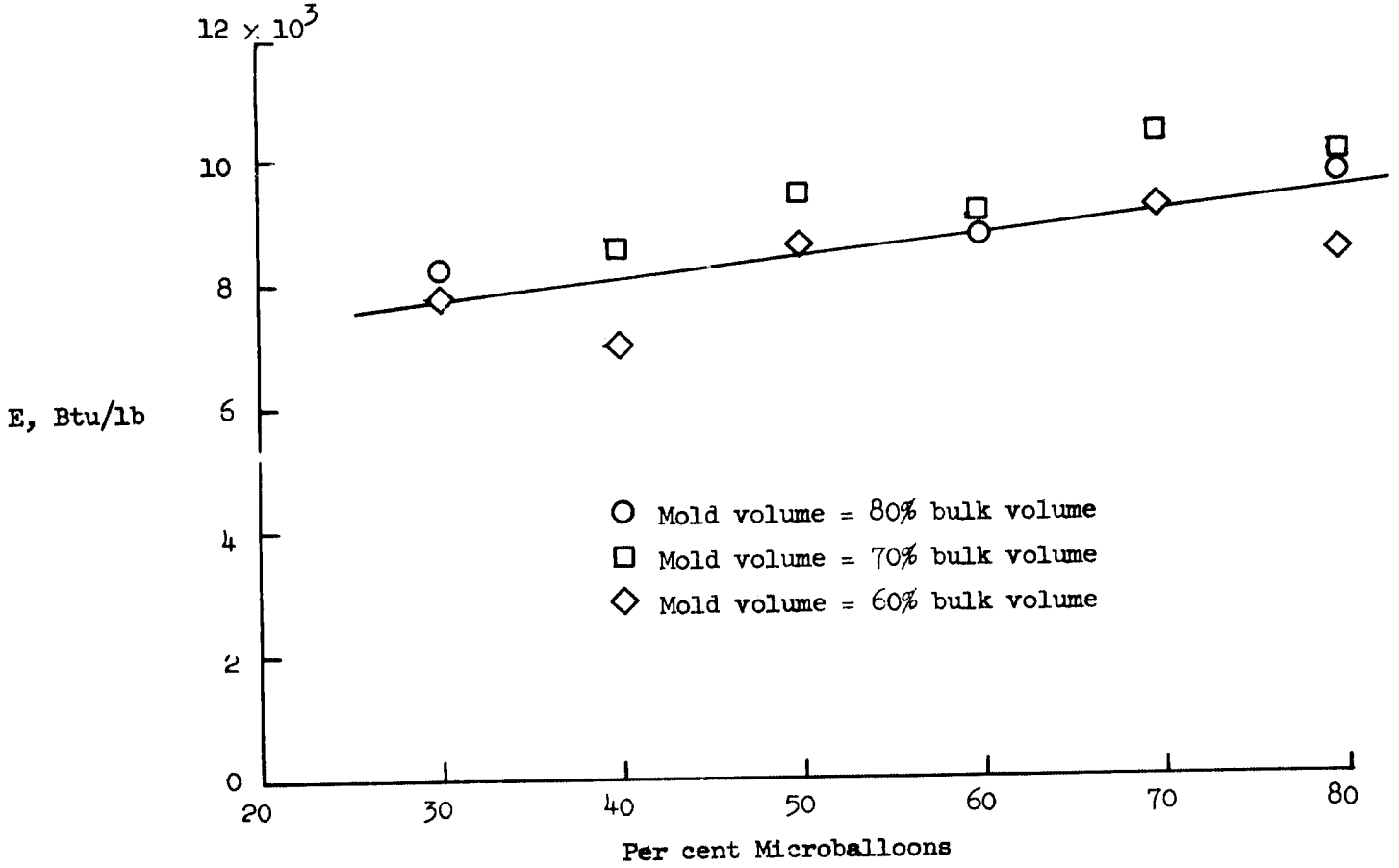

Figure 8.- Effect of phenolic Microballoon content on effectiveness (one-to-one ratio of nylon to phenolic resin).

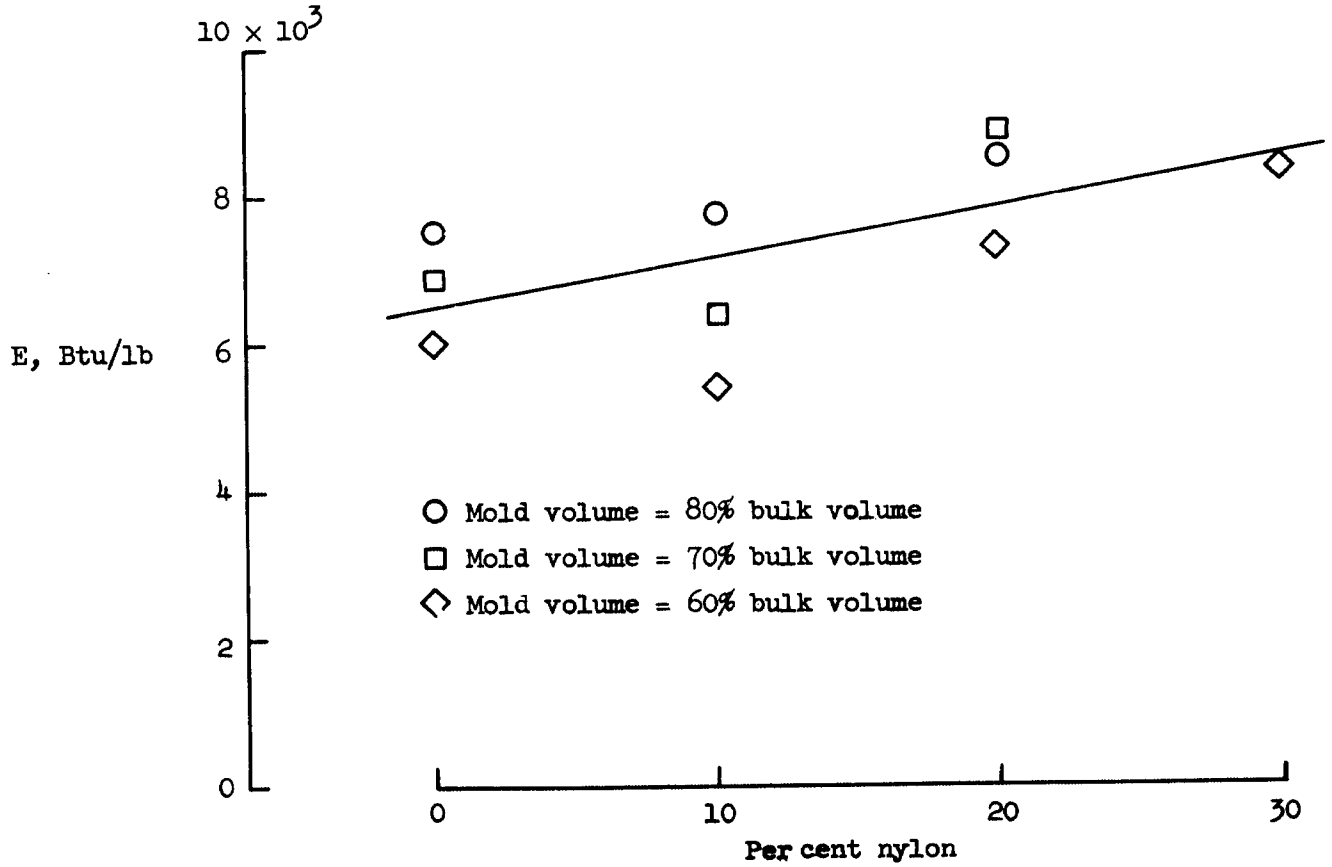

Figure 9.- Effect of nylon content on effectiveness (60 per cent phenolic Microballoons).

that has been evaluated extensively (Ref. 7) was tested at the same condition as the low-density materials listed in Table III. The effectiveness E of some of the low-density materials was 1.5 times greater than the 56-lb/ft^3 material. The physical integrity, however, of the high-density char was superior to that of the low-density chars. This condition was evidenced by smaller spacing between the cracks and by no spalling (Fig. 10).

Effect of honeycomb. The previous discussion has pointed out that all of the low-density composites when charred, experienced cracking to varying degrees. Furthermore, some of the lowest-density moldings for the various materials experienced spallation. For these materials the assumption that oxidation is the only surface removal mechanism is violated. However, since a honeycomb matrix is commonly used to improve the physical integrity of the char of ablation materials, a model (Table III) of the material that contained a 3.5-lb/ft^3 phenolic-glass honeycomb matrix was tested.

The ablative effectiveness E of the honeycomb-supported material was equivalent (Table III) to that of the same density material without the honeycomb. Furthermore, the physical appearance and integrity of the char were improved significantly (Fig. 11) as evidenced by no spalling and less surface recession.

Material performance for various test conditions. After completion of the tests to determine the effect of density and composition variations, one ablation material was selected (30 per cent phenolic, 10 per cent nylon, and 60 per cent phenolic Microballoons) for which

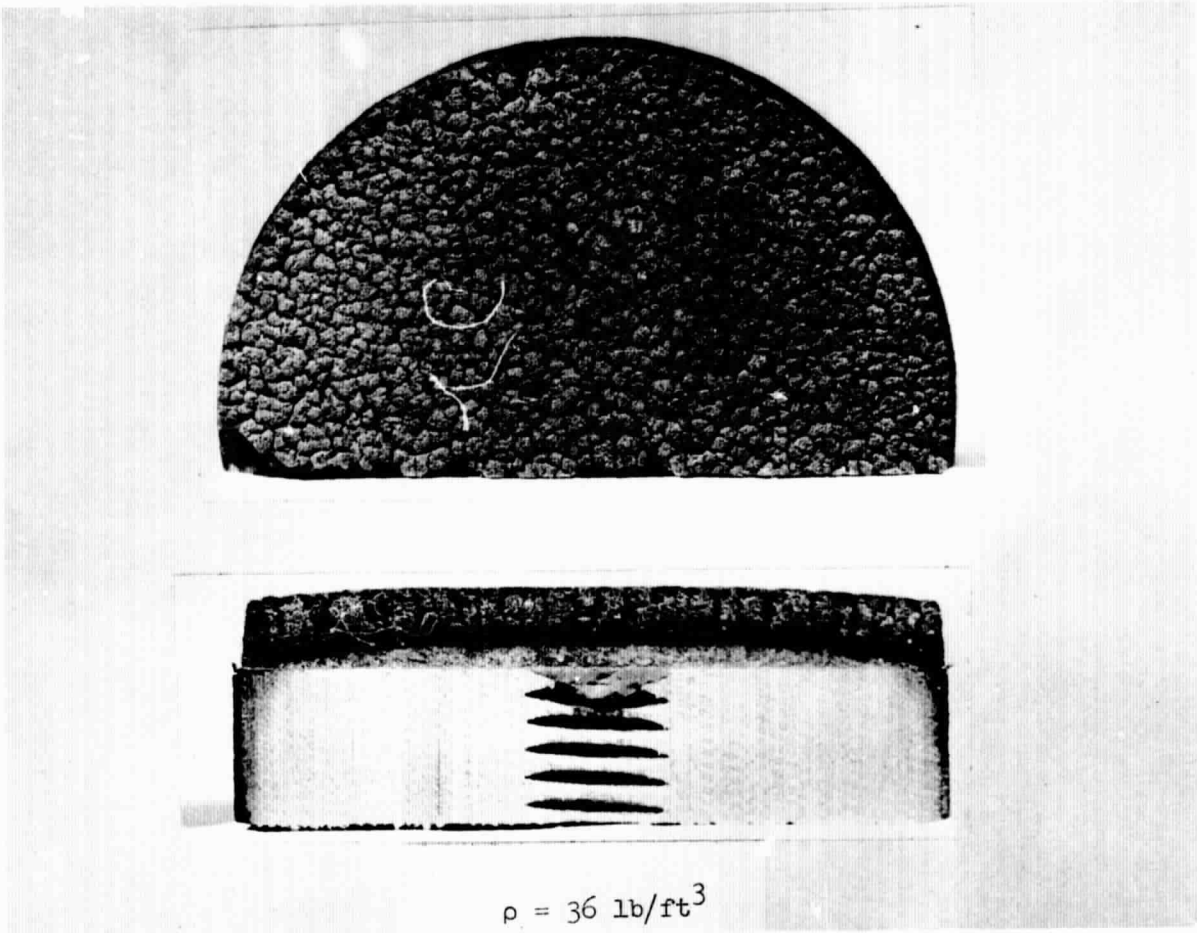

Figure 10.- Surface and cross-section views of 25 per cent phenolic, 40 per cent nylon, and 35 per cent Microballoons after testing.

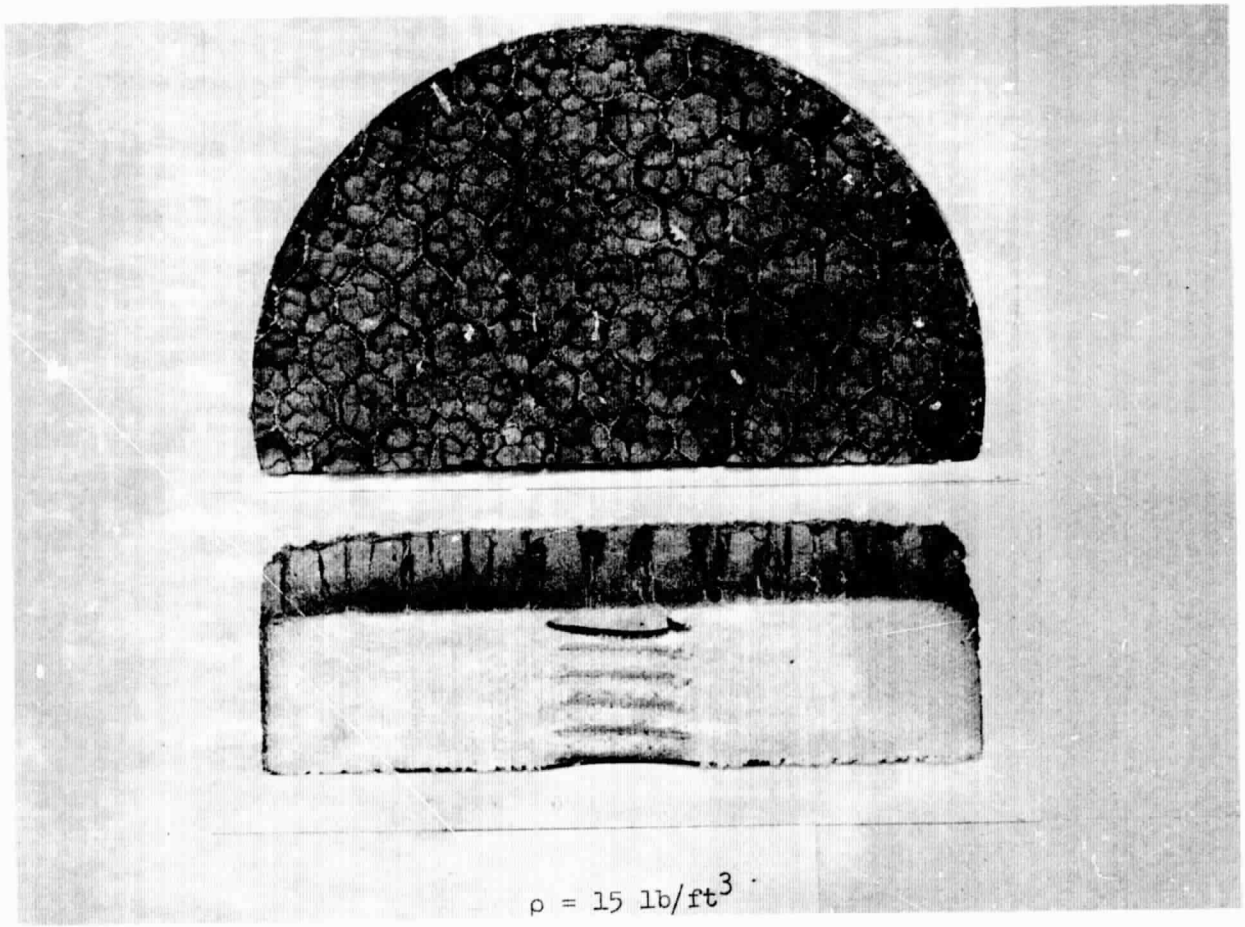

Figure 11.- Surface and cross-section views of 30 per cent phenolic, 10 per cent nylon, and 60 per cent Microballoons in a 3.5-lb/ft^3 phenolic-glass honeycomb after testing.

performance was to be determined at various test conditions. The material, including the honeycomb matrix, had a nominal density of 14 lb/ft^3. The honeycomb used was a phenolic-glass honeycomb having a density of 2.6 lb/ft^3. The results of the tests conducted for this material and the test conditions are listed in Table IV.

The back surface temperature histories for four ablation models that were tested at various stagnation pressures, enthalpies, and heating rates are shown in Figure 12. As would be expected, the time for a given temperature rise decreases with increasing heating rate. The time required for a temperature rise of 300° F is used in computing the ablative effectiveness of a material.

The performance of the 30-10-60 material on an ablative effectiveness basis is shown in Figure 13, where the effectiveness is plotted as a function of cold-wall heating rate for various stagnation pressures and test stream oxygen concentrations. The two effectiveness curves are least-squares fits for the data points resulting from the tests made in test streams containing 3 and 23 per cent oxygen concentrations. The trend is for the effectiveness to increase with increasing heating rate; however, this effect is strongly dependent on the test stream oxygen concentration. Furthermore, the effectiveness of this material does not appear to be dependent on the stagnation pressures for which it was subjected (0.05 to 0.20 atm). In examining the effectiveness data shown in Figure 13 along with the test-stream enthalpy and oxygen concentrations in Table IV, it becomes apparent that the performance of the 30-10-60 material is extremely sensitive to heating rate, oxygen concentration, and enthalpy test parameters.

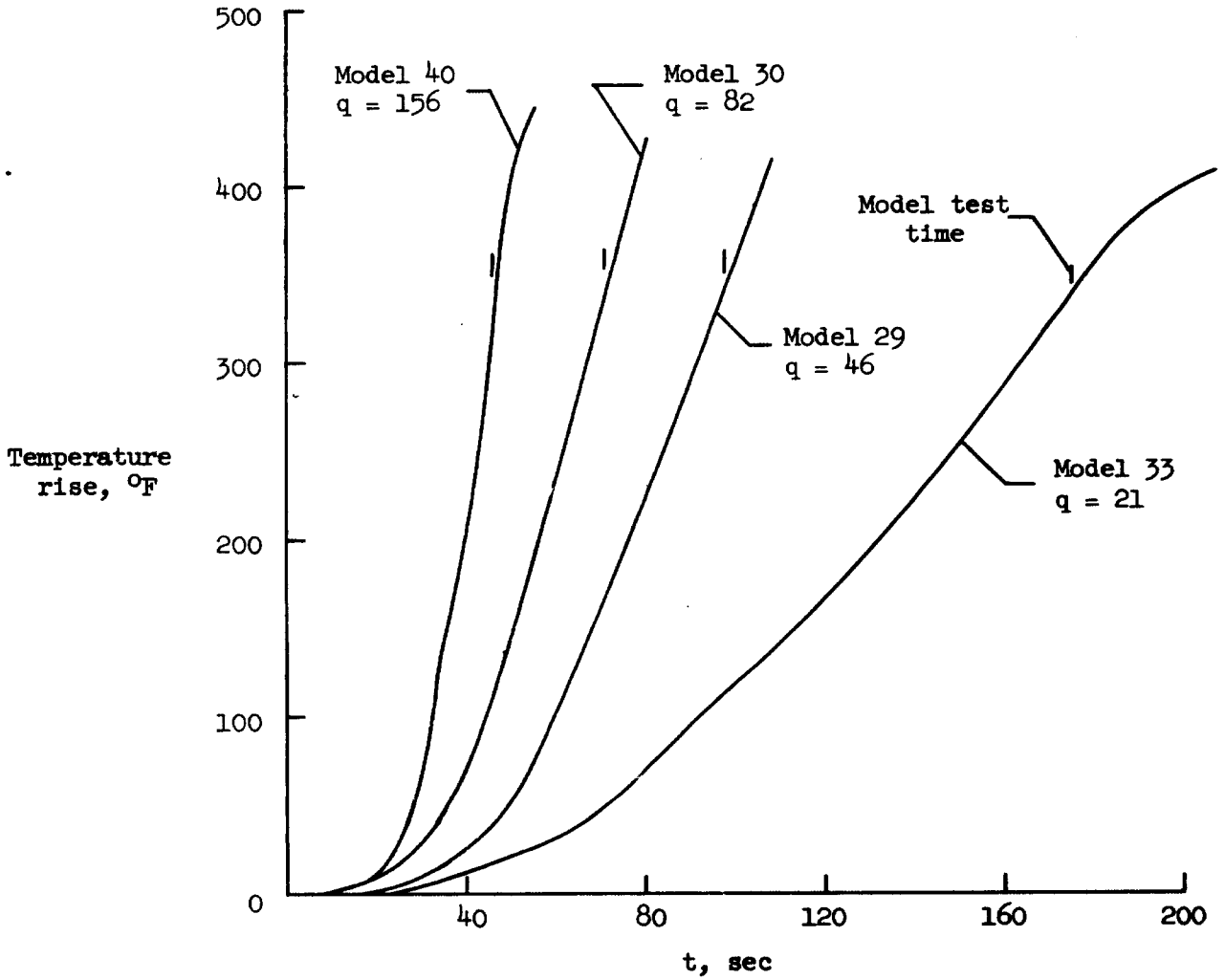

Figure 12.- Representative back surface temperature histories.

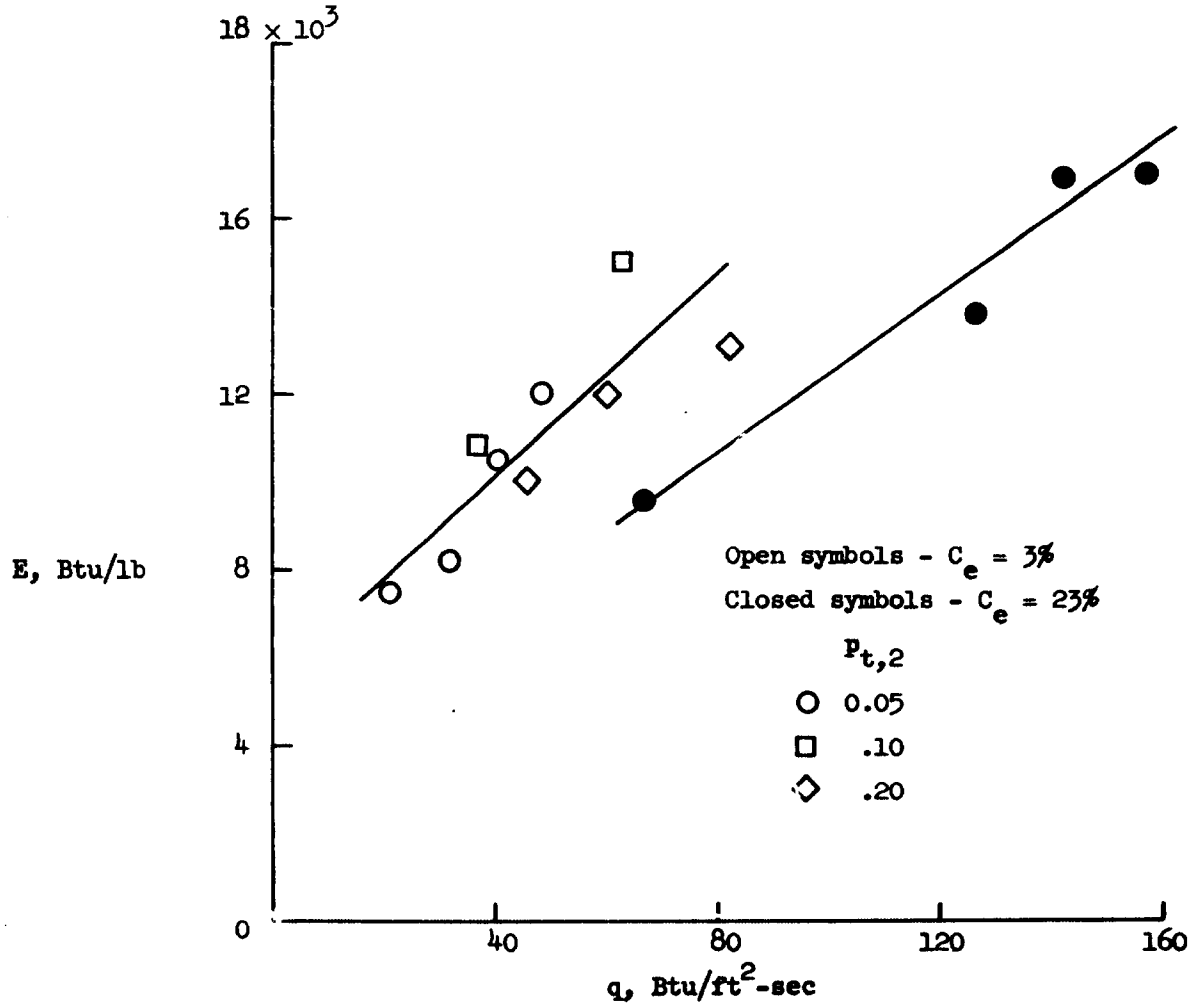

Figure 13.- Ablative effectiveness of a 30 per cent phenolic, 10 per cent nylon, and 60 per cent Microballoons ablator as a function of heating rate (ρ = 14 lb/ft^3).

However, this sensitivity is not unique to the 14-lb/ft^3 phenolic-nylon ablator because similar results have been obtained from studies (Ref. 10) made with higher-density phenolic-nylon ablators.

The effects of the test environment are also evident when examining the appearance of the charred models (Fig. 14). In general, the physical integrity of the char was good in that it remained in place during the test for all test conditions. The most obvious effect on the char was the test stream oxygen concentration. For the models tested in a 3-per cent-oxygen test stream, the surface recession was negligible; however, for the models tested in a 23-per cent-oxygen test stream, the surface recession was from 0.20 to 0.25 inch.

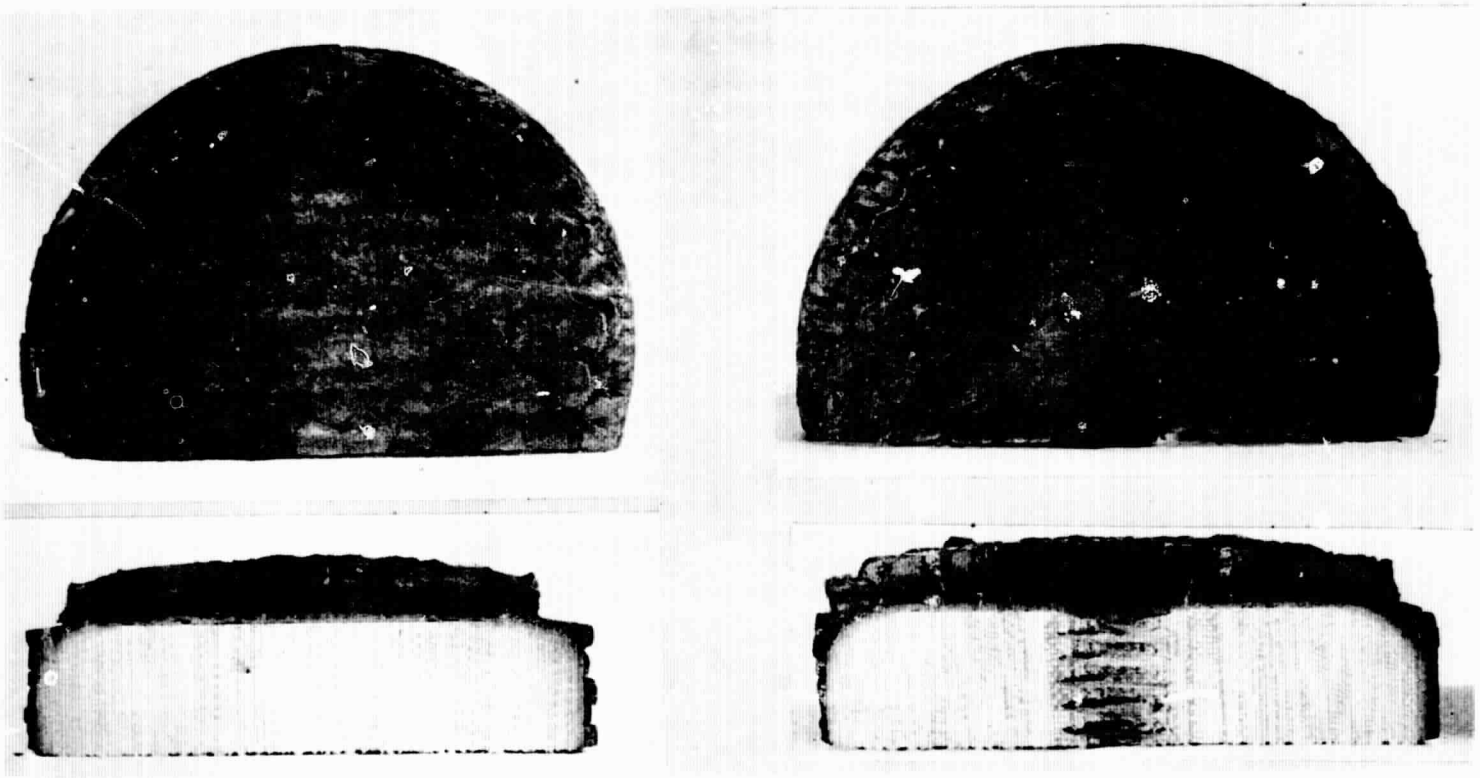

(a) Model 28; $q = 60$, $C_e = 3\%$, $h_e = 2300$.

(b) Model 29; $q = 46$, $C_e = 3\%$, $h_e = 1800$.

Figure 14.- Surface and cross-section views of 30 per cent phenolic, 10 per cent nylon, and 60 per cent Microballoons after testing.

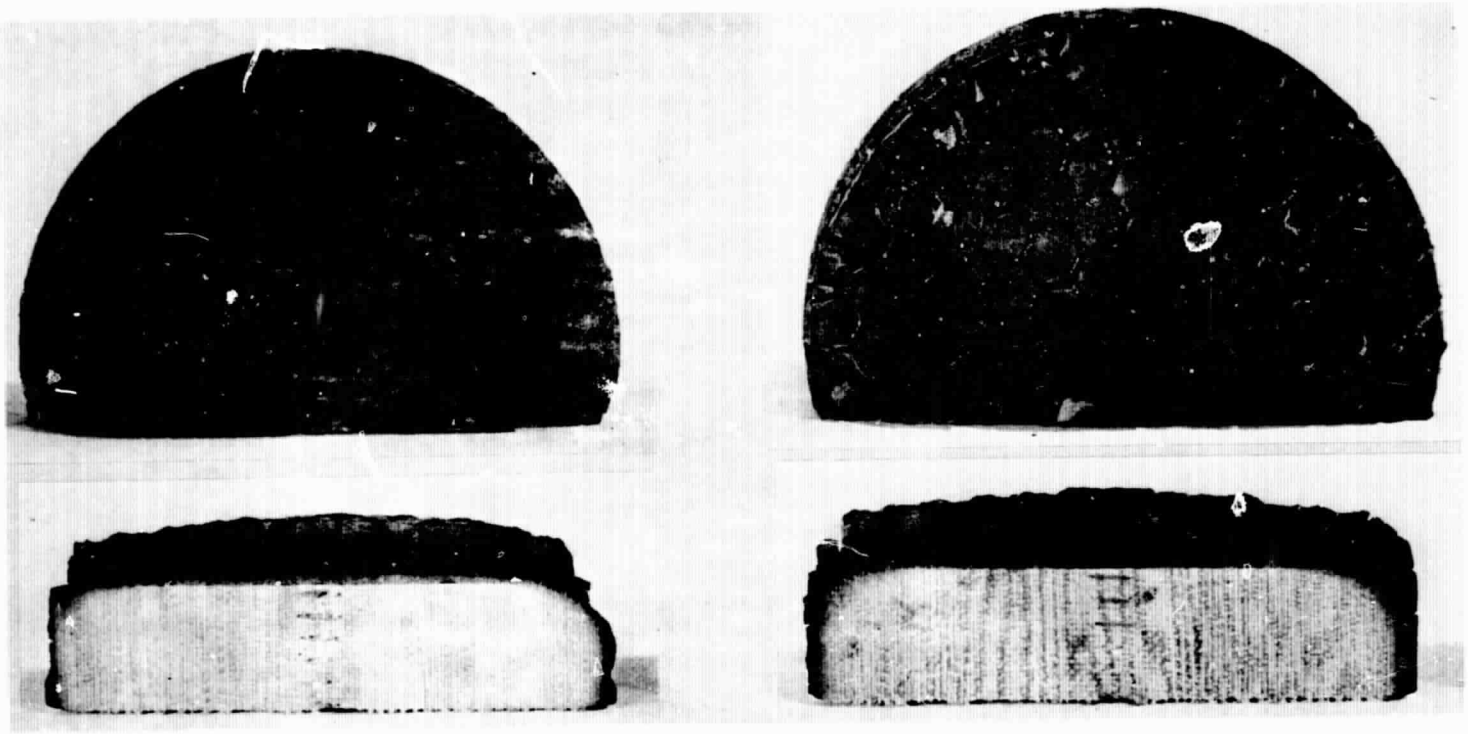

(c) Model 30; $q = 82$, $C_e = 3\%$, $h_e = 3100$.

(d) Model 31; $q = 37$, $C_e = 3\%$, $h_e = 1900$.

Figure 14.- Continued.

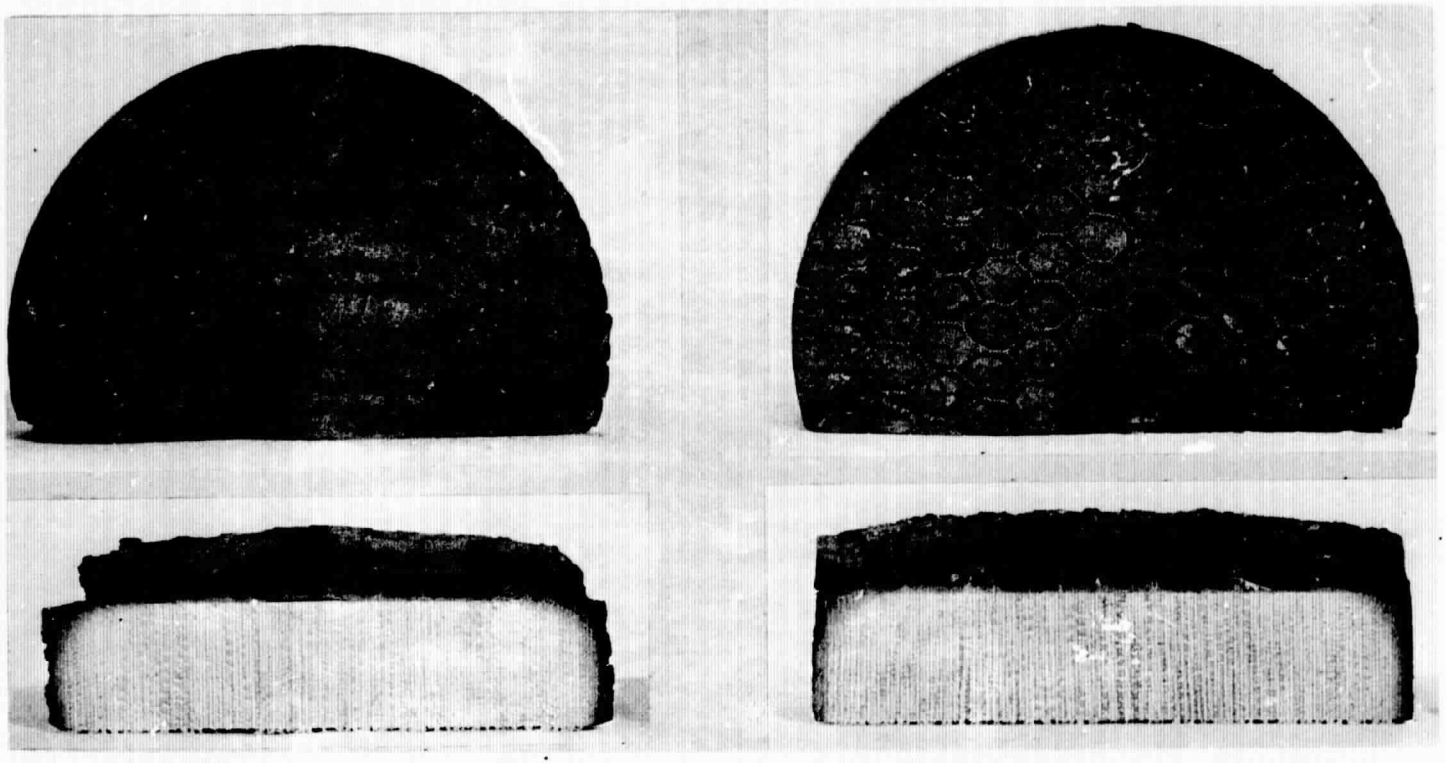

(e) Model 32; q = 62,
C_e = 3%, h_e = 3300.

(f) Model 33; q = 21,
C_e = 3%, h_e = 1600.

Figure 14.- Continued.

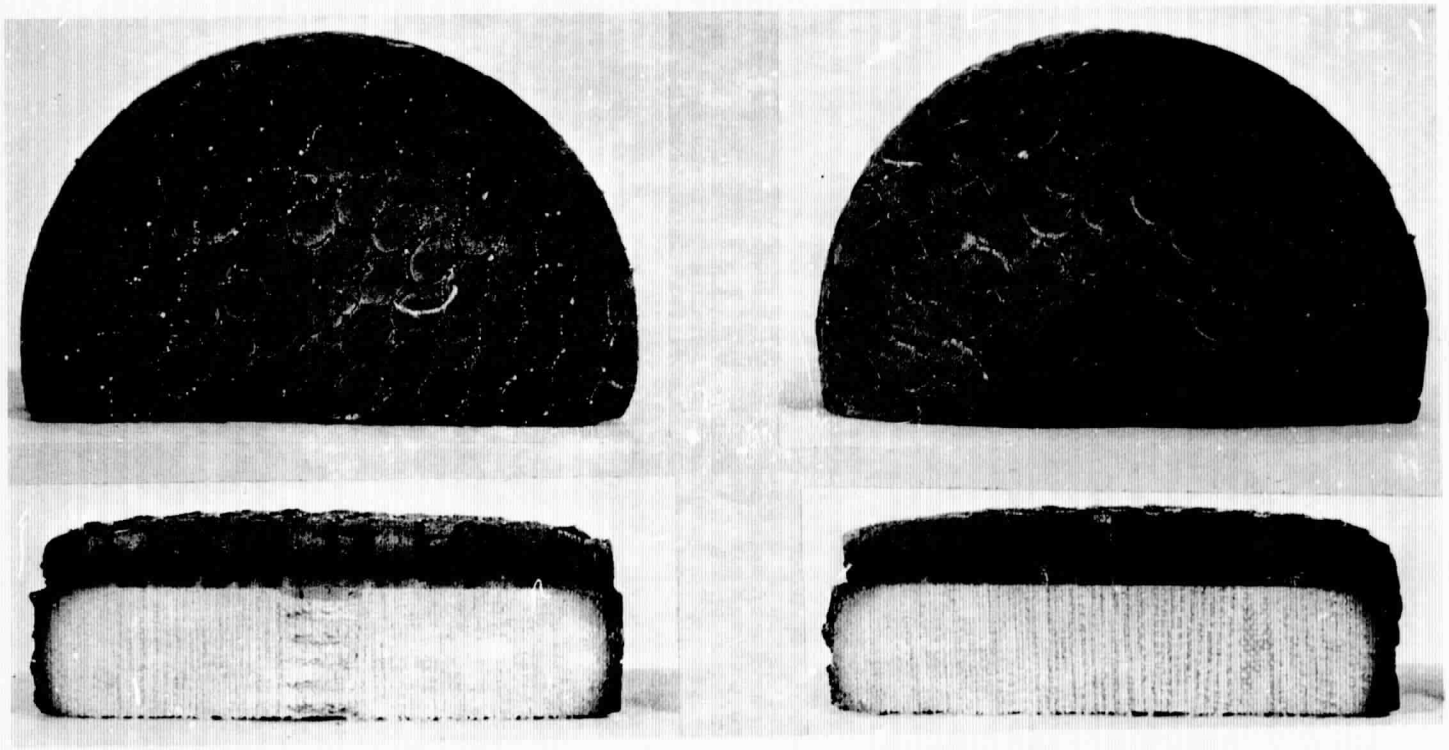

(g) Model 34; q = 32, C_e = 3%, h_e = 2300.

(h) Model 35; q = 40, C_e = 3%, h_e = 3000.

Figure 14.- Continued.

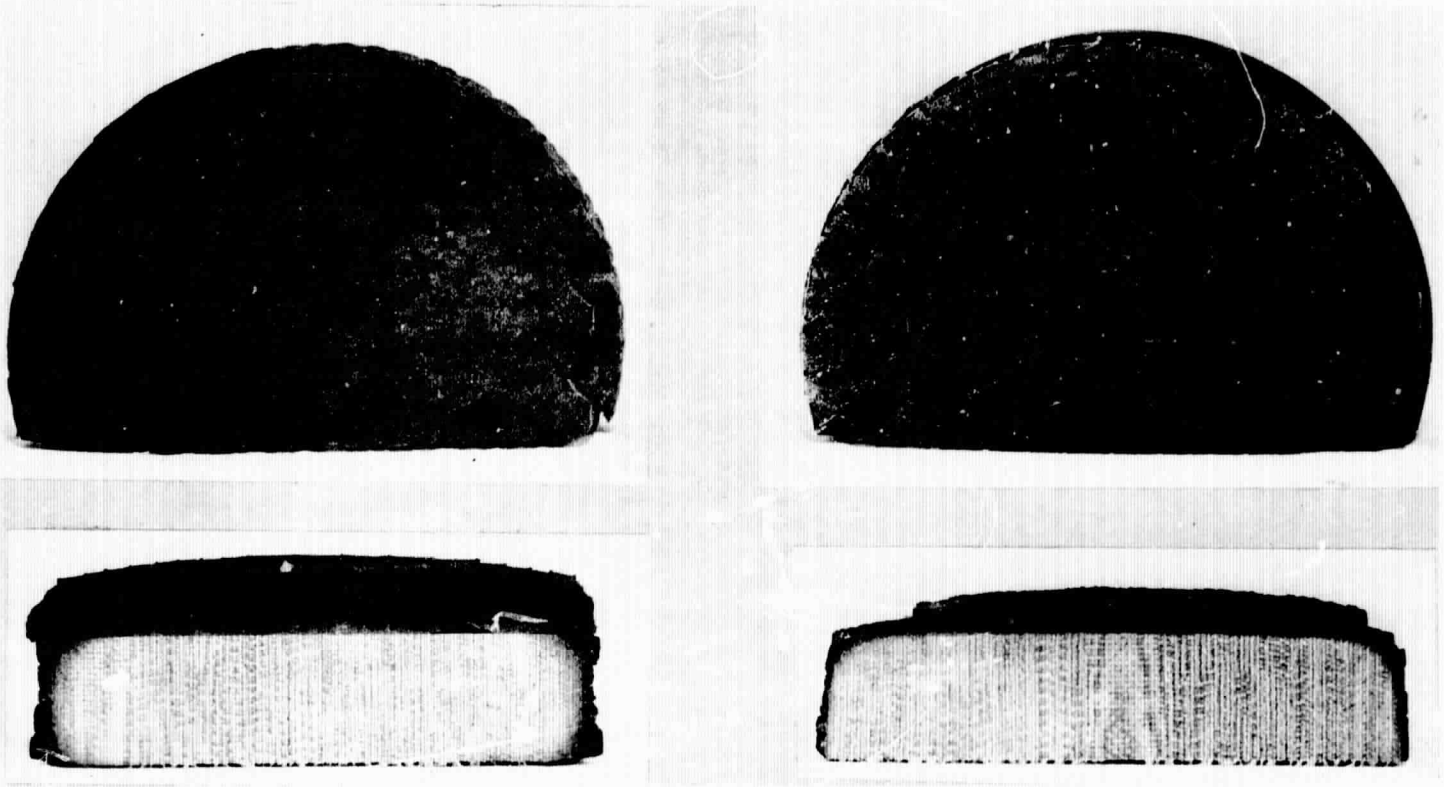

(i) Model 36; $q = 48$, $C_e = 3\%$, $h_e = 3600$.

(j) Model 37; $q = 66$, $C_e = 23\%$, $h_e = 5000$.

Figure 14.- Continued.

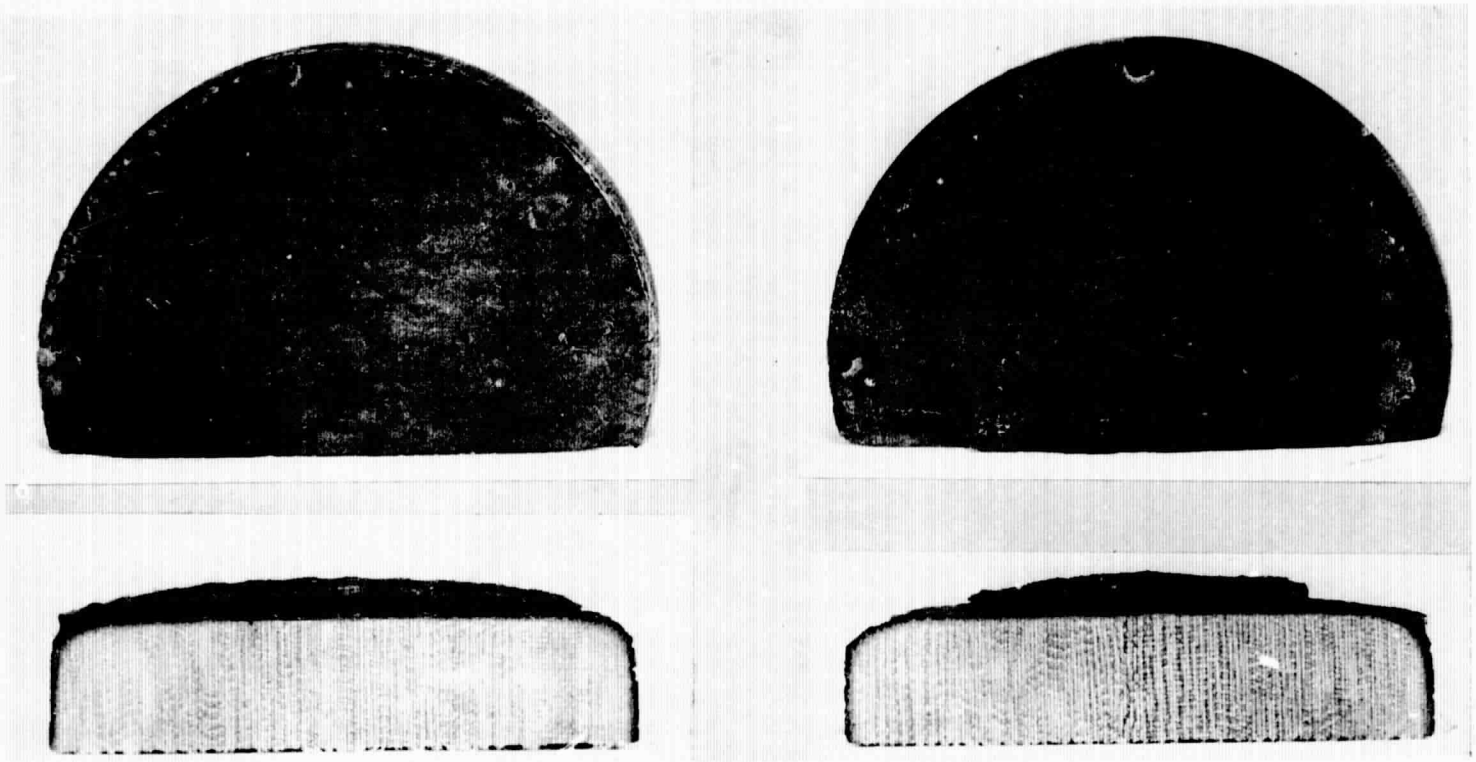

(k) Model 38; q = 125, C_e = 23%, h_e = 8800.

(l) Model 39; q = 141, C_e = 23%, h_e = 9500.

Figure 14.- Continued.

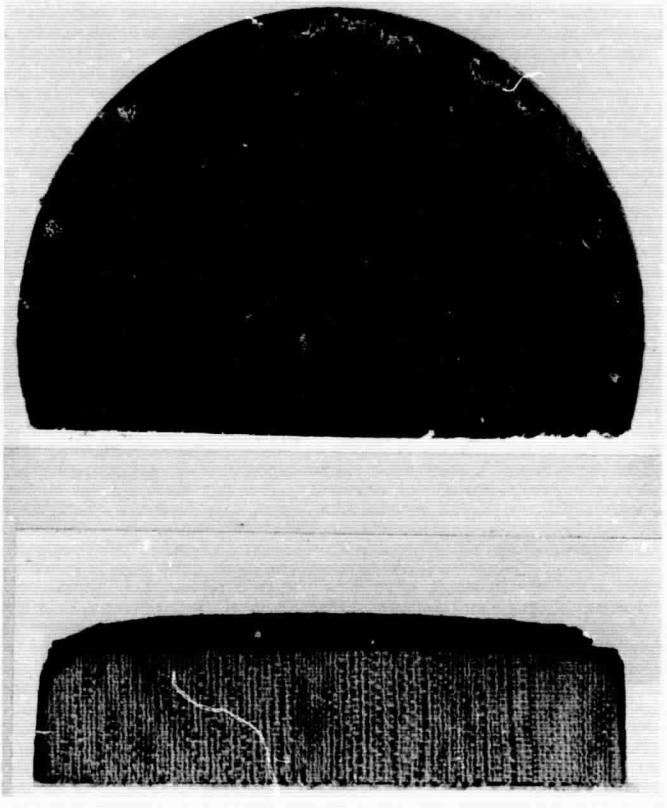

(m) Model 40; q= 156,
C_e = 23%, h_e = 10000.

Figure 14.- Concluded.

CHAPTER V

APPLICATION ANALYSIS

As part of the low-density phenolic-nylon ablator study, an application analysis was made to determine the ablative heat shield weight requirements of the windward portion of one-half of a 13° half-angle cone with a spherically blunt tip using 14- and 36-lb/ft^3 phenolic-nylon ablators. The heat shield weight requirements were determined for the blunted cone at angles of attack ranging from approximately $(L/D)_{max}$ to $(C_L)_{max}$.

Entry Body Configuration Considered

Since local heating effects were to be considered in determining the heat shield weight requirements, an entry body configuration was selected on a basis of amenability to calculation of local heating and aerodynamic behavior. The selection was also made with the intention of selecting a configuration that could be considered a reasonable approximation of a manned lifting-body entry vehicle. The configuration selected is shown in Figure 15. As for the geometric characteristics of the body, it is one-half of a 13° half-angle cone with a spherically blunt tip having a 1.4-ft radius. The body length is 28 ft. The planform loading used in this analysis was 50 lb/ft^2, resulting in a total vehicle weight of 12,142 lbs.

With regards to the extent by which the selected body configuration approximates some of the present manned lifting-body entry vehicles, it is noted that the Ames M-2 Lifting Body was evolved from

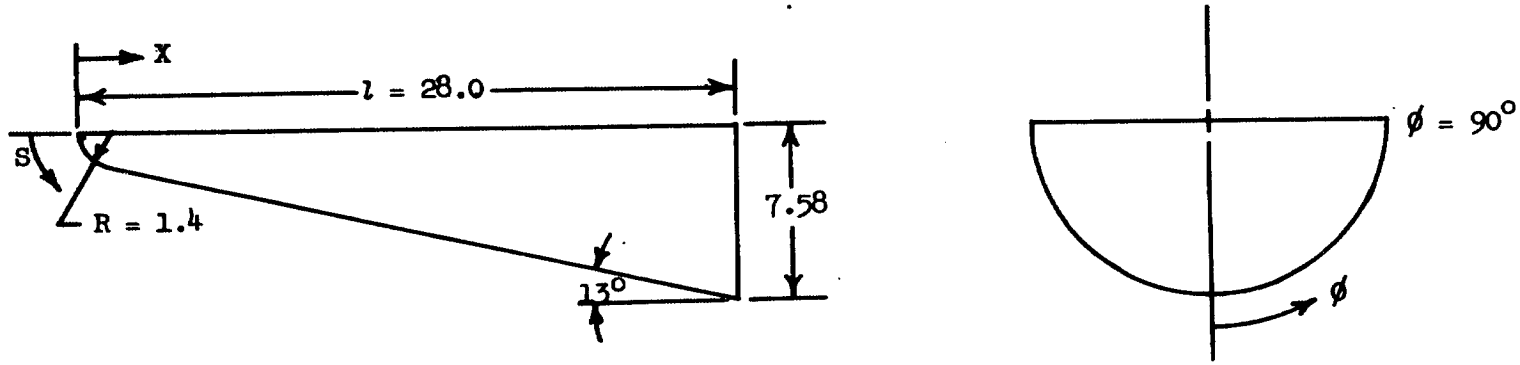

Figure 15.- Entry body configuration for which ablative weight requirements were determined.

one-half of a 15° half-angle cone with a spherically blunt tip (Ref. 18). However, the blunt half cone was extensively boattailed and twin vertical surfaces and a canopy were added. Consequently, the aerodynamic characteristics as well as the ablative requirements would be different from that of the body configuration selected.

Aerodynamic Characteristics

The aerodynamic force coefficients, lift and drag, were calculated for the blunted half cone from Newtonian theory from Reference 19. The results of these calculations are shown in Figure 16 where L/D and C_L are plotted as a function of angle of attack. The angle of attack variation considered in this analysis was 1° to 40°, providing aerodynamic force coefficients from those for approximately $(L/D)_{max}$ to those for $(C_L)_{max}$. Since the vehicle was always at an angle of attack, the top surface of the vehicle was shielded from the flow and therefore did not contribute to the aerodynamic forces.

Trajectories

Four trajectories describing the flight environment for the blunt half cone vehicle at L/D values of 0.67, 0.93, 1.49, and 2.1 were generated on a high speed digital computer program. The L/D values correspond respectively to angles of attack of 40°, 30°, 15°, and 1°. For the constant L/D trajectories considered in this analysis, entry was assumed to start at an altitude of 400,000 ft., at an inertial flight path angle of -1.5°, and at an inertial velocity of 26,000 ft/sec. A planform wing loading of 50 lb/ft^2 was used throughout the calculations.

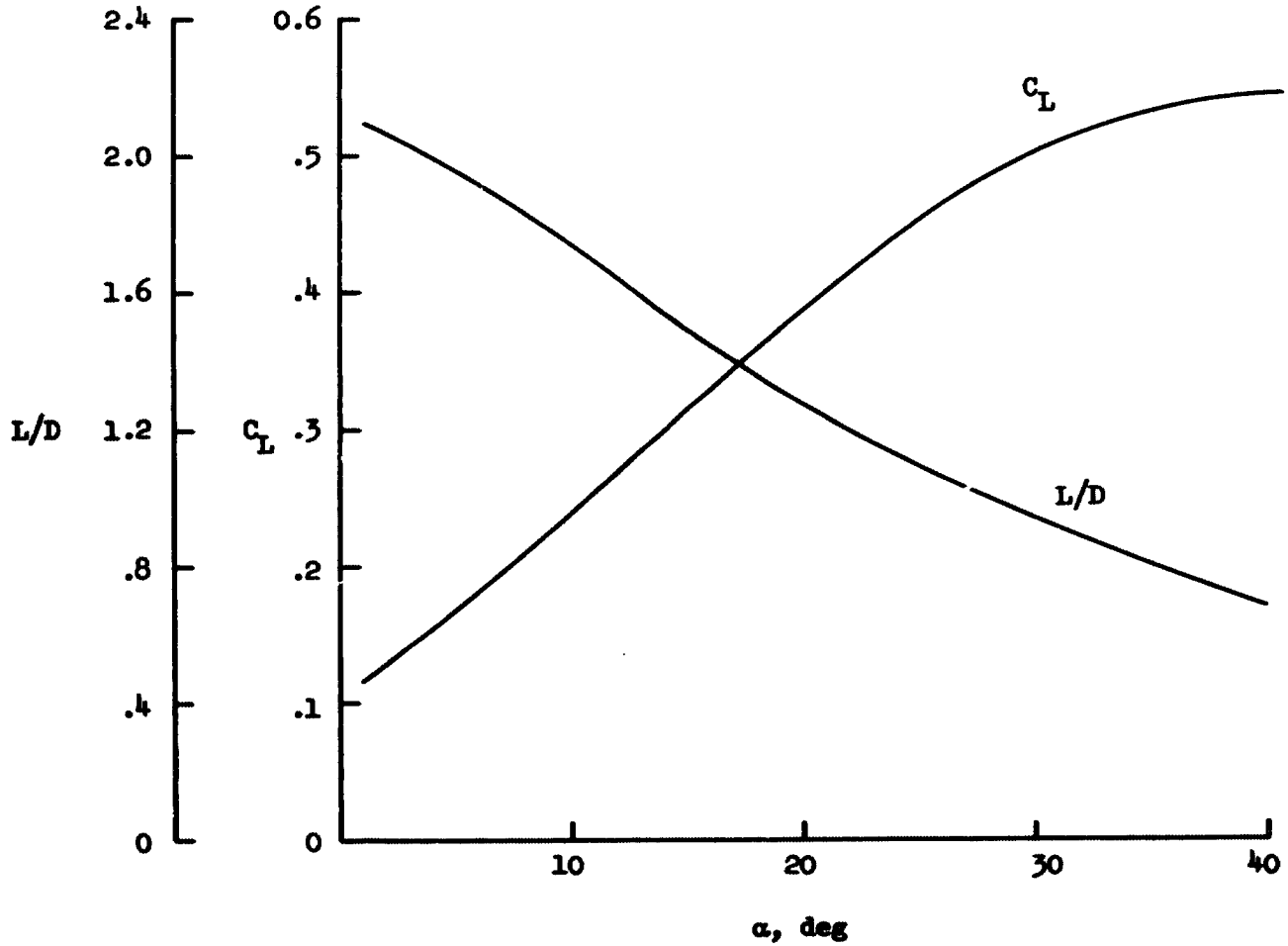

Figure 16.- Aerodynamic characteristics of 13° blunted half cone.

The entry trajectories along with the environmental parameters for angle of attacks of 1°, 15°, 30°, and 40° are illustrated in Figures 17 and 18. The entry trajectories were constrained so that when the vehicle reached a 0° flight path angle (pull out), the vehicle was roll modulated about the velocity vector to maintain constant altitude. When the vehicle was rolled back to 0°, equilibrium glide at the specified value of L/D was flown to touchdown.

In examining Figure 17, it is seen that as the angle of attack increases from approximately $(L/D)_{max}$ to $(C_L)_{max}$, entry is made at higher altitudes. The effects of angle of attack variations are also evident when examining Figure 18 where the environmental parameters are shown to be a strong function of the entry attitude.

Heat Transfer Distributions

When the aerodynamic heating to entry vehicles is analyzed, no one point or line on the vehicle can possibly show, in general, a variation of entry heating rate with angle of attack that is typical of the entire vehicle (Ref. 6). Consequently, either theoretical methods or experimental data must be available that allow the determination of the heating over that portion of the vehicle being analyzed.

For the present analysis, theoretical and empirical methods were used to determine the stagnation-point heating on the spherical nose and the local heating on the afterbody as some fraction of the stagnation heating. The laminar stagnation heating correlation of Reference 20, which contains the correction for dissociation and the ratio of external

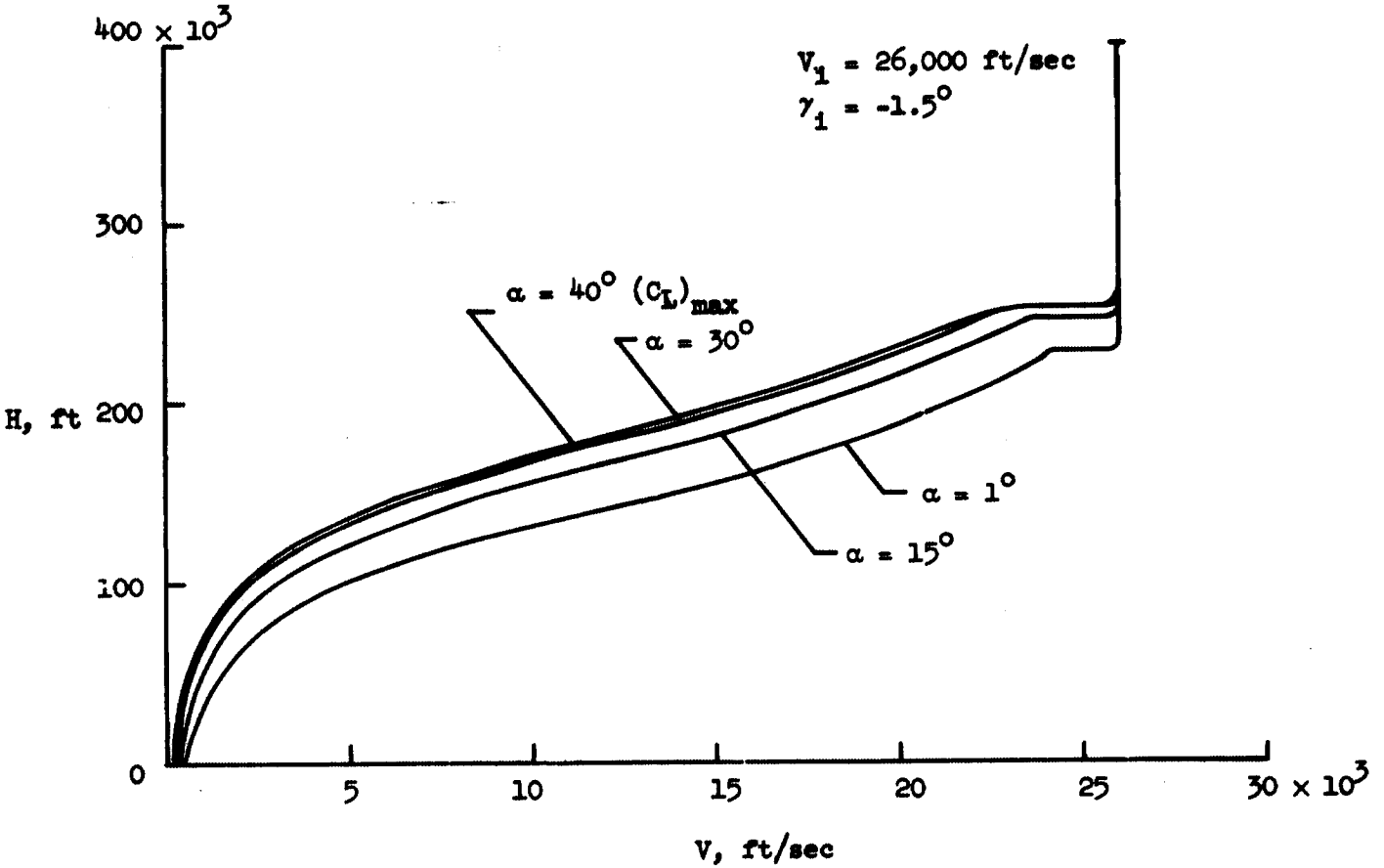

Figure 17.- Entry trajectories for 13° blunted half cone.

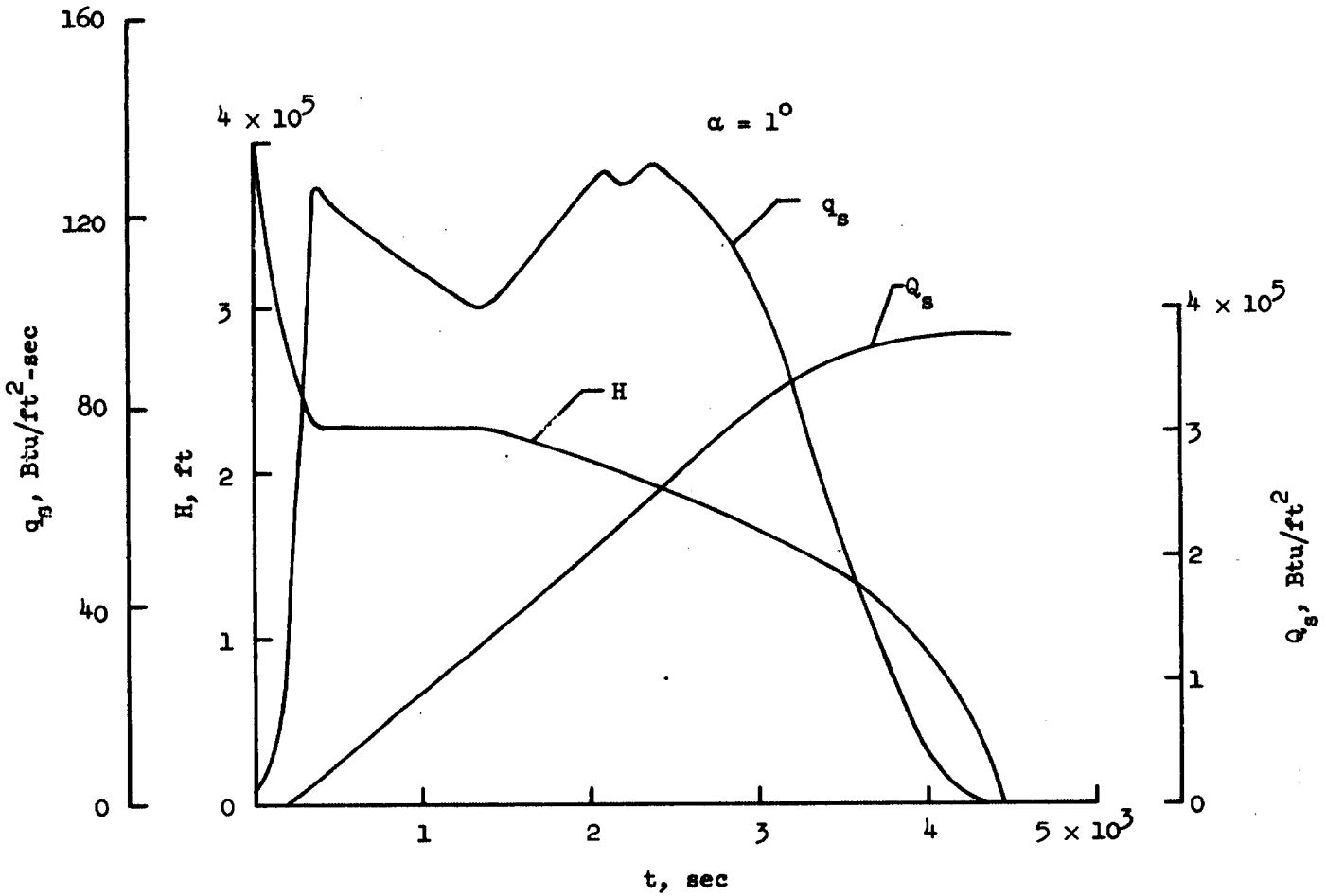

(a) Values of q_s, Q_s, and H for $\alpha = 1^\circ$.

Figure 18.- Trajectory environmental parameters for 13° blunted half cone.

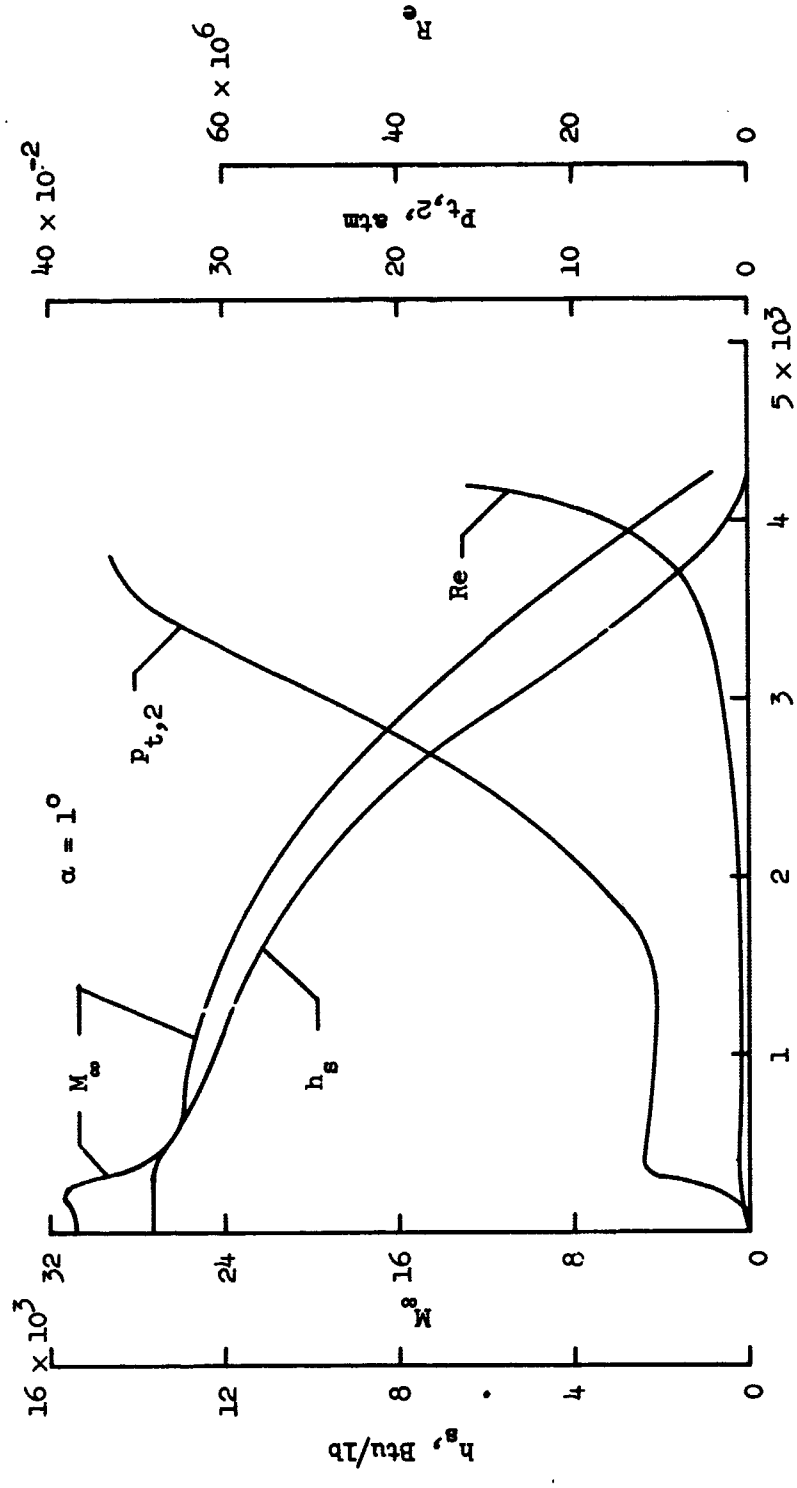

(b) Values of h_s, $p_{t,2}$, M_∞, and Re for $\alpha = 1^\circ$.

Figure 18.- Continued.

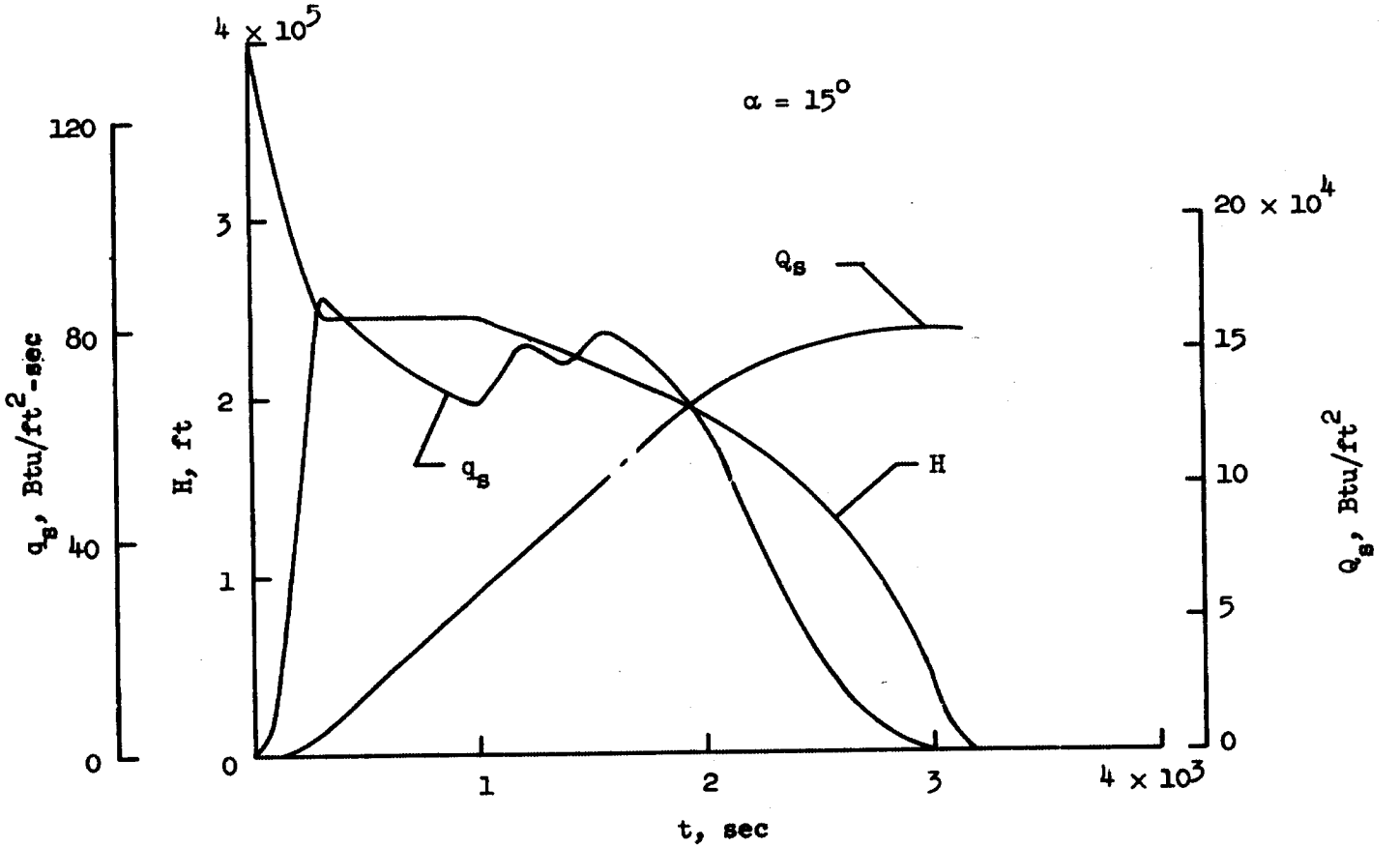

(c) Values of q_s, Q_s, and H for $\alpha = 15^{\circ}$.

Figure 18.- Continued.

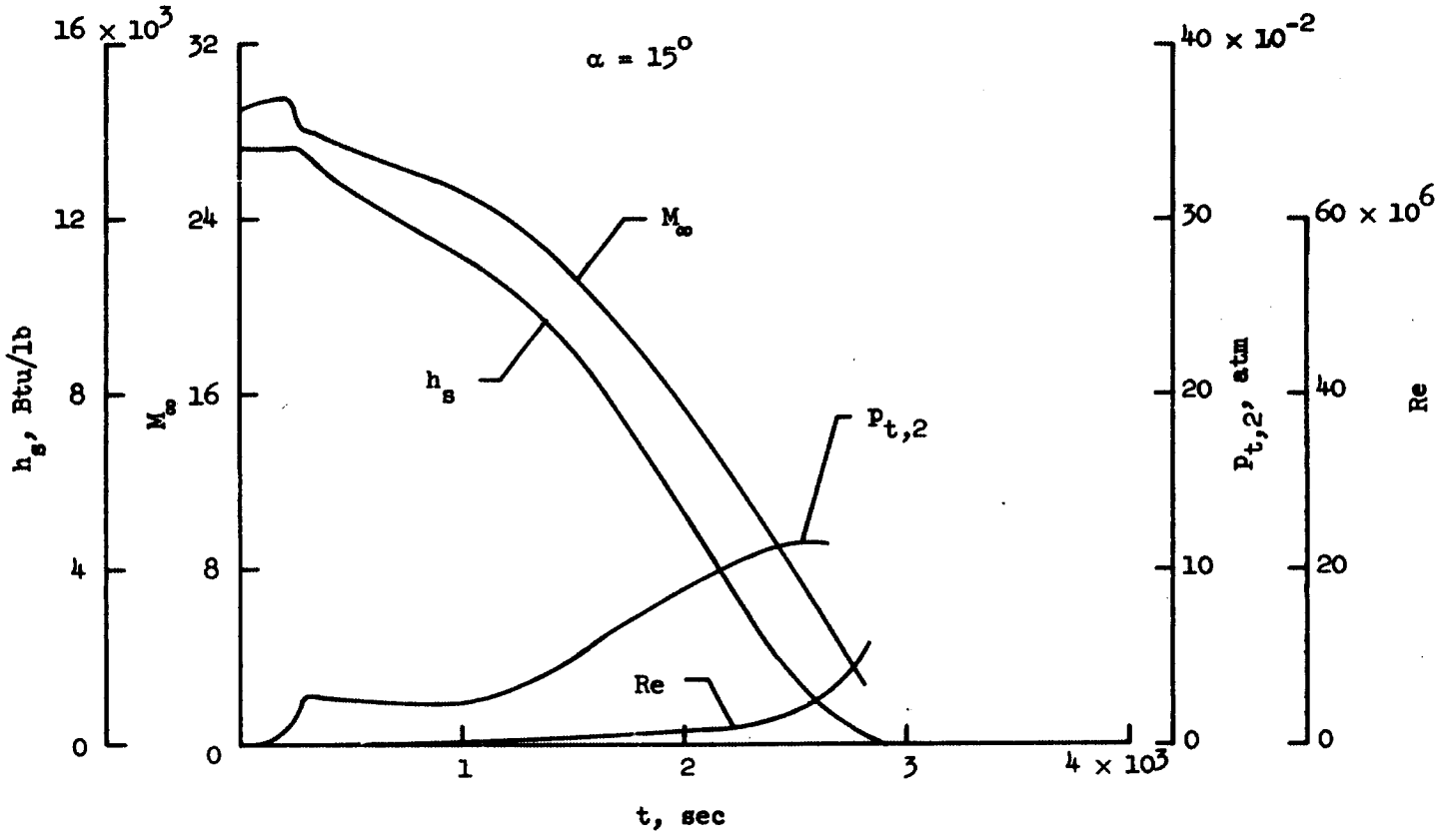

(d) Values of h_s, $p_{t,2}$, M_∞, and Re for $\alpha = 15^\circ$.

Figure 18.- Continued.

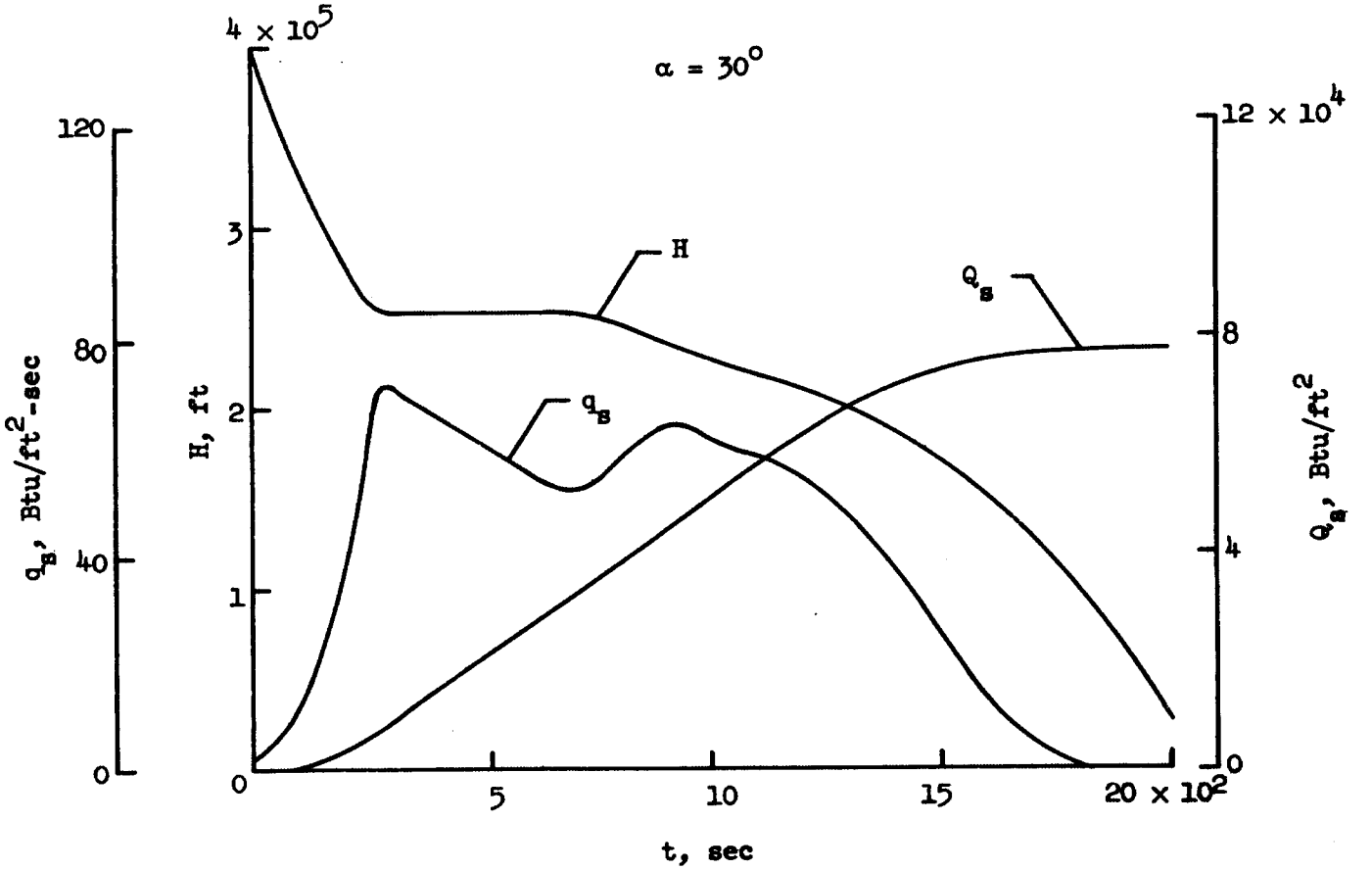

(e) Values of q_s, Q_s, and H for $\alpha = 30^\circ$.

Figure 18.- Continued.

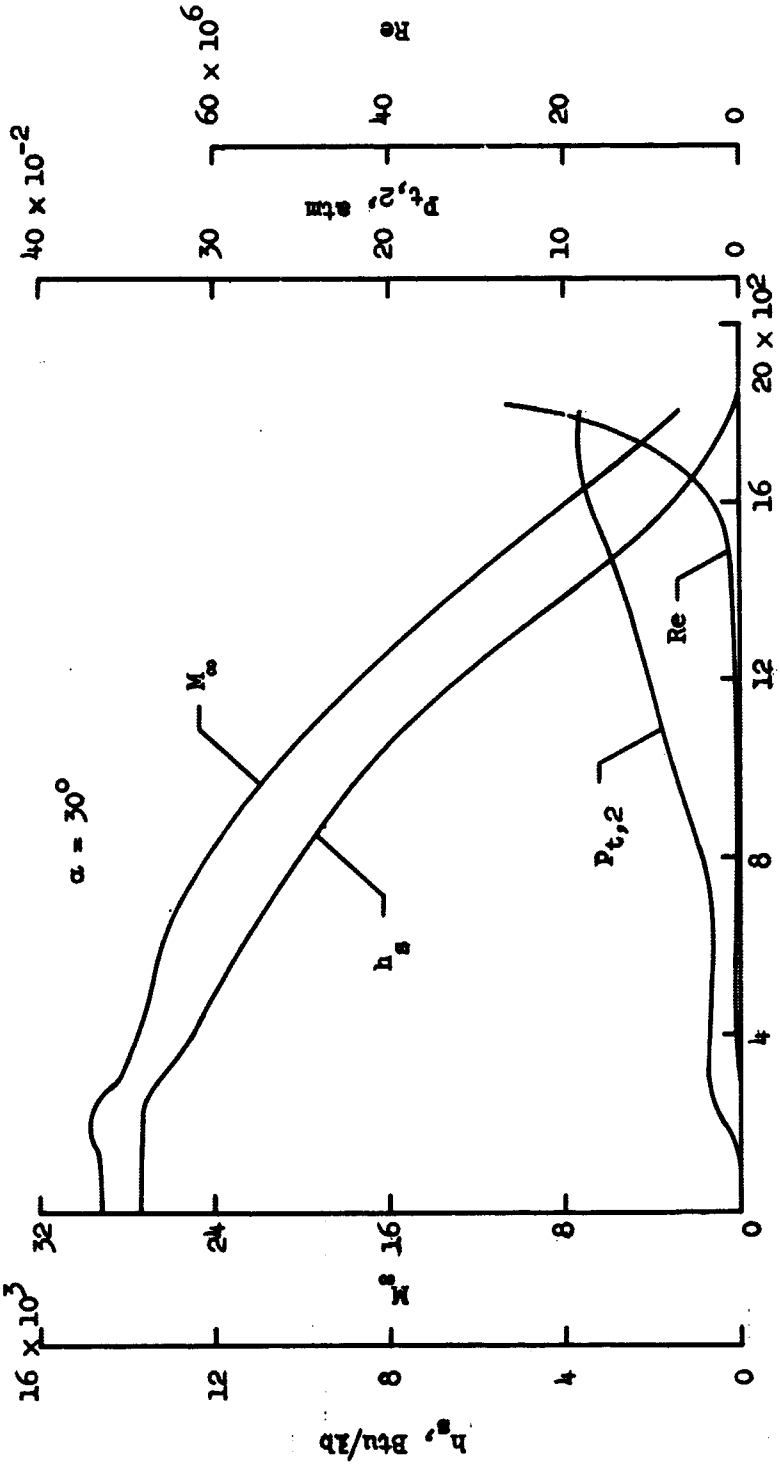

(f) Values of h_s, $P_{t,2}$, M_∞, and Re for $\alpha = 30^\circ$.

Figure 18.- Continued.

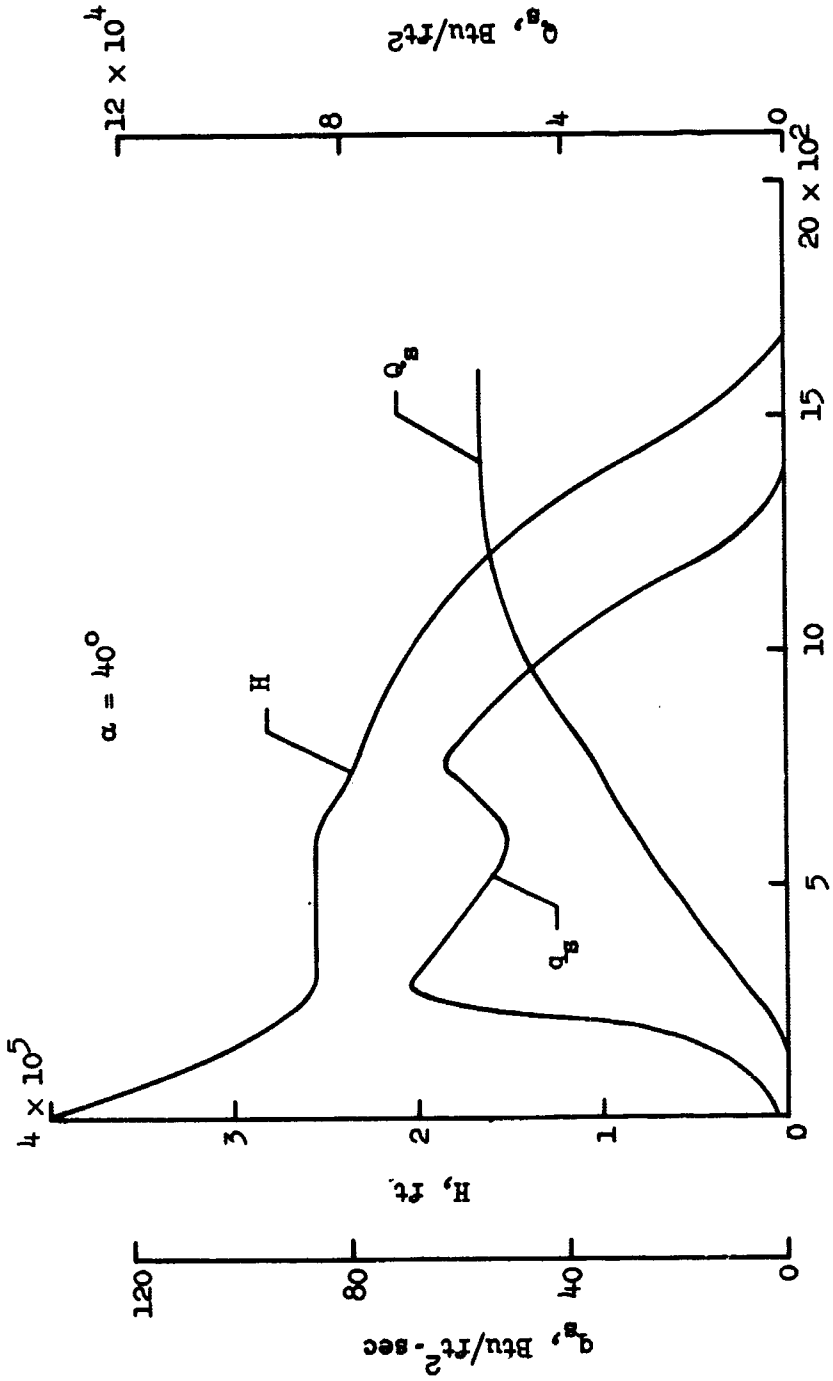

(g) Values of q_s, Q_s, and H for $\alpha = 40^o$.

Figure 18.- Continued.

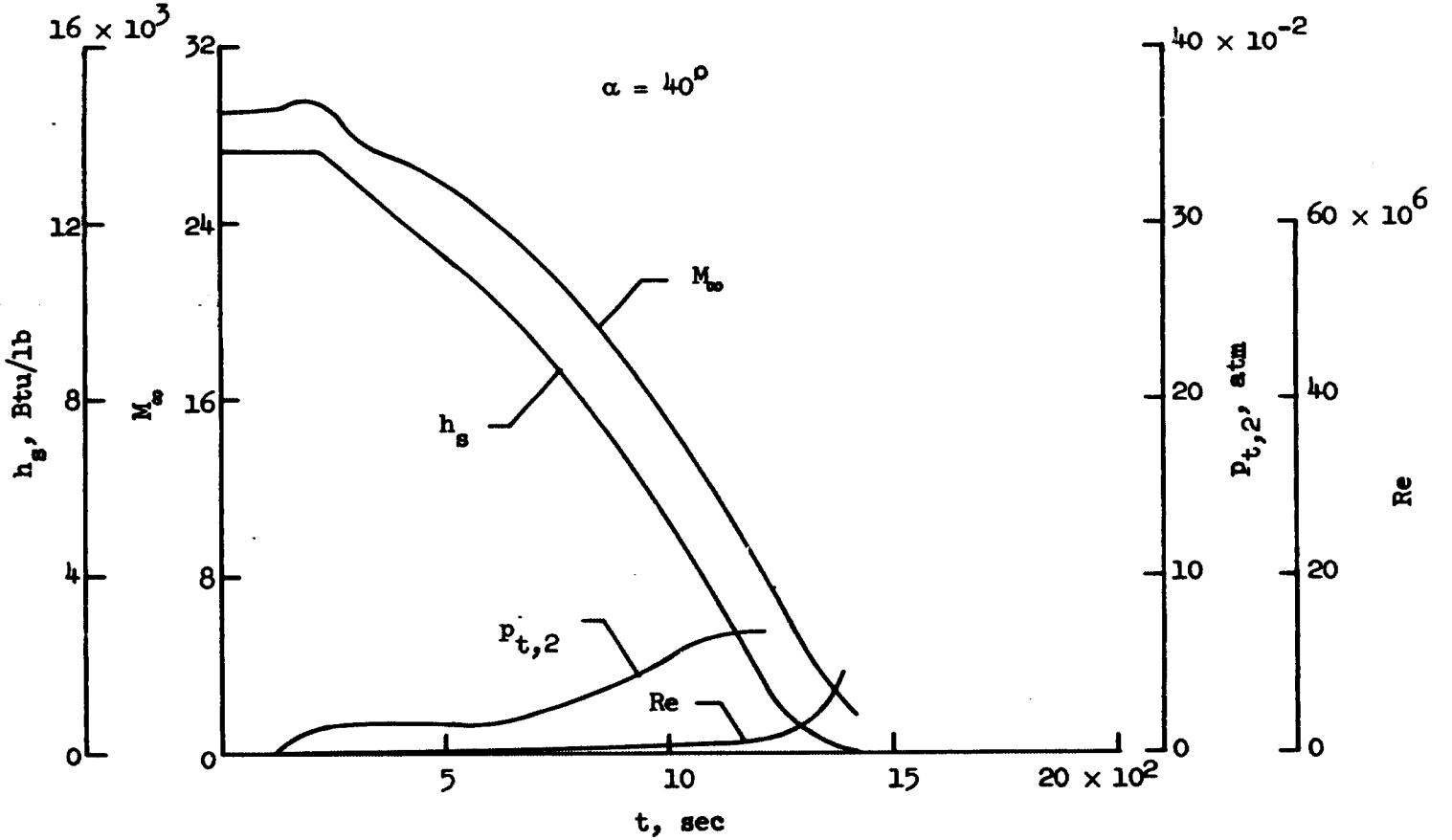

(h) Values of h_s, $p_{t,2}$, M_∞, and Re for $\alpha = 40^{\circ}$.

Figure 18.- Concluded.

enthalpy to wall enthalpy, was used in determining the stagnation heating rates shown in Figure 18. The stagnation heating correlation is given as:

$$q_s = \frac{17{,}800\ \sqrt{\rho}\ V^{3.15}}{\sqrt{R}} \qquad (21)$$

where ρ is the atmospheric density, V the vehicle velocity, and R the nose radius.

The ratio of the local to the stagnation heating was determined by using a relatively simple method (Ref. 21) for computing the laminar heating over hypersonic vehicles at an angle of attack and with a highly cooled surface. This method uses the "axisymmetric analogue" (Refs. 22 and 23) for transforming the general three-dimensional boundary-layer equations into the same form as those for an axisymmetric body at zero angle of attack when the coordinate directions are taken along and perpendicular to the inviscid streamlines and when the cross flow (i.e., the component of boundary layer flow normal to an inviscid streamline and along the body surface) is assumed small. The "axisymmetric analogue" transformation makes it possible to calculate the heating rate along a streamline by any method applicable to a body of revolution at zero angle of attack providing the pressure distribution and coordinate scale factor are known along this streamline. For the calculations made herein, the pressure distribution was modified Newtonian and the laminar heating rates were determined by using the method of Lester Lees (Ref. 24).

The method used to determine the heating rate distributions has provided good results when compared with experimental heating distributions. As is shown in Reference 21, the predicted heating distributions to a blunted 25° half-angle cone at various angles of attack are usually within 10 per cent of the experimental values. Additional discussion of this method is found in Reference 21.

The calculated heating rate ratio q/q_s to the windward center line of the blunt half cone for angles of attack of 1°, 15°, 30°, and 40° is shown in Figure 19 and shows the extent by which the heating rate ratio increased with angle of attack for a given S/R station. Also, the circumferential heating rate ratio at S/R stations of 1.34 (tangent point) and 10 is shown in Figure 20 for each of the four angles of attack. The maximum stagnation-point heating rate as a function of angle of attack is shown in Figure 21. The heating rate to several S/R stations along the windward center line for the point of maximum heating on the trajectories are also shown in Figure 21. The effect of angle of attack on the lower-surface heating is reverse of that to the stagnation-point heating.

In addition to the maximum heating rates, the total heat loads must be considered in determining the heat shield requirements for an entry vehicle. The stagnation-point heat load along with the heat load to the windward center line at various S/R stations are shown as a function of angle of attack in Figure 22. The heat load parameter shows a different change with angle of attack than the heating rate parameter.

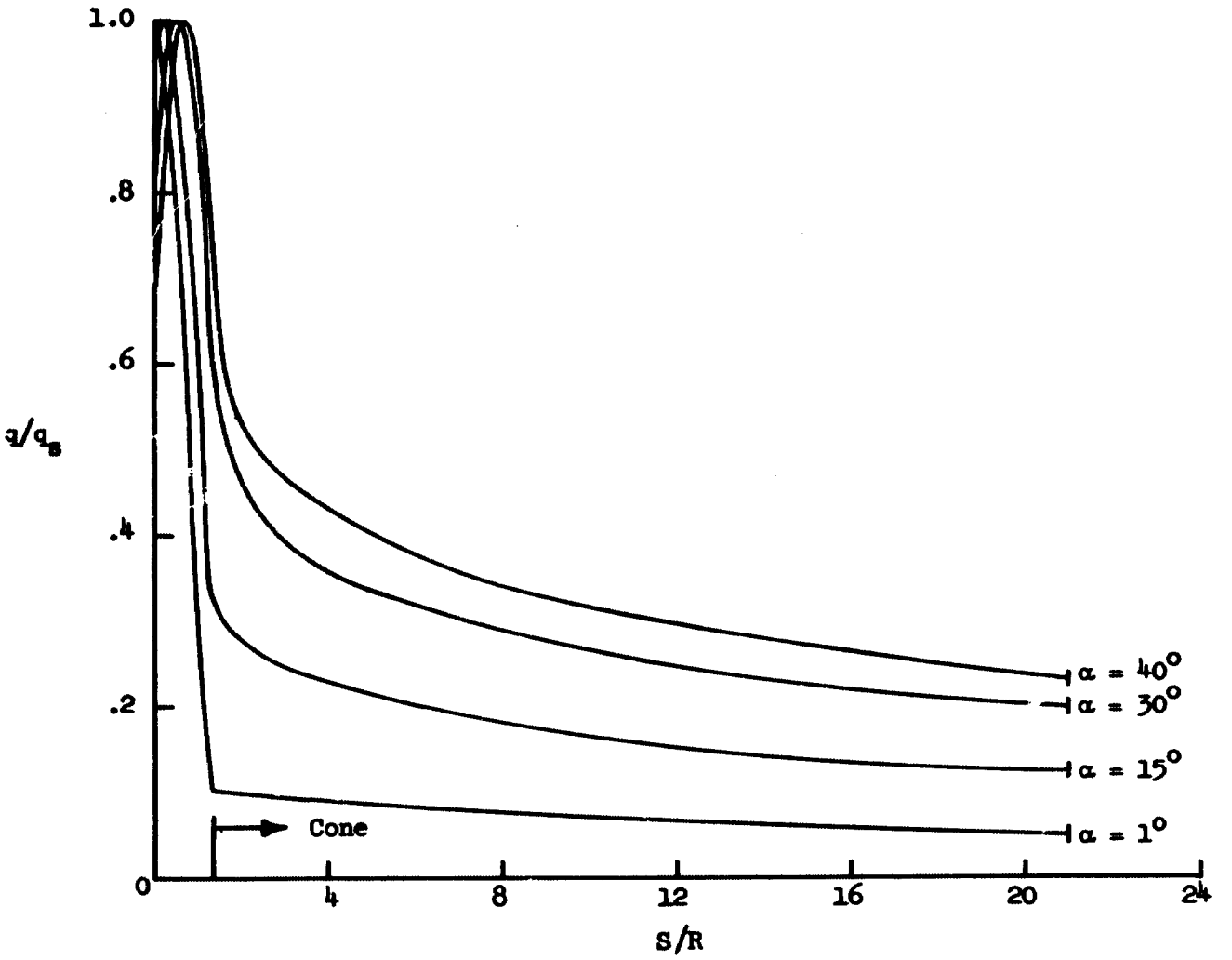

Figure 19.- Laminar heating distribution along the windward center line of 13° blunted half cone.

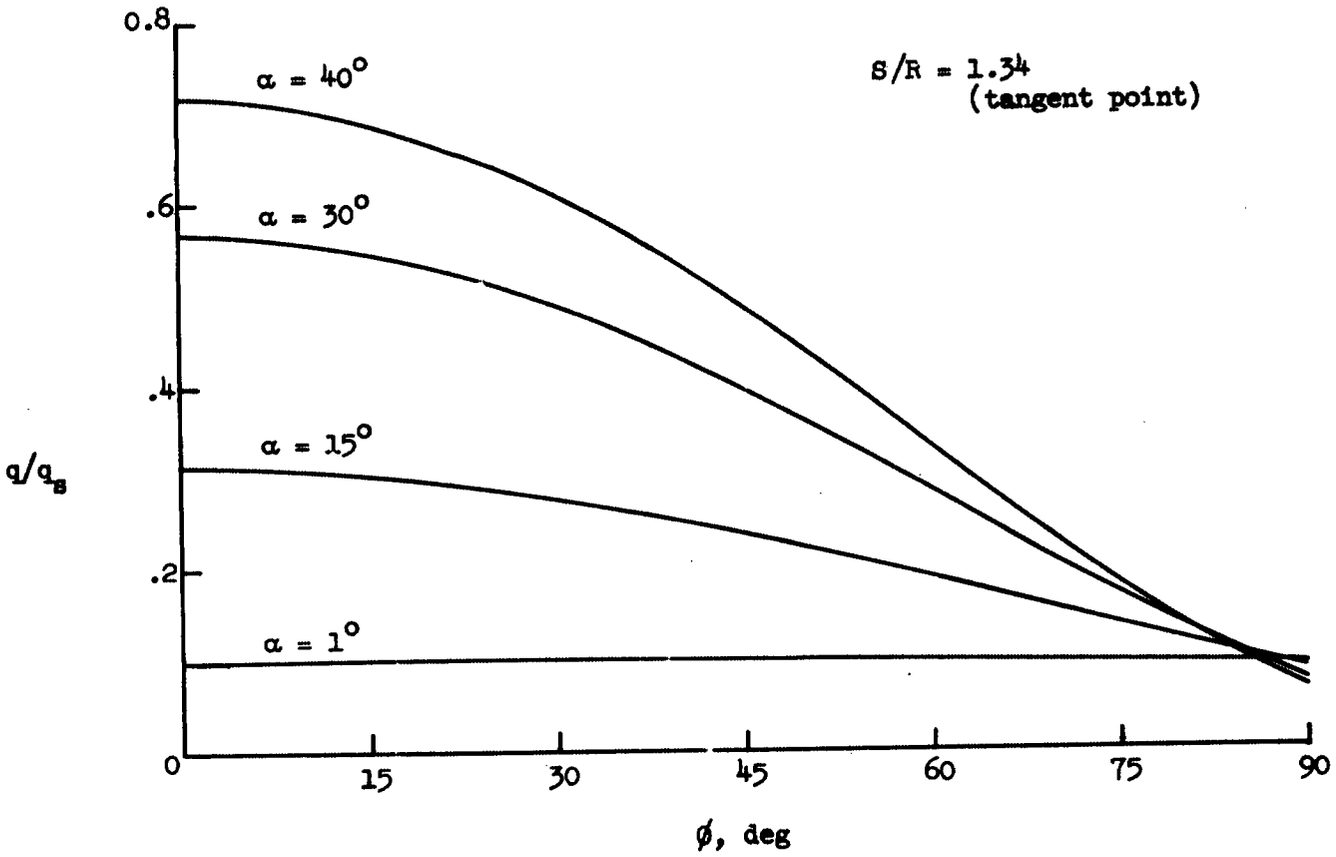

(a) S/R = 1.34.

Figure 20.- Circumferential heating distribution for 13° blunted half cone.

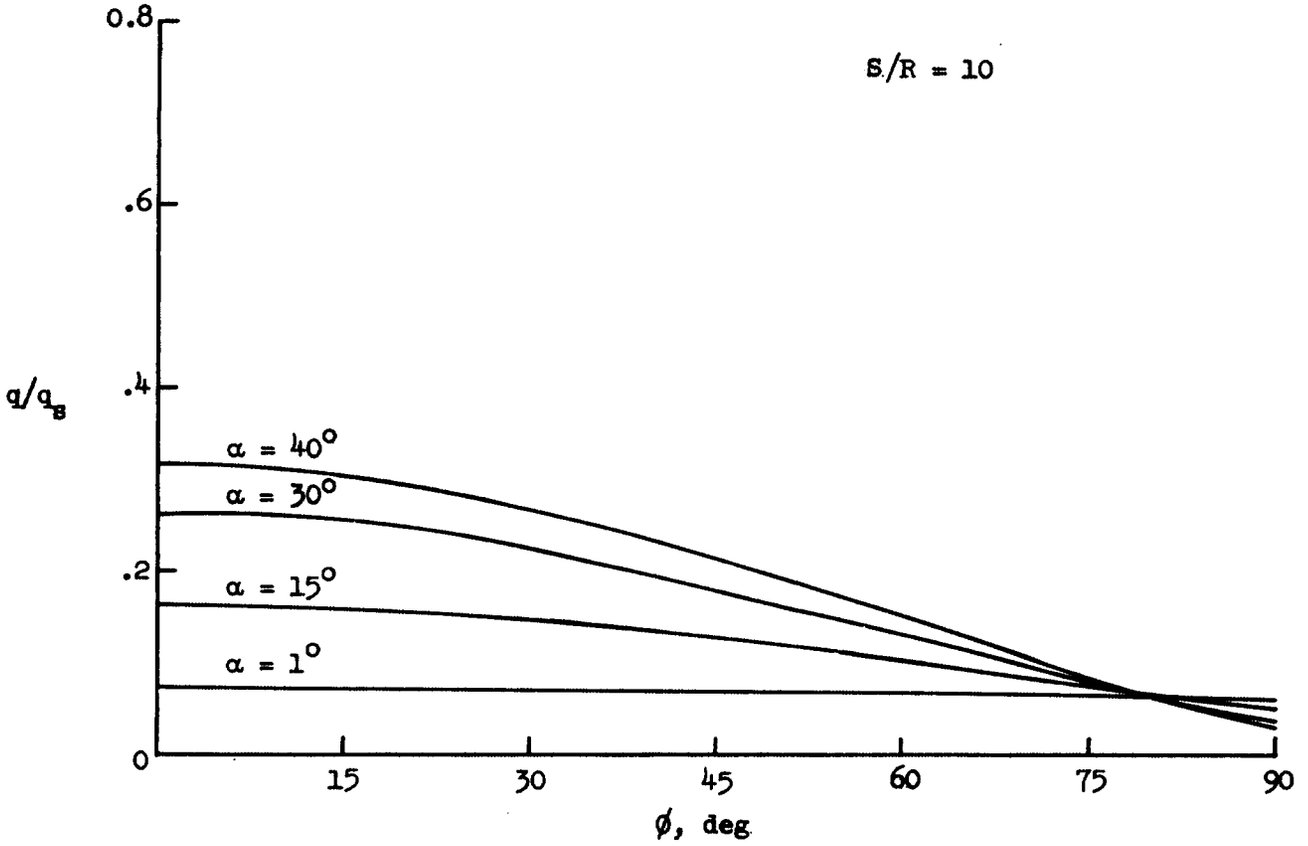

(b) S/R = 10.

Figure 20.- Concluded.

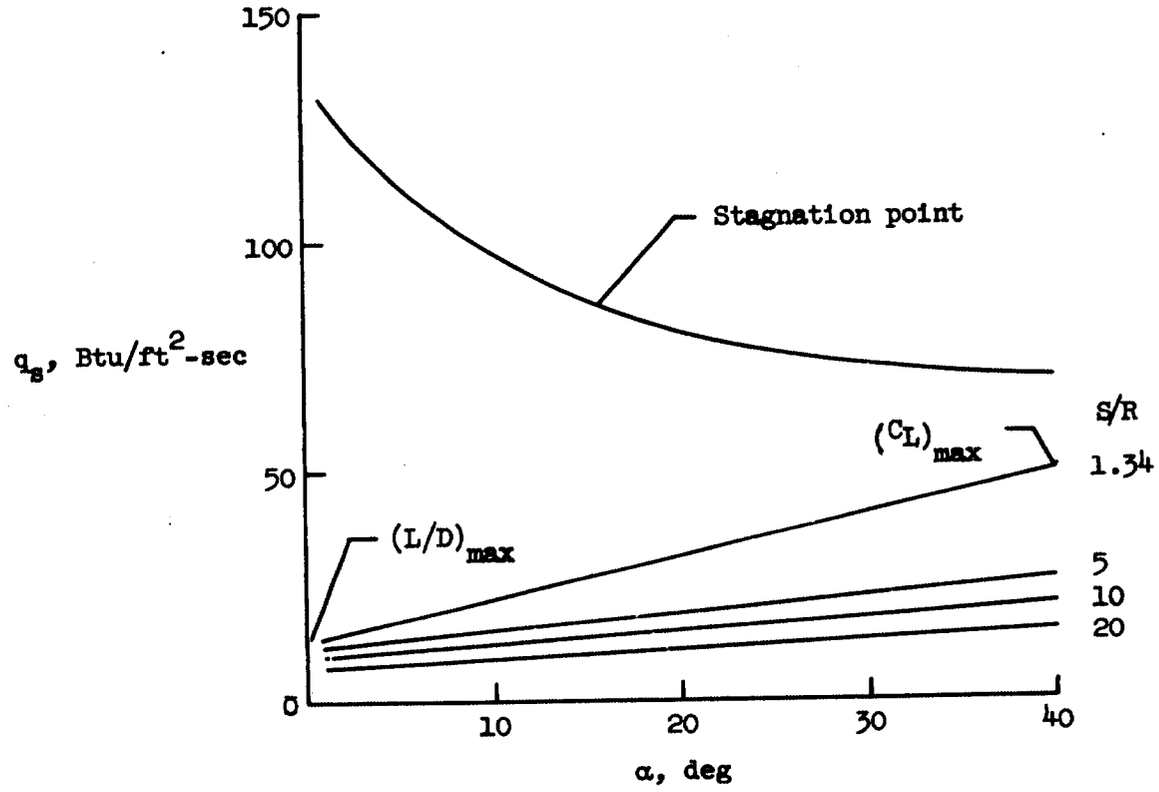

Figure 21.- Maximum heating rates at various locations along the windward center line as a function of angle of attack.

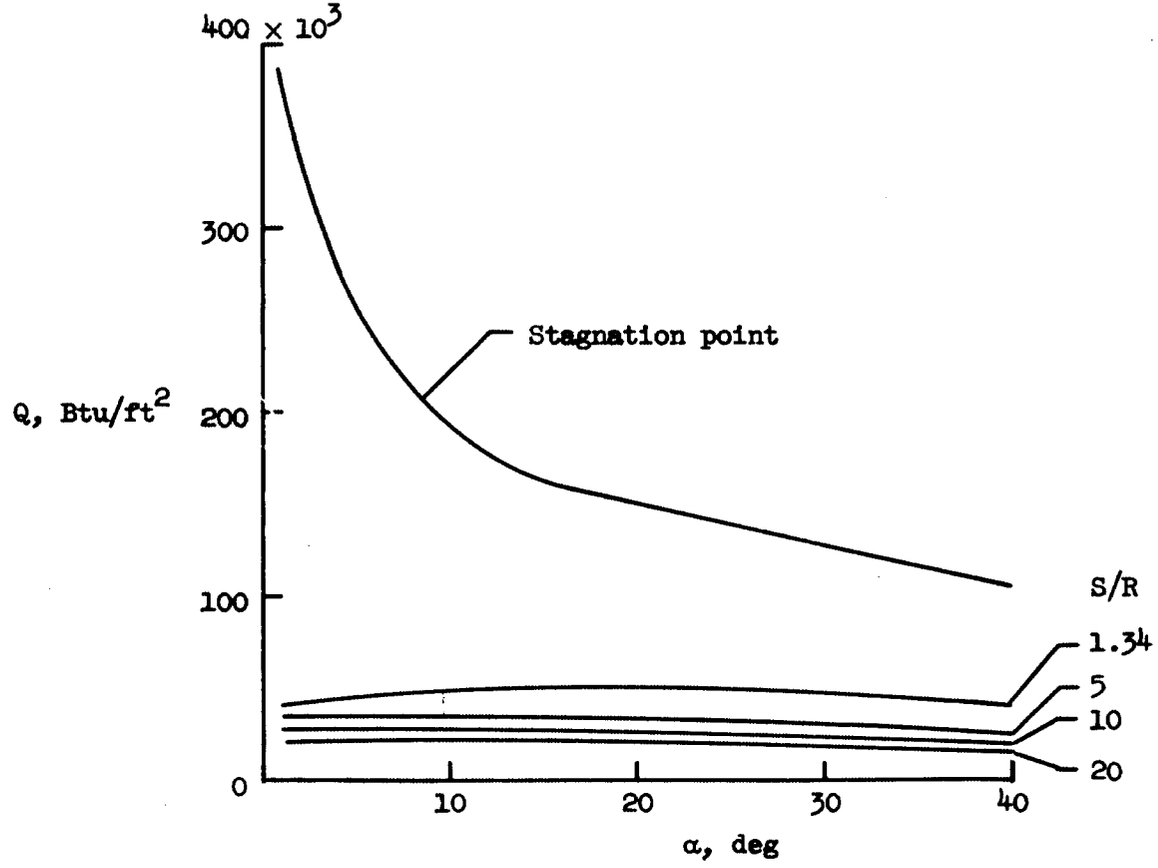

Figure 22.- Total heat load at various locations along the windward center line as a function of angle of attack.

For the angle of attack range considered, an angle of 40° is the optimum attitude of the vehicle with respect to the total heat load parameter.

In order to calculate heat shield weight requirements, the heating distribution must be known as a function of the surface area. This distribution has been calculated and is shown in Figure 23 as the heating rate ratio q/q_s as a function of per cent of vehicle surface area for each of the four entry attitudes. By integrating the heating distribution over the windward surface of the vehicle, the total heat loads can be obtained for each angle of attack (Fig. 24). The results show a consistent reduction in the total heat load as angle of attack increases toward $(C_L)_{max}$. The variations in total heat load will be reflected in the ablative weight requirements that will be discussed subsequently.

Ablative Weight Requirements

The ablative weight requirements of a blunted 13° half cone for entry at angles of attack of 1°, 15°, 30°, and 40° were determined for two phenolic-nylon ablation materials, one having a density of 36 lb/ft^3 and one having a density of 14 lb/ft^3. The ablative weight requirements were those necessary to limit the back surface temperature rise of a substructure having a heat capacity of 0.235 $Btu/ft^2-{}^{\circ}F$ to 300° F. The calculations were made by use of the charring ablator program, the trajectory environmental conditions, and the heating distributions previously discussed.

The material properties used for the 36-lb/ft^3 ablator (Table I) were those that have been used previously (Ref. 15) to obtain good agreement between calculated and experimental results. The material

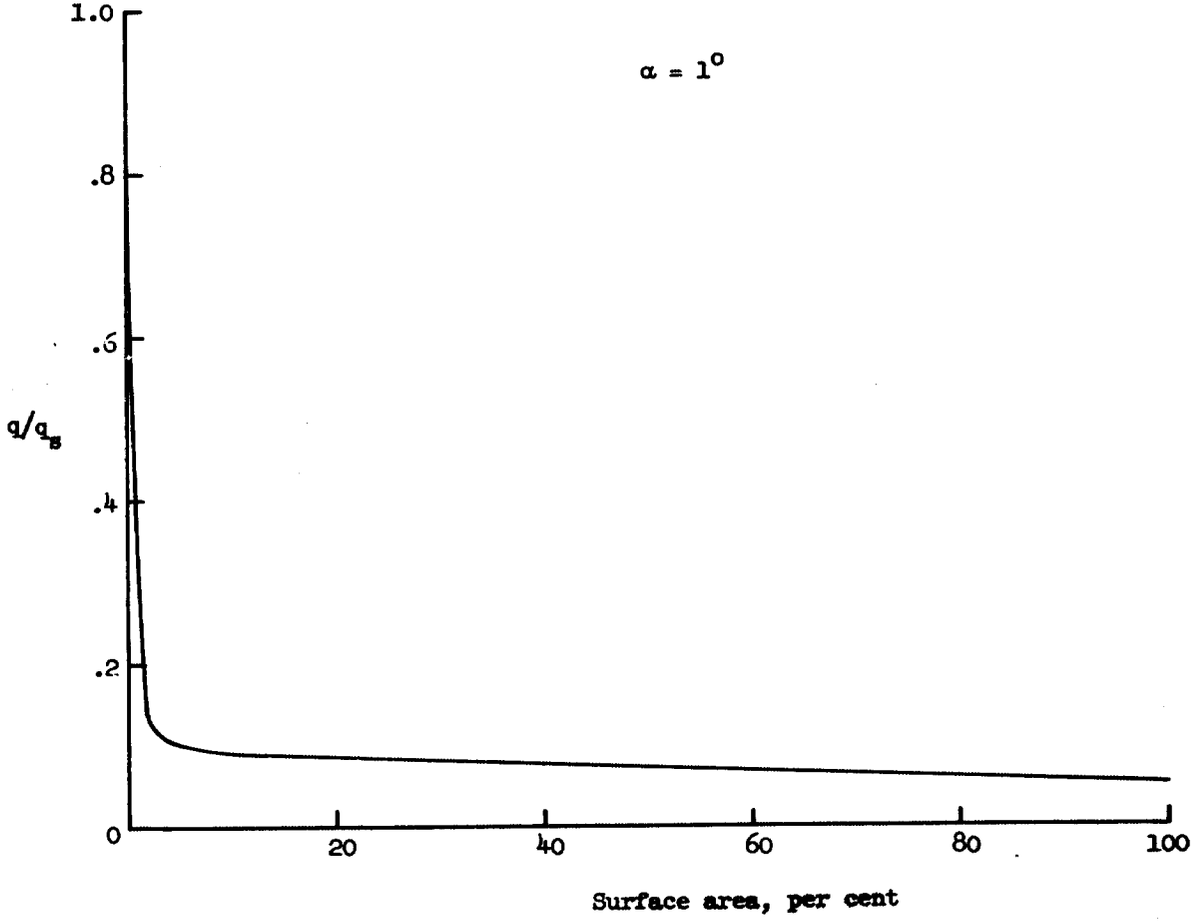

(a) $\alpha = 1^o$.

Figure 23.- Heating rate distribution over the windward surface of 13^o blunted half cone.

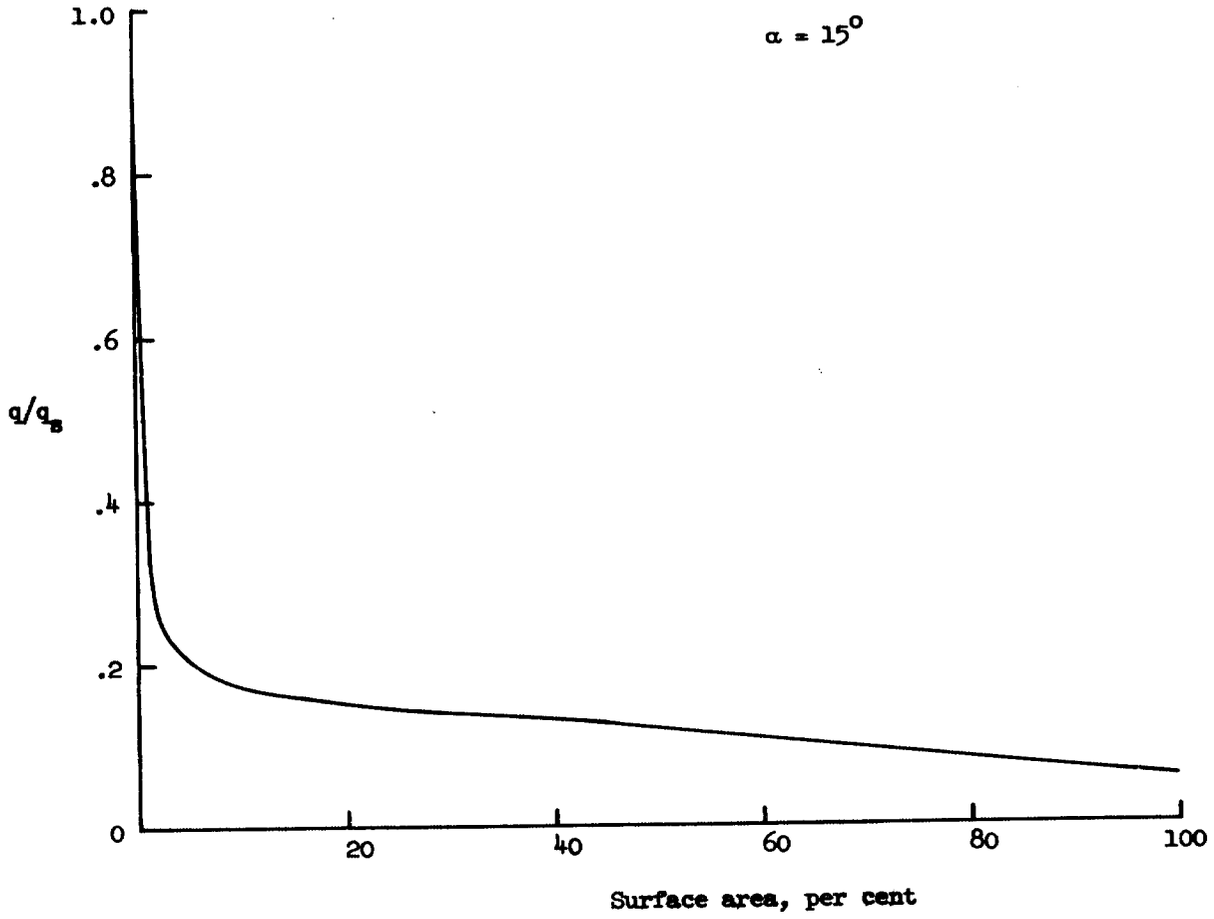

(b) $\alpha = 15^o$.

Figure 23.- Continued.

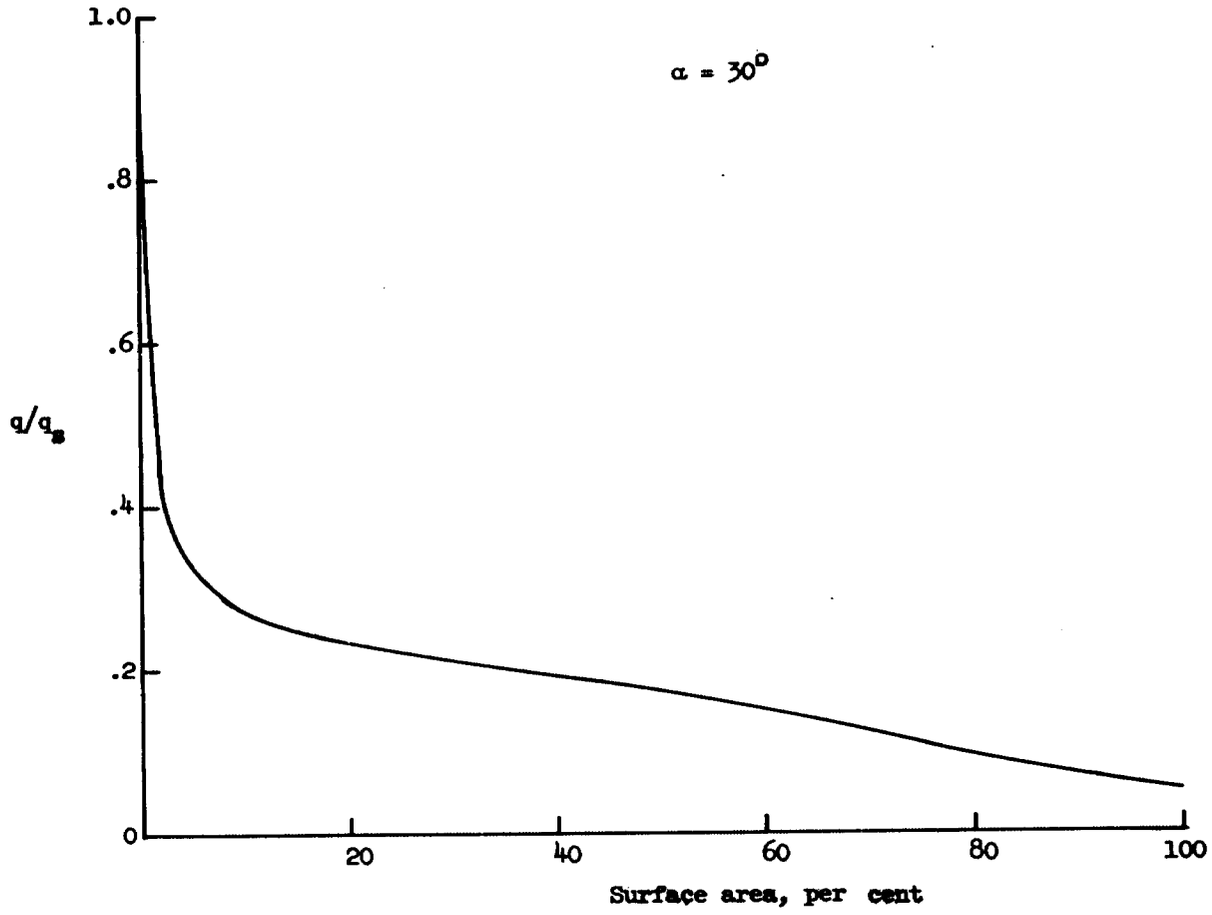

(c) $\alpha = 30^\circ$.

Figure 23.- Continued.

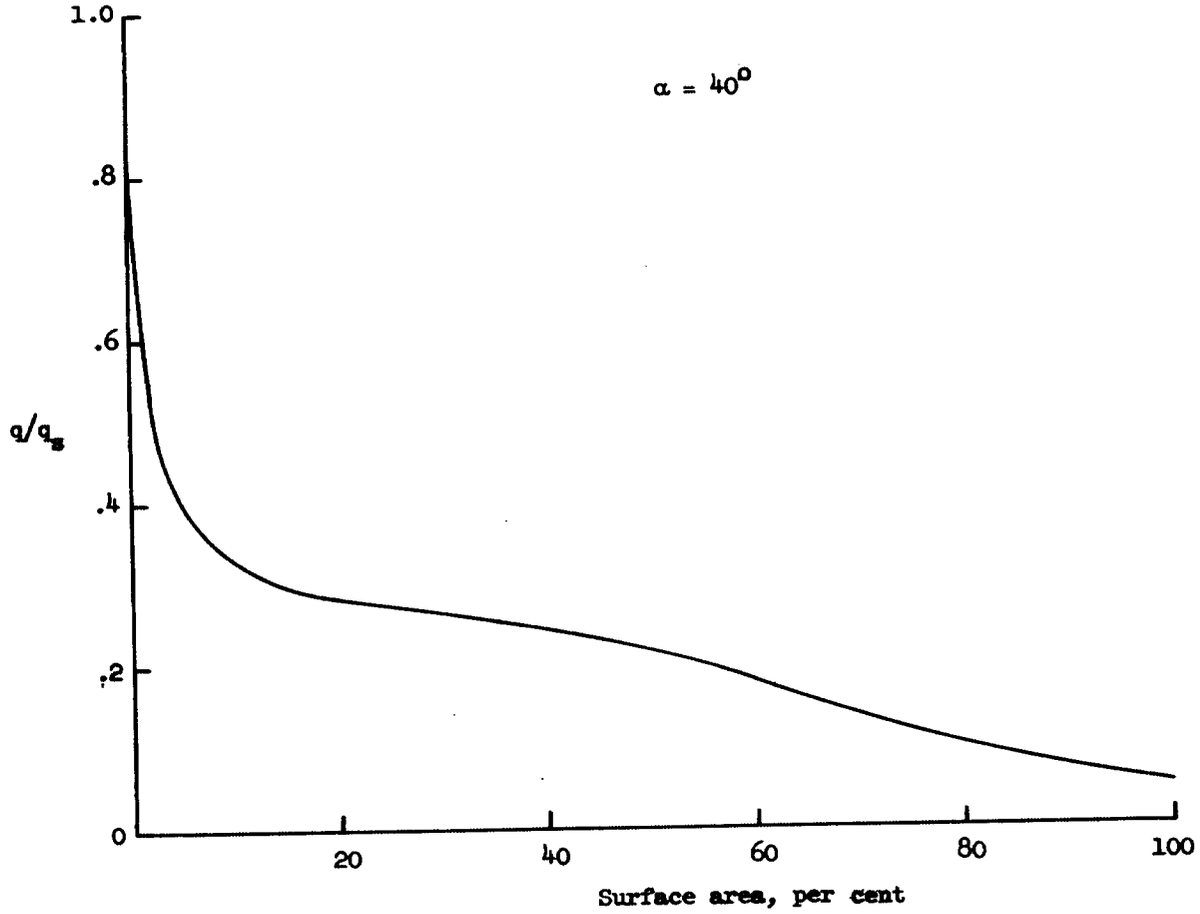

(d) $\alpha = 40^\circ$.

Figure 23.- Concluded.

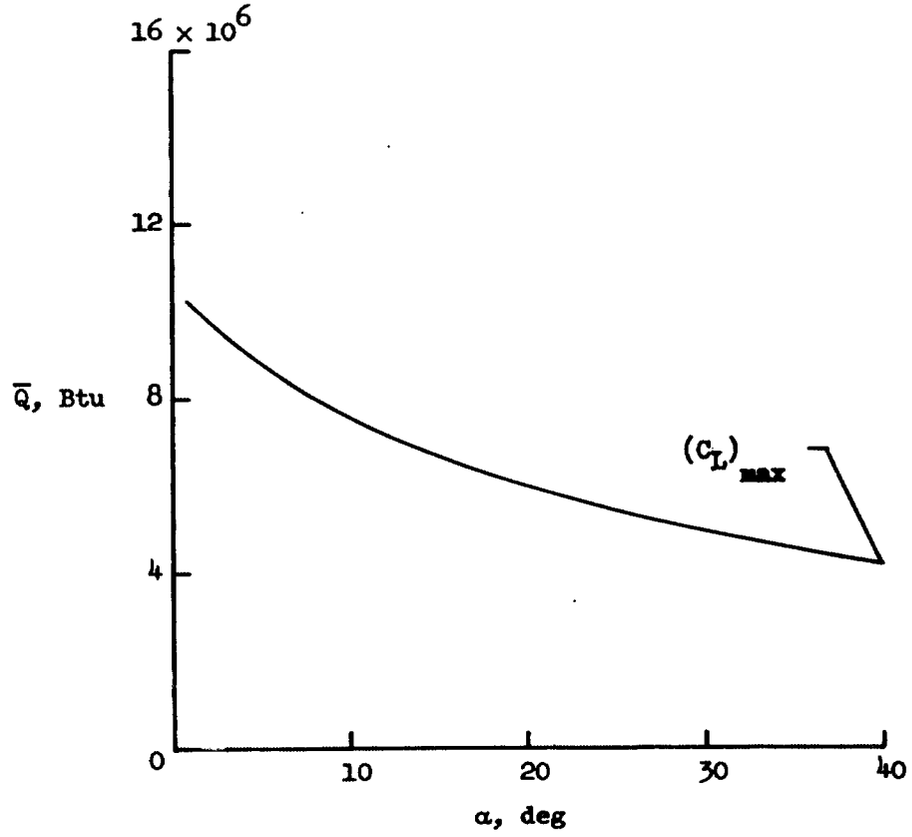

Figure 24.- Total heat load accommodated by 13° blunted cone during entry as a function of angle of attack.

properties used for the 14-lb/ft^3 ablator (Table I) were obtained by adjusting the thermal conductivities and densities of the charred and uncharred materials until the calculated thermal response of the low-density material was approximately that of the experimental results. With the exception of the thermal conductivities and densities, the material properties of the 14-lb/ft^3 ablator were assumed to be the same as the properties of the 36-lb/ft^3 ablator. This assumption appears reasonable since the two ablators consist of the same material components; however, the percentages of the component materials used were not the same for the high and low density ablators (Table III). Consequently, the need exists for thermophysical property measurements on the low-density ablators in order that more reliable inputs may be used in calculating the performance of the low-density ablators.

The environmental parameters used in the charring ablator program were stagnation cold-wall heating rates and enthalpy as a function of time along with the oxygen concentration (C_e = 23 per cent). The ablative weight requirements were determined for various heating rate ratios q/q_s while considering the enthalpy at the edge of the boundary layer to be the same as that at the stagnation point.

The results of the ablative heat shield weight calculations as a function of heating rate ratio q/q_s for entry at angles of attack of 1°, 15°, 30°, and 40° are shown in Figures 25(a) and 25(b) for the 36- and 14-lb/ft^3 ablators respectively. These results show that the entry attitude of a lifting-body entry vehicle has a significant

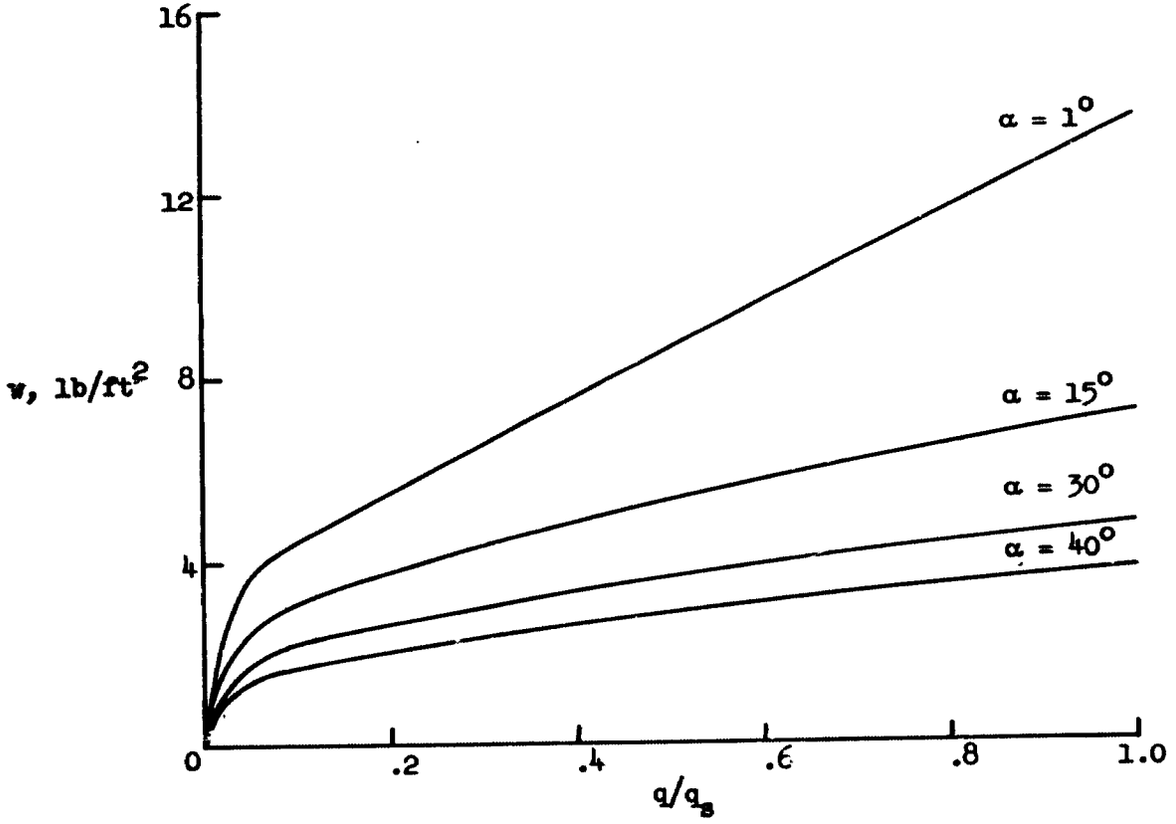

(a) 36 lb/ft^3 phenolic nylon.

Figure 25.- Effect of angle of attack on unit weight of ablation material required to limit back surface temperature rise to 300° F.

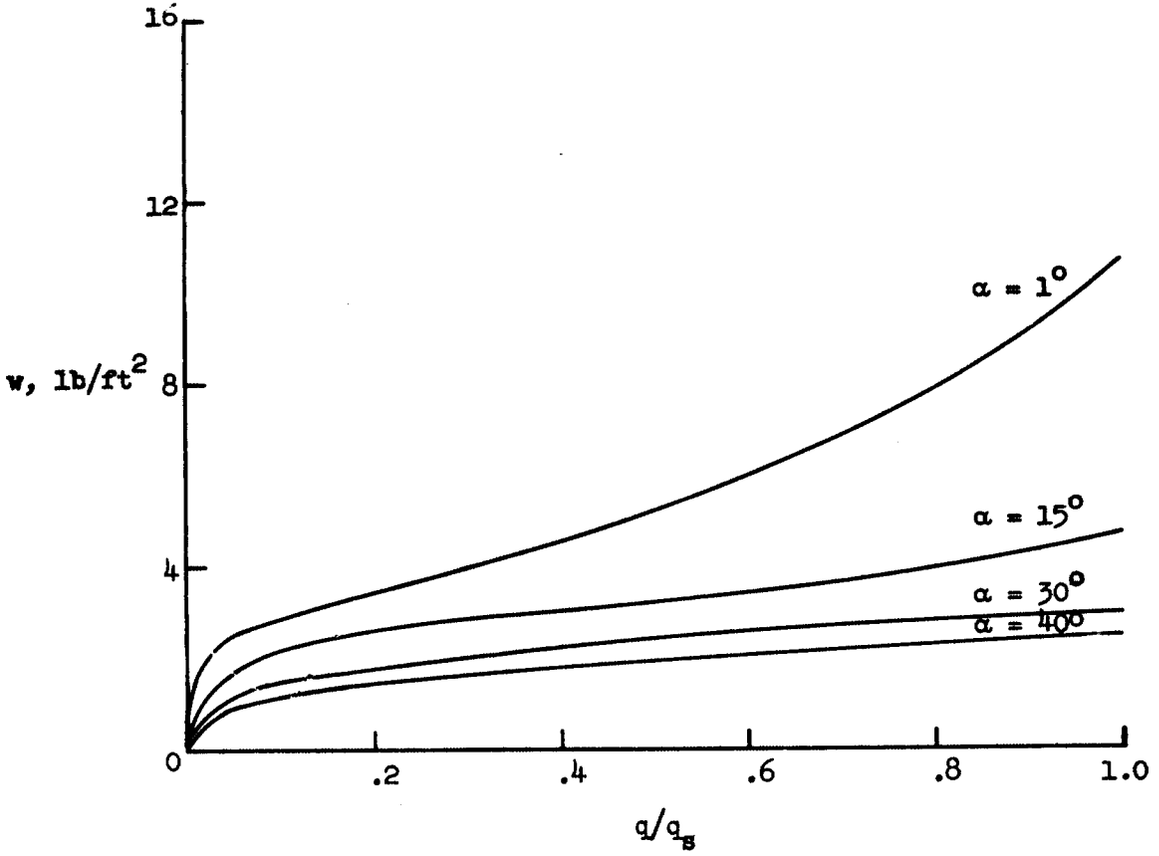

(b) 14 lb/ft^3 phenolic nylon.

Figure 25.- Concluded.

effect on the weight of ablation material required and that for any given entry attitude the ablative weight requirement can be reduced significantly by using a 14-lb/ft^3 rather than a 36-lb/ft^3 phenolic-nylon ablator.

Figures 26(a) and 26(b) show the ablative weight distributions over the windward surface of the entry vehicle. The unit weight of ablation material required to limit the back surface temperature rise to 300° F is plotted against per cent of windward surface area for each angle of attack for a 36-lb/ft^3 (Fig. 26(a)) and a 14-lb/ft^3 (Fig. 26(b) ablator. The total weight of ablation material required is obtained by integrating the appropriate weight-distribution curve over the windward surface area of the vehicle. The results of such integrations are shown in Figure 27, where the total ablative weight requirements are plotted against angle of attack. The fact that the total ablative weight requirement decreases with increasing angle of attack is a manifestation of the lower heat loads (Fig. 24) and, in general, the lower heating rates (Fig. 21) experienced at the larger angles of attack. The extent of the effect of varying the angle of attack from approximately that for $(L/D)_{max}$ to that for $(C_L)_{max}$ was to decrease the total ablative heat-shield weight requirement by approximately 50 per cent for both ablators.

When the effect of the density of the ablator on the total ablative weight requirement (Fig. 27) is examined, it is apparent that an appreciable reduction in the total ablative weight requirement can be realized by reducing the density of the phenolic-nylon ablator from

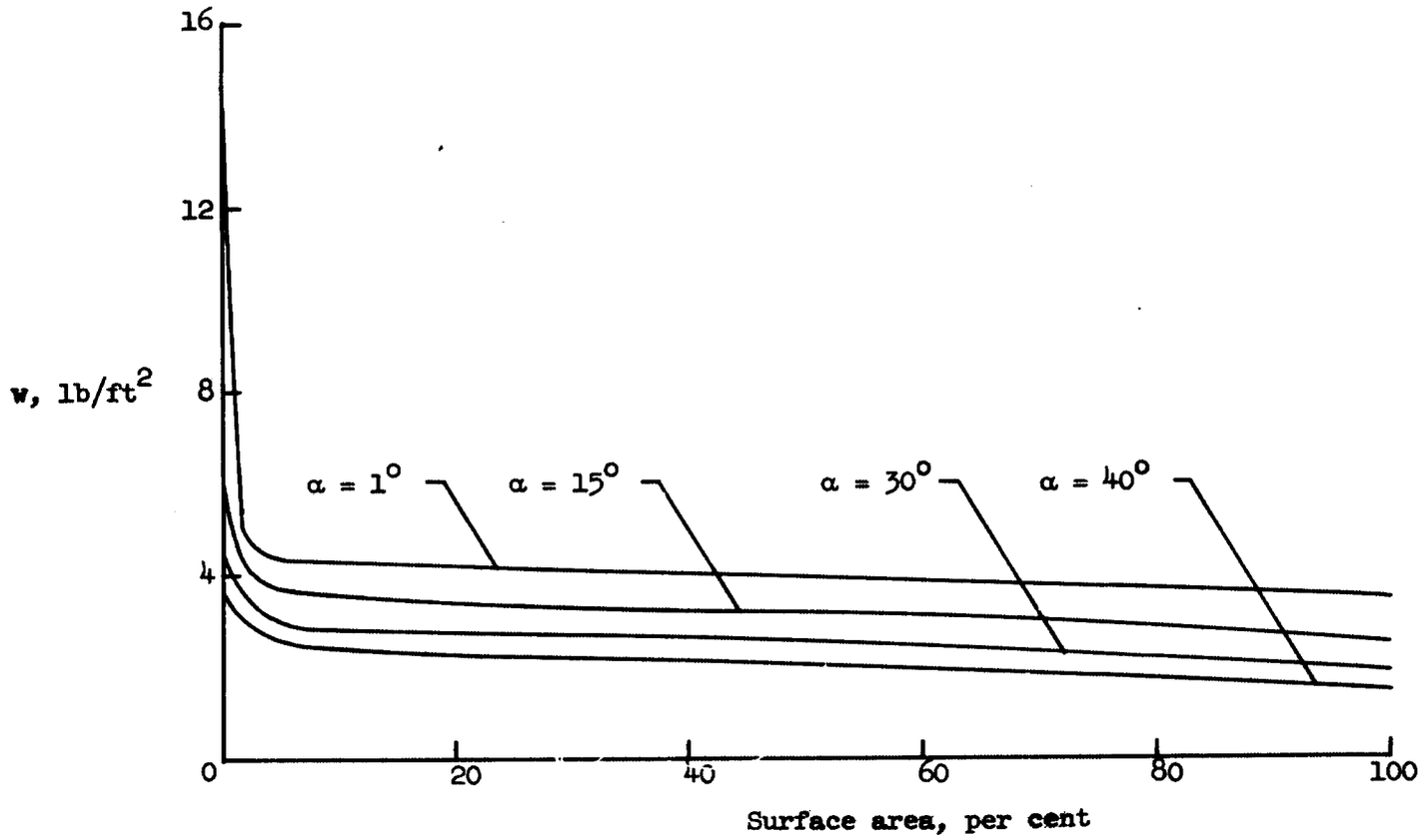

(a) 36 lb/ft^3 phenolic nylon.

Figure 26.- Unit weight distribution of ablation material over windward surface of 13° blunted half cone.

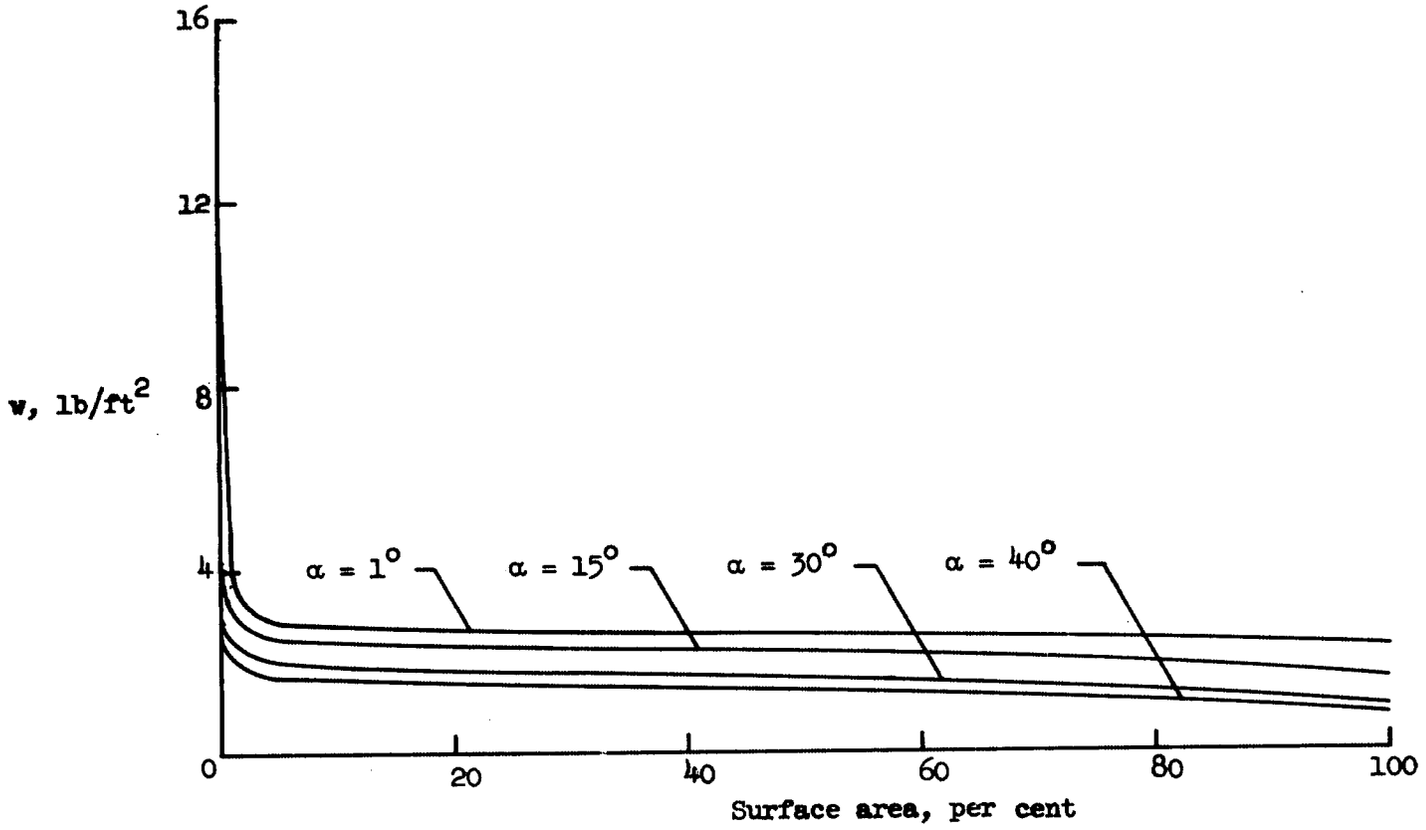

(b) 14 lb/ft^3 phenolic nylon.

Figure 26.- Concluded.

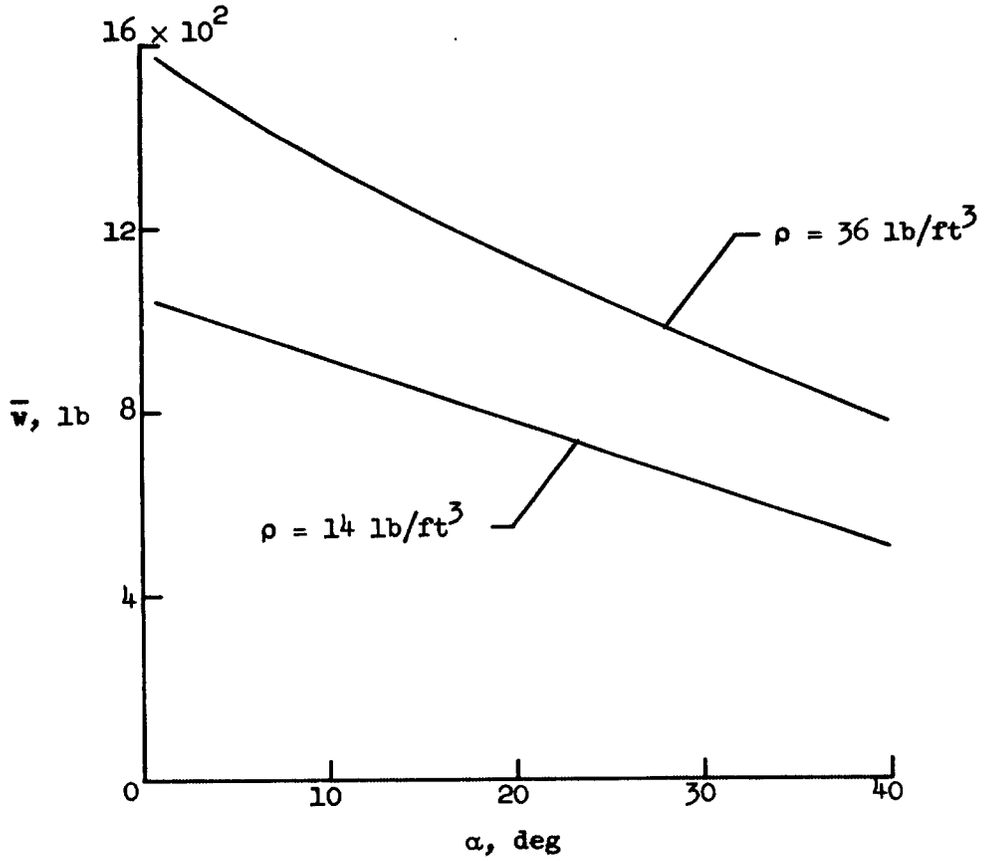

Figure 27.- Total ablative weight requirement of the windward surface of a 13° blunted half cone using 14 and 36 lb/ft^3 phenolic nylon ablators.

36 lb/ft^3 to 14 lb/ft^3. In fact, an average ablative heat shield weight reduction of 34 per cent was obtained by using a 14-lb/ft^3 rather than a 36-lb/ft^3 phenolic-nylon ablator. This weight reduction was essentially independent of the entry attitude of the lifting-body entry vehicle. Even though the entry attitudes considered for the 13° blunted half cone had a greater effect on the total ablative heat-shield weight requirement than the density variation considered, it is apparent that significant weight reductions were obtained for a given angle of attack by using the 14-lb/ft^3 ablator rather than the 36-lb/ft^3 ablator.

Consequently, the use of a low-density ablator, such as the 14-lb/ft^3 phenolic-nylon ablator considered in this study, appears to be justifiable not only from the performance of such materials in ground test facilities, but also from the results of the analysis made with regard to possible applications of such materials.

CHAPTER VI

CONCLUSIONS

A study has been made of the ablative performance of phenolic-nylon materials having densities of 10 lb/ft^3 to 20 lb/ft^3 and of the potential benefits that a low-density ablator might have with respect to ablative heat-shield weight requirements for a lifting-body entry vehicle. Results of the study lead to the following conclusions:

1. The ablative effectiveness of some of the low-density materials was about 1.5 times that of a 36-lb/ft^3 material when subjected to cold-wall heating rates of 20 Btu/ft^2-sec.

2. The trend for the low-density materials is for the ablative effectiveness to decrease with increasing density.

3. The ablative effectiveness of the phenolic-nylon materials improved as the percentage of phenolic Microballoons was increased. However, the physical characteristics of the uncharred and charred materials limits the amount of Microballoons that can be used in an ablative material.

4. The physical integrity of the char of low-density phenolic-nylon materials can be significantly improved, without reducing the ablative insulative properties of the material, by placing the material in a phenolic-glass honeycomb.

5. The ablative effectiveness of a 14-lb/ft^3 material when subjected to various test conditions increased with increasing heating rates and decreased with increasing test stream oxygen concentrations.

Furthermore, the char of the 14-lb/ft^3 material, supported in a phenolic-glass honeycomb, maintained good physical integrity as evidenced by no spallation for all test conditions. The test conditions were representative of those experienced by a lifting-body entry vehicle at various times during the entry trajectory.

6. Analysis indicates that the environmental parameters experienced by a lifting body entry vehicle are strongly dependent on the entry attitude. In particular, the heating load and, in general, the heating rates experienced by the most windward ray of a 13° blunted half cone decreased with increasing angle of attack (lift). Furthermore, the total integrated heat load to the windward side of the entry vehicle for $(C_L)_{max}$ entry ($\alpha = 40^\circ$) was only 41 per cent of the total heat load experienced at approximately $(L/D)_{max}$ entry ($\alpha = 1^\circ$).

7. Analysis of the ablative heat shield weight requirements of the windward side of a 13° blunted half cone indicates that the total weight of ablation material required to limit the back surface temperature rise to 300° F can be reduced by as much as 34 per cent by using a 14-lb/ft^3 ablator rather than a 36-lb/ft^3 ablator.

8. Consideration should be given to low-density ablators, such as the 14-lb/ft^3 ablator considered in this study, in future heat shield design studies for lifting-body entry vehicles. If the low-density materials are used, the single-wall heat shield design may become more competitive with the double-wall heat shield design with respect to total heat shield weight.

REFERENCES

1. Meltzer, J.; Slaughter, J. I.; and Sallis, D. V.: Thermal Protection System for the SV-5 (PRIME) Ablative Lifting Reentry Vehicle. Aerospace Corp. TRD-669(6108-27)-1, Oct. 22, 1965.
2. Fallis, William B.: Feasibility Study of Minimum Manned Lifting Body Entry Vehicle. Vol. I. Final Report, Northrop Norair Publication NB 66-9, Jan. 1966.
3. LaPorte, A. H.: Research on Refurbishable Thermostructural Panels for Manned Lifting Entry Vehicles. NASA CR-638, 1966.
4. Newell, J.: A Study of Thermo-Structural Design Concepts for Lifting Entry Vehicles. NASA CR-240, 1965.
5. Chapman, A. J.: An Experimental Evaluation of Three Types of Thermal Protection Materials at Moderate Heating Rates and High Total Heat Loads. NASA TN D-1814, July 1963.
6. Dunavant, James C.; and Edwards, William R.: The Effects of Vehicle Attitude on Heat Transfer to the Surface of Lifting Vehicles Entering the Atmosphere. Paper presented at the AIAA Third Aerospace Sciences Meeting, New York, N.Y., Jan. 24-26, 1966.
7. Swann, Robert T.; Brewer, William D.; and Clark, Ronald K.: Effect of Composition, Density, and Environment on the Ablative Performance of Phenolic Nylon. NASA TN D-3908, 1967.
8. Moss, James N.; and Howell, William E.: Recent Developments in Low-Density Ablators. Paper presented at 12th National SAMPE Symposium, Anaheim, California, Oct. 10-12, 1967.

9. Swann, Robert T.; Pittman, Claud M.; and Smith, James C.: One-Dimensional Numerical Analysis of the Transient Response of Thermal Protection Systems. NASA TN D-2876, 1965.

10. Dow, Marvin B.; and Swann, Robert T.: Determination of Effects of Oxidation on Performance of Charring Ablators. NASA TR R-196, 1964.

11. Nolan, Edward J.; and Scala, Sinclaire M.: Aerothermo-Dynamic Behavior of Pyrolytic Graphite During Sustained Hypersonic Flight. ARS Jour. Vol. 32, No. 1, Jan. 1962, pp. 26-35.

12. Swann, Robert T.: Approximate Analysis of the Performance of Char-Forming Ablators. NASA TR R-195, 1964.

13. Dorrance, William H.: Viscous Hypersonic Flow. McGraw-Hill Book Co., Inc., 1962.

14. Nelson, James B.: Determination of Kinetic Parameters of Six Ablation Polymers by Thermogravimetric Analysis. NASA TN D-3919, 1967.

15. Brewer, William D.; Stroud, C. W.; and Clark, Ronald K.: Effect of Chemical State of Pyrolysis Gases on Lifting Body Heat-Shield Weight. (Proposed NASA TN).

16. Wing, L. D.; and Eilerston, W. H.: Research Studies and Analysis to Define Manned Lifting Entry Flight Environment. NASA CR-639, 1966.

17. Swann, Robert T.; Dow, Marvin B.; and Tompkins, Stephen S.: Analysis of the Effects of Environmental Conditions on the

Performance of Charring Ablators. J. Spacecraft Rockets, Vol. 3, No. 1, Jan. 1966, pp. 61-67.

18. Syvertson, C. A.; Swenson, B. L.; Anderson, J. L.; and Kenyon, G. D.: Some Considerations of the Performance of a Maneuverable, Lifting-Body, Entry Vehicle. Space Rendezvous, Rescue, and Recovery. Vol. 16, part one of Advances in the Aeronautical Sciences. N. V. Peterson, ed. 1963, pp 898-918.

19. Wells, William R.; and Armstrong, William O.: Tables of Aerodynamic Coefficients Obtained from Developed Newtonian Expressions for Complete and Partial Conic and Spheric Bodies at Combined Angles of Attack and Slideslip with Some Comparison with Hypersonic Experimental Data. NASA TR R-127, 1962.

20. Detra, R. W.; Kemp, N. H.; and Riddell, F. R.: Addendum to "Heat Transfer to Satellite Vehicles Re-entering the Atmosphere." Jet Propulsion, Vol. No. 12, Dec. 1957, pp. 1256-1257.

21. DeJarnette, Fred, R.: A Simplified Method for Calculating Heat Transfer Over Bodies at an Angle of Attack. Paper presented at the Southeastern Symposium on Missiles and Aerospace Vehicles Sciences, Am. Astronautical Society, Huntsville, Alabama, Dec. 5-7, 1966.

22. Cooke, J. C.: An Axially Symmetric Analogue for General Three-Dimensional Boundary Layers, ARC R & M No. 3200 (London), June 1959.

23. Beckwith, I. E.: Similarity Solutions for Small Cross Flows in Laminar Compressible Boundary Layers, NASA TR R-107, 1961.

24. Lees, Lester: Laminar Heat Transfer Over Blunt-Nosed Bodies at Hypersonic Flight Speeds, Jet Propulsion, Vol. 26, No. 4, April 1956, pp. 259-269, 274.

TABLE I

MATERIAL PROPERTIES OF 14-AND 36-LB/FT^3 PHENOLIC-NYLON ABLATORS

Uncharred material properties	14-lb/ft^3 Material	36-lb/ft^3 Material
Density, lb/ft^3	14	36
Effective heat of pyrolysis, Btu/lbm	550	550
A', lb/ft^2-sec	1.58×10^6	1.58×10^6
B', $^\circ$R	2.32×10^4	2.32×10^4
Specific heat of gaseous products of pyrolysis, Btu/lb		
At 0° F	0.58	0.58
At 160° F	0.94	0.94
At 340° F	1.54	1.54
At 520° F	3.06	3.06
At 700° F	4.10	4.10
At 880° F	3.78	3.78
At 1060° F	2.21	2.21
At 1240° F	1.42	1.42
At 1600° F	1.18	1.18
At 1800° F	1.09	1.09
At 2540° F	1.00	1.00
At 3040° F	1.00	1.00
Specific heat, Btu/lb		
At 80° F	0.36	0.36
At 200° F	.42	.42
At 300° F	.48	.48
At 400° F	.54	.54
At 500° F	.60	.60
At 600° F	.66	.66
At 700° F	.71	.71
At 800° F	.74	.74
Thermal conductivity, Btu/ft-sec-$^\circ$ F		
At 80° F	1.29×10^{-5}	1.08×10^{-5}
At 240° F	1.35	1.36
At 440° F	1.42	1.72
At 640° F	1.47	2.08
At 820° F	1.50	2.22
At 1040° F	2.50	2.80

TABLE I

MATERIAL PROPERTIES OF 14-AND 36-LB/FT^3
PHENOLIC-NYLON ABLATORS - Continued

Charred material properties	14-lb/ft^3 Material	36-lb/ft^3 Material
Density, lb/ft^3	8.4	17
Emissivity	0.8	0.8
A, lb/ft^2-sec-atm	1.0×10^{10}	1.0×10^{10}
B, $^\circ$R	7.6×10^4	7.6×10^4
Heat of combustion of char, Btu/lb	4300	4300
Specific heat, Btu/lb		
At 80° F	0.39	0.39
At 1000° F	0.39	0.39
At 2000° F	0.52	0.52
At 3000° F	0.52	0.52
Thermal conductivity, Btu/ft-sec-$^\circ$F		
At 80° F	1.0×10^{-5}	2.5×10^{-5}
At 500° F	1.8	2.5
At 1000° F	3.4	2.5
At 1500° F	5.8	8.0
At 2500° F	11.7	30.0
At 3500° F	20.0	60.0

TABLE II. TEST FACILITIES OPERATIONAL PARAMETERS

Operational parameters	Test facility	
	5-Megawatt[a]	1-Megawatt[b]
Total enthalpy, Btu/lb	750 - 4500	4000 - 16000
Stagnation pressure, atm	0.04 - 0.4	0.02 - 0.06
Cold-wall heating rate, $Btu/ft^{1.5}$-sec	10 - 70	30 - 150
Mass flow rate, lb/sec	0.1 - 1.0	.01 - .05
Run time, sec	100 - 500	Continuous
Model body diameter, inch	3	3
Power level, MW	0.25 - 5	0.06 - 1.2
Mach number	3.4 - 4.3	3.2 - 3.4
Reynolds number, $ft^{-1} \times 10^6$	.05 - .50	.004 - .012

[a] Using a 9.65° conical nozzle with a 1.5-inch-diameter throat and a 6-inch-diameter exit.

[b] Using a 8.18° conical nozzle with a 1-inch-diameter throat and a 4-inch-diameter exit.

TABLE III. SUMMARY OF TEST RESULTS FOR VARIOUS PHENOLIC-NYLON MATERIALS

[q = 20 Btu/ft^2-sec; $p_{t,2}$ = 0.04 atm; h_e = 1700 Btu/lb; test gas = 3% O_2 and 97% N_2]

Model	Composition percentage by weight			Density lb/ft^3	Time for 300° F rise, sec	E, Btu/lb
	Phenolic	Nylon	Microballoons			
1	10	10	80	10.3	148	9 600
2	10	10	80	11.8	173	10 000
3	10	10	80	13.9	178	8 400
4	15	15	70	12.6	200	10 300
5	15	15	70	14.6	195	9 100
6	20	20	60	10.1	120	7 900
7	20	20	60	12.4	185	8 600
8	20	20	60	14.2	194	8 900
9	20	20	60	16.6	222	7 300
10	20	20	60	20.1	228	7 100
11	25	25	50	14.1	171	9 400
12	25	25	50	17.5	192	6 600
13	30	30	40	16.0	211	8 400
14	30	30	40	19.5	209	6 800
15	35	35	30	15.4	188	8 200
16	35	35	30	20.0	233	7 700
17	40	0	60	13.1	149	7 700
18	40	0	60	14.5	129	6 900
19	40	0	60	16.5	152	6 000
20	30	10	60	11.9	143	7 800
21	30	10	60	14.8	150	6 400
22	30	10	60	17.6	140	5 400
23	30	10	60	12.9	174	8 400
24	30	10	60	13.1	148	8 800
25[a]	30	10	60	15.0	144	6 600
26	10	30	60	14.6	198	8 700
27	25	40	35	35.0	272	6 200

[a]Material was in a phenolic-glass honeycomb.

TABLE IV. SUMMARY OF TEST CONDITIONS AND TEST RESULTS FOR A 14 lb/ft^3 PHENOLIC-NYLON ABLATOR[a]

[30 per cent phenolic, 10 per cent nylon, and 60 per cent Microballoons]

Model	q, Btu/ft^2-sec	he, Btu/lb	$p_{t,2}$, atm	Mass flow rate, lb/sec		Time for 300° F rise, sec	Density, lb/ft^3	E, Btu/lb
				N_2	O_2			
5-Megawatt test facility								
28	60	2300	0.200	0.504	0.016	89	13.7	12 000
29	46	1800	.196	.553	.017	91	13.0	10 000
30	82	3100	.195	.453	.014	66	12.9	13 000
31	37	1900	.106	.278	.008	128	13.6	10 800
32	62	3300	.098	.213	.007	109	13.9	15 000
33	21	1600	.058	.148	.005	164	14.2	7 400
34	32	2300	.050	.120	.004	124	15.2	8 100
35	40	3000	.048	.106	.003	118	13.8	10 500
36	48	3600	.050	.106	.003	106	12.9	12 100
1-Megawatt test facility								
37	66	5000	0.042	0.028	0.008	65	13.6	9 600
38	125	8800	.097	.025	.008	50	14.5	13 800
39	141	9500	.050	.024	.007	51	12.9	17 000
40	156	10000	.053	.024	.007	45	12.7	17 000

[a]In a phenolic-glass honeycomb.